

**SYSTEMATIC APPROACH FOR CHEMICAL REACTIVITY
EVALUATION**

A Dissertation

by

ABDULREHMAN AHMED ALDEEB

Submitted to the Office of Graduate Studies of
Texas A&M University
in partial fulfillment of the requirements for the degree of

DOCTOR OF PHILOSOPHY

December 2003

Major Subject: Chemical Engineering

**SYSTEMATIC APPROACH FOR CHEMICAL REACTIVITY
EVALUATION**

A Dissertation

by

ABDULREHMAN AHMED ALDEEB

Submitted to the Office of Graduate Studies of
Texas A&M University
in partial fulfillment of the requirements for the degree of

DOCTOR OF PHILOSOPHY

Approved as to style and content by:

M. Sam Mannan
(Chair of Committee)

Kenneth R. Hall
(Member)

Mark T. Holtzapple
(Member)

Jerald A. Caton
(Member)

Kenneth R. Hall
(Head of Department)

December 2003

Major Subject: Chemical Engineering

ABSTRACT

Systematic Approach for Chemical Reactivity

Evaluation. (December 2003)

Abdulrehman Ahmed Aldeeb, B.S., Jordan University of Science & Technology;

M.S., The University of Texas at Arlington

Chair of Advisory Committee: Dr. M. Sam Mannan

Under certain conditions, reactive chemicals may proceed into uncontrolled chemical reaction pathways with rapid and significant increases in temperature, pressure, and/or gas evolution. Reactive chemicals have been involved in many industrial incidents, and have harmed people, property, and the environment.

Evaluation of reactive chemical hazards is critical to design and operate safer chemical plant processes. Much effort is needed for experimental techniques, mainly calorimetric analysis, to measure thermal reactivity of chemical systems. Studying all the various reaction pathways experimentally however is very expensive and time consuming. Therefore, it is essential to employ simplified screening tools and other methods to reduce the number of experiments and to identify the most energetic pathways.

A systematic approach is presented for the evaluation of reactive chemical hazards. This approach is based on a combination of computational methods, correlations, and experimental thermal analysis techniques. The presented approach will help to focus

the experimental work to the most hazardous reaction scenarios with a better understanding of the reactive system chemistry.

Computational methods are used to predict reaction stoichiometries, thermodynamics, and kinetics, which then are used to exclude thermodynamically infeasible and non-hazardous reaction pathways. Computational methods included: (1) molecular group contribution methods, (2) computational quantum chemistry methods, and (3) correlations based on thermodynamic-energy relationships. The experimental techniques are used to evaluate the most energetic systems for more accurate thermodynamic and kinetics parameters, or to replace inadequate numerical methods. The Reactive System Screening Tool (RSST™) and the Automatic Pressure Tracking Adiabatic Calorimeter (APTAC™) were employed to evaluate the reactive systems experimentally. The RSST™ detected exothermic behavior and measured the overall liberated energy. The APTAC™ simulated near-adiabatic runaway scenarios for more accurate thermodynamic and kinetic parameters.

The validity of this approach was investigated through the evaluation of potentially hazardous reactive systems, including decomposition of *di-tert*-butyl peroxide, copolymerization of styrene-acrylonitrile, and polymerization of 1,3-butadiene.

To my parents: Ahmed and Fatima

To my brothers: Fahed, Abdulrazaq, Fadi, Mohammad, and Abdullah

ACKNOWLEDGEMENTS

The author wishes to express his sincere gratitude to his supervisor, Professor M. Sam Mannan, for his guidance, inspiration, friendship, and support throughout this research. Thanks also go to a member of the committee, Professor Kenneth Hall for his unlimited support. Special thanks also go to Professors Mark Holtzapple and Jerald Caton for their cooperation and serving as advising committee members.

It is a pleasure to recognize the extent to which conversations and collaboration with Dr. William Rogers contributed to this project. Dr. Rogers has been an invaluable source of knowledge and encouragement.

Gratitude is expressed to the Mary Kay O'Connor Process Safety Center (MKOPSC) for supporting this research project and the Chemical Engineering Department at Texas A&M University for supporting me financially pursuing my degree.

I am grateful to the Texas A&M University Supercomputing Facility staff for their technical support in conducting the theoretical calculations in this research. Also, many thanks go to the MKOPSC and Chemical Engineering Department staff for their help to make this research project reach this final stage.

I would like also to thank the National Research Institute of Fire and Disaster, Tokyo, Japan for inviting me to their laboratory to conduct the C80D heat flow analysis.

Finally, sincere admiration goes to my parents and brothers for their love and encouragement. I offer sincere thank to Nader and Eman for the unlimited family environment they created.

TABLE OF CONTENTS

	Page
ABSTRACT	iii
DEDICATION	v
ACKNOWLEDGEMENTS	vi
TABLE OF CONTENTS	vii
LIST OF TABLES	xi
LIST OF FIGURES	xvi
LIST OF SYMBOLS	xxi
LIST OF ABBREVIATIONS	xxv
 CHAPTER	
I INTRODUCTION	1
II APPROACHES IN CHEMICAL REACTIVITY	4
1. Précis	4
2. Traditional Approaches of Evaluation	5
2.1. Qualitative Methods	6
2.1.1. Reactive Chemical Listing	6
2.1.2. Molecular Structure Considerations	7
2.1.3. Chemical Incompatibility	8
2.2. Quantitative Methods	9
2.2.1. Thermodynamic Calculations	9
2.2.2. Experimental Analysis	12
3. Conclusions	14
III SYSTEMATIC APPROACH FOR CHEMICAL REACTIVITY EVALUATION	15
1. Précis	15

CHAPTER	Page
2. Characterization of Chemical Reactivity	16
3. Description of the Approach	17
3.1. Level 1: Screening Evaluation	19
3.2. Level 2: Theoretical Evaluation	19
3.2.1. Molecular Group Contribution Methods	20
3.2.2. Computational Quantum Chemistry Methods	21
3.2.3. Correlations Based on Thermodynamic Energy Relationships	25
3.3. Level 3: Experimental Analysis	28
4. Reactive Systems Under Investigation	30
5. Conclusions	32
 IV RESEARCH METHODOLOGY AND PROCEDURES	 33
1. Précis	33
2. Theoretical Evaluation Methods	33
2.1. Molecular Group Contribution Methods	34
2.2. Computational Quantum Chemistry Methods	35
2.3. Thermodynamic-Energy Correlations	37
3. Experimental Thermal Analysis	38
3.1. Reactive System Screening Tool	39
3.1.1. Apparatus Description	40
3.1.2. Operating Modes and Procedures	42
3.1.3. Data Quality	43
3.2. Heat Flux Calorimeter	44
3.2.1. Apparatus Description	45
3.2.2. Operating Modes and Procedures	45
3.2.3. Data Quality	45
3.3. Automatic Pressure Tracking Adiabatic Calorimeter	45
3.3.1. Apparatus Description	46
3.3.2. Operating Modes and Procedures	49
3.3.3. Data Quality	53
4. Experimental Data Analysis	54
4.1. Kinetic Modeling	57
4.2. Thermal Inertia	61
 V THERMAL DECOMPOSITION OF DI-TERT-BUTYL PEROXIDE IN TOLUENE	 64
1. Précis	64
2. Application of the Systematic Approach	67
3. Pre-screening Evaluation	68

CHAPTER	Page
4. Computational Models	70
5. Experimental Analysis	82
5.1. Materials	83
5.2. Apparatus	84
5.3. Data Analysis	84
5.4. RSST™ Thermal Analysis	84
5.5. C80D Thermal Analysis	93
5.6. APTAC™ Thermal Analysis	95
5.7. DTBP in Benzene Analysis	104
5.8. Experimental Analysis Discussion	114
6. Conclusions	121
VI THERMAL COPOLYMERIZATION OF STYRENE-ACRYLONITRILE.....	123
1. Précis	123
2. Thermal Hazards Evaluation	126
3. Computational Models	127
4. Experimental Analysis	134
4.1. Materials	136
4.2. Apparatus	137
4.3. Data Analysis	137
4.4. RSST™ Thermal Analysis	137
4.5. APTAC™ Thermal Analysis	144
4.6. Experimental Analysis Discussion	153
5. Conclusions	159
VII THERMAL POLYMERIZATION OF 1,3-BUTADIENE	161
1. Précis	161
2. Thermal Hazards Evaluation	163
3. Computational Models	165
3.1. Dimerization of Butadiene	166
3.2. Polymerization of Butadiene	171
4. Experimental Analysis	175
4.1. Materials	175
4.2. Apparatus	176
4.3. Data Analysis	178
4.4. 1,3-Butadiene in the Absence of Oxygen	178
4.5. 1,3-Butadiene in the Presence of Oxygen	185
5. Results Discussion	193
6. Conclusions	197

CHAPTER	Page
VIII CONCLUSIONS AND RECOMMENDATIONS	199
1. Conclusions	199
2. Recommendations	201
REFERENCES	203
VITA	211

LIST OF TABLES

TABLE	Page
5.1	Gibbs free energy of DTBP decomposition components calculated using four levels of theory 73
5.2	Gibbs free energy of elementary reactions of DTBP decomposition calculated using four levels of theory 74
5.3	Gibbs free energy of DTBP decomposition pathways calculated using four levels of theory 74
5.4	Enthalpy of DTBP decomposition components calculated using four levels of theory 75
5.5	Enthalpy of elementary reaction of DTBP decomposition calculated using four levels of theory 76
5.6	Enthalpies of DTBP decomposition pathways calculated using four levels of theory 76
5.7	Activation energy of DTBP decomposition elementary reactions calculated using the Polanyi and Marcus equations and the B3LYP/6-31G(d) enthalpy of reaction 77
5.8	Activation energy of DTBP decomposition elementary reactions calculated using the Polanyi and Marcus equations and the CBS-4M enthalpy of reaction 78
5.9	Enthalpy of DTBP decomposition calculated with six levels of theory for the Pathway I 81
5.10	Summary of the RSST™ DTBP in toluene samples 85
5.11	Experimental results of DTBP decomposition in toluene with the RSST™ 87
5.12	Summary of the RSST™ thermodynamic and kinetic parameters of DTBP decomposition in toluene 90

TABLE	Page
5.13 Maximum self-heating and pressurization rates of DTBP decomposition in toluene using the RSST™	92
5.14 The C80D onset temperature and heat of reaction of DTBP decomposition in toluene	95
5.15 Summary of the APTAC™ DTBP in toluene samples	96
5.16 Experimental results of DTBP decomposition in toluene with the APTAC™	99
5.17 Summary of the APTAC™ thermodynamic and kinetic parameters of DTBP decomposition in toluene	101
5.18 Maximum self-heating and pressurization rates of DTBP decomposition in toluene using the APTAC™	103
5.19 Summary of the RSST™ DTBP in benzene samples	105
5.20 Experimental results of DTBP decomposition in benzene with the RSST™	107
5.21 Summary of the RSST™ thermodynamic and kinetic parameters of DTBP decomposition in benzene	108
5.22 Maximum self-heating and pressurization rates of DTBP decomposition in benzene using the RSST™	110
5.23 Summary of the APTAC™ DTBP in benzene samples	111
5.24 Experimental results of DTBP decomposition in benzene with the APTAC™	112
5.25 Summary of the APTAC™ thermodynamic and kinetic parameters of DTBP decomposition in benzene	114
5.26 Maximum self-heating and pressurization rates of DTBP decomposition in benzene using the APTAC™	116

TABLE	Page
5.27 Heat of reaction comparison of experimental measurements and theoretical calculations	119
5.28 Literature heat of reaction and Arrhenius parameters for DTBP decomposition in toluene	120
5.29 Summary of the APTAC TM corrected parameters of DTBP in toluene at $\phi \approx 1$	120
5.30 <i>P</i> -value statistical analysis of the APTAC TM DTBP in toluene and benzene	122
6.1 Heats of reaction for styrene and acrylonitrile homopolymerization and styrene-acrylonitrile cross-polymerization using the semi-empirical level of theory AM1	131
6.2 Heats of reaction of selected propagation steps for styrene-acrylonitrile cross-polymerization using the density functional level of theory B3LYP/6-31G(d)	135
6.3 Styrene-acrylonitrile monomers feed ratios	136
6.4 Summary of the experimental parameters of the SAN copolymerization samples with the RSST TM	138
6.5 Summary of the measured temperatures of the SAN copolymerization samples with the RSST TM	140
6.6 Summary of the experimental thermodynamic and kinetic parameters of the SAN copolymerization with the RSST TM	142
6.7 Maximum self-heating and pressurization rates of SAN copolymerization in the RSST TM	144
6.8 Summary of the experimental results of the SAN copolymerization samples with the APTAC TM	147
6.9 Summary of the experimental thermodynamic and kinetic parameters of the SAN copolymerization with the APTAC TM	149

TABLE	Page
6.10 Maximum self-heating and pressurization rates of SAN copolymerization in the APTAC™	152
6.11 Enthalpy of vaporization corrections for the APTAC™ heats of reaction of styrene-acrylonitrile copolymerization	157
6.12 Summary of the APTAC™ corrected parameters of SAN copolymerization at $\phi \approx 1$	158
7.1 Gibbs free energies and enthalpies (in Hartree/particle) of 1,3-butadiene dimerization components calculated using three levels of theory	169
7.2 Gibbs free energies and heats of reactions (in kcal/gmol) of 1,3-butadiene dimerization calculated using three levels of theory	170
7.3 Heats of reactions (in kcal/gmol) of 1,3-butadiene dimerization to form the four major products calculated using four levels of theory	171
7.4 Gibbs free energies and enthalpies (in Hartree/particle) of 1,3-butadiene reaction with singlet oxygen components calculated using three levels of theory	172
7.5 Gibbs free energies and heats of reactions (in kcal/gmol) of 1,3-butadiene with singlet oxygen reactions calculated using three levels of theory	173
7.6 Heats of reaction for butadiene polymerization propagation steps calculated using HF/6-31G(d) level of theory	174
7.7 Summary of the experimental results of butadiene tests in the absence of oxygen with the APTAC™	180
7.8 Summary of the experimental thermodynamic and kinetic parameters of butadiene reaction in the absence of oxygen with the APTAC™	183
7.9 Maximum self-heating and pressurization rates of butadiene reaction in the absence of oxygen with the APTAC™	185
7.10 Summary of the experimental results of butadiene tests in the presence of oxygen with the APTAC™	188

TABLE	Page
7.11 Summary of the experimental thermodynamic and kinetic parameters of butadiene reaction in the presence of oxygen with the APTAC TM	190
7.12 Maximum self-heating and pressurization rates of the butadiene reaction in the presence of oxygen with the APTAC TM	193
7.13 Literature values of 1,3-butadiene dimerization	196
7.14 Summary of the corrected experimental parameters of butadiene reactions with the APTAC TM at $\phi \approx 1$	197

LIST OF FIGURES

FIGURE	Page
3.1	Systematic approach for chemical reactivity evaluation 18
3.2	Validation of Polanyi equation for 45 homolytic cleavage reactions 27
4.1	Typical temperature and pressure profiles of the RSST™ test 40
4.2	Overall schematic of the RSST™ test cell and containment vessel 41
4.3	Schematic of APTAC™ reaction and pressure vessels 47
4.4	Typical heat-wait-search operation mode of the APTAC™ 50
4.5	Temperature-pressure profiles of the APTAC™ heat-wait-search mode 50
4.6	Temperature and pressure profiles during APTAC™ relative calibration 55
4.7	Pressure data during relative calibration of APTAC™ thermocouples 55
4.8	Water vapor pressure of the APTAC™ and steam tables 56
4.9	Self-heating rate of 30 wt% DTBP in toluene over 9 months 56
5.1	<i>Di-tert-butyl</i> peroxide molecular structure and physical properties 66
5.2	Proposed reaction pathways of DTBP decomposition in toluene 71
5.3	DTBP decomposition in toluene temperature profiles using the RSST™ 86
5.4	DTBP decomposition in toluene pressure profiles using the RSST™ 86
5.5	First-order kinetics of DTBP decomposition in toluene with the RSST™ 89

FIGURE	Page
5.6 Self-heating rate of DTBP decomposition in toluene using the RSST™	91
5.7 Pressurization rate of DTBP decomposition in toluene using the RSST™	92
5.8 Heat flow profiles of DTBP decomposition in toluene using the C80D	94
5.9 C80D pressurization rate profiles of DTBP decomposition in toluene	94
5.10 DTBP decomposition in toluene temperature profiles using the APTAC™	97
5.11 DTBP decomposition in toluene pressure profiles using the APTAC™	97
5.12 First-order kinetics of DTBP decomposition in toluene with the APTAC™	100
5.13 Self-heating rate of DTBP decomposition in toluene using the APTAC™	102
5.14 Pressurization rate of DTBP decomposition in toluene using the APTAC™	102
5.15 DTBP decomposition in benzene temperature profiles using the RSST™	106
5.16 DTBP decomposition in benzene pressure profiles using the RSST™	106
5.17 First-order kinetics of DTBP decomposition in benzene with the RSST™	108
5.18 Self-heating rate of DTBP decomposition in benzene using the RSST™	109
5.19 Pressurization rate of DTBP decomposition in benzene using the RSST™	109

FIGURE	Page
5.20 DTBP decomposition in benzene temperature profiles using the APTAC™	111
5.21 DTBP decomposition in benzene pressure profiles using the APTAC™	112
5.22 First-order kinetics of DTBP decomposition in benzene with the APTAC™	113
5.23 Self-heating rate of DTBP decomposition in benzene using the APTAC™	115
5.24 Pressurization rate of DTBP decomposition in benzene using the APTAC™	115
5.25 Measured overall heats of reaction of DTBP decomposition in toluene	117
6.1 Typical free radical copolymerization reaction of two monomers, A and B	125
6.2 Possible free radical homopolymerization and copolymerization pathways for the styrene and acrylonitrile monomers	129
6.3 Styrene and acrylonitrile reactive ends as identified in this research	129
6.4 Examples of styrene and acrylonitrile monomers copolymerization reactions	130
6.5 SAN copolymerization temperature profiles with the RSST™	139
6.6 SAN copolymerization pressure profiles with the RSST™	139
6.7 First-order kinetics of SAN copolymerization with the RSST™	141
6.8 Self-heating rates of SAN copolymerization with the RSST™	143
6.9 Pressurization rates of SAN copolymerization with the RSST™	143
6.10 SAN copolymerization temperature profiles with the APTAC™	146

FIGURE	Page
6.11 SAN copolymerization pressure profiles with the APTAC™	146
6.12 Maximum temperature and pressure for the SAN reactions	148
6.13 First-order kinetics of SAN copolymerization with the APTAC™	149
6.14 Self-heating rates of SAN copolymerization with the APTAC™	151
6.15 Pressurization rates of SAN copolymerization with the APTAC™	151
6.16 Comparison of measured heats of reaction of SAN copolymerization	154
7.1 1,3-butadiene molecular structure and physical properties	162
7.2 Proposed reaction pathways of 1,3-butadiene dimerization	168
7.3 1,3-butadiene reaction with singlet oxygen to form 3,6-dihydro-1,2-dioxin	172
7.4 Modes of addition reactions of 1,3-butadiene	174
7.5 Schematic of special APTAC™ setup to transfer butadiene to the test cell	177
7.6 Butadiene temperature profiles in the absence of oxygen	179
7.7 Butadiene pressure profiles in the absence of oxygen	179
7.8 Second-order kinetics of 1,3-butadiene dimerization	182
7.9 Self-heating rate of 1,3-butadiene dimerization	184
7.10 Pressurization rate of 1,3-butadiene dimerization	184
7.11 Butadiene temperature profiles in the presence of oxygen	187
7.12 Butadiene pressure profiles in the presence of oxygen	187
7.13 First-order kinetics of 1,3-butadiene polymerization	189

FIGURE	Page
7.14 Self-heating rate of 1,3-butadiene polymerization	191
7.15 Pressurization rate of 1,3-butadiene polymerization	191
7.16 Two-stage reaction of 1,3-butadiene in the presence of oxygen	192

LIST OF SYMBOLS

A	Frequency parameter, s^{-1} (first-order); $m^3 \text{ mol}^{-1} s^{-1}$ (second-order)
C	Concentration of the reactant, mol L^{-1}
C_c	Heat capacity of cell, $\text{cal g}^{-1} \text{ }^\circ\text{C}^{-1}$
C_o	initial concentration of the reactant, mol L^{-1}
C_s	Heat capacity of sample, $\text{cal g}^{-1} \text{ }^\circ\text{C}^{-1}$
dT/dt	Sample heating rate, $^\circ\text{C min}^{-1}$
$(dT/dt)_{\text{max}}$	Maximum sample self-heating rate, $^\circ\text{C min}^{-1}$
dP/dt	Sample pressurization rate, psi min^{-1}
$(dP/dt)_{\text{max}}$	Maximum sample pressurization rate, psi min^{-1}
E_A	Activation energy, kcal mol^{-1}
E_A^o	Intrinsic barrier of reaction, kcal mol^{-1}
H	Chemical substance enthalpy, kcal mol^{-1}
k	Reaction rate constant, s^{-1} (first-order); $m^3 \text{ mol}^{-1} s^{-1}$ (second-order)
k_{ij}	Reaction rate constant for polymerization reaction of monomers i and j ; i and j are A, B, S
k^*	Pseudo zero-order rate constant, s^{-1} (first-order); $m^3 \text{ mol}^{-1} s^{-1}$ (second-order)

m	Reactant mass, g
m_c	Mass of test cell, g
m_s	Mass of sample, g
n	Reaction order
N	Number of moles of chemical substance
N_o	Initial number of moles of chemical substance
P	Pressure, psia
r	Reaction rate, s^{-1} (first-order); $m^3 mol^{-1} s^{-1}$ (second-order)
r_i	Monomer i reactivity ratio, i is A, B, or S
R	Gas constant, $1.987 cal/mol K^{-1}$
S	Chemical substance entropy, $kcal mol^{-1}$
t	Time, min
t_{MR}	Time at the maximum rate, min
T	Temperature, $^{\circ}C$
T_{bp}	Boiling point of the reaction mixture, $^{\circ}C$
T_{max}	Maximum temperature reached by reaction, $^{\circ}C$
T_{MR}	Temperature of the maximum self-heating rate, $^{\circ}C$
T_{NR}	Reaction temperature of no return, $^{\circ}C$

T_o	Reaction onset temperature, °C
$T_{o,adj}$	Adjusted to adiabatic conditions reaction onset temperature, °C
$T_{process}$	Process normal operating temperature, °C
TMR_{ad}	Time to maximum rate at adiabatic conditions, min
$TMR_{ad,meas}$	Measured time to maximum rate at adiabatic conditions, min
$TMR_{ad,adj}$	Adjusted time to maximum rate at adiabatic conditions, min
x	Fraction of reactant in the sample solution
V	Reacting volume, L

Greek letters

α	Confidence interval coefficient
ΔG_f	Chemical substance Gibbs free energy of formation, kcal mol ⁻¹
ΔG_r	Gibbs free energies of reaction, kcal mol ⁻¹
ΔG_r^{idg}	Ideal gas phase Gibbs free energy of reaction, kcal mol ⁻¹
ΔG_r^{mix}	Mixing and solvent Gibbs free energy effects of reaction, kcal mol ⁻¹
ΔG_r^{press}	Pressure Gibbs free energy effects of reaction, kcal mol ⁻¹
ΔH_f	Chemical substance enthalpy of formation, kcal mol ⁻¹
ΔH_r	Enthalpy of decomposition reaction, kcal mol ⁻¹

ΔH_r^{idg}	Ideal gas phase enthalpy of reaction, kcal mol ⁻¹
ΔH_r^{mix}	Mixing and solvent enthalpic effects of reaction, kcal mol ⁻¹
$\Delta H_r^{\text{press}}$	Pressure enthalpic effects of reaction, kcal mol ⁻¹
ΔH_{vap}	Enthalpy of vaporization or sublimation, kcal mol ⁻¹
ΔS_r	Entropy of reaction, kcal mol ⁻¹
ΔS_r^{idg}	Ideal gas phase entropy of reaction, kcal mol ⁻¹
ΔS_r^{mix}	Mixing and solvent entropic effects, kcal mol ⁻¹
$\Delta S_r^{\text{press}}$	Pressure entropic effects, kcal mol ⁻¹
ΔT_{ad}	Adiabatic temperature rise, °C
$\Delta T_{\text{ad,adj}}$	Adjusted adiabatic temperature rise, °C
$\Delta T_{\text{ad,meas}}$	Measured adiabatic temperature rise, °C
ν_i	Stoichiometric coefficient of species i
ϕ	Thermal inertia factor
γ_P	Transfer coefficient

LIST OF ABBREVIATIONS

A	Acrylonitrile
A/D	Analog to Digital
AM1	Austin Model 1
APTAC TM	Automated Pressure Tracking Adiabatic Calorimeter
ARC TM	Accelerated Rate Calorimeter
ARSST TM	Advanced Reactive System Screening Tool
ASTM	American Society for Testing and Materials
BD	1,3-Butadiene
<i>c</i> -BD	<i>cis</i> -1,3-Butadiene
<i>t</i> -BD	<i>trans</i> -1,3-Butadiene
BHT	Butylated Hydroxy Toluene
CBS	Complete Basis Set
CHETAH TM	Chemical Thermodynamic and Energy Release Evaluation Program
COD	<i>cis, cis</i> -Cycloocta-1,5-Diene
CSB	Chemical Safety Board
DFT	Density Functional Theory
DHD	3,6-Dihydro-1,2-Dioxin
DSC	Differential Scanning Calorimeter
DTBP	<i>Di-tert</i> -Butyl Peroxide

<i>c</i> -DVCB	<i>cis</i> -1,2-Divinylcyclobutane
<i>t</i> -DVCB	<i>trans</i> -1,2-Divinylcyclobutane
HF	Hartree Fock <i>ab initio</i> Method
NFPA	National Fire Protection Association
NRIFD	National Research Institute for Fire and Disaster
OB	Oxygen Balance
OSHA	Occupational Safety and Health Administration
PSM	Process Safety Management
RSST™	Reactive System Screening Tool
S	Styrene
SAN	Styrene-Acrylonitrile
SO	Singlet Oxygen
TBC	<i>t</i> -Butylcatechol
TST	Transition State Theory
VCH	4-Vinylcyclohexane
VSP™	Vent Sizing Package

CHAPTER I

INTRODUCTION

Under certain conditions, reactive chemicals can release very large and potentially dangerous amounts of energy, which may result in huge pressure increases. This dangerous combination can lead to reactions that differ from the primary process reactions, mainly by the rate at which they progress. Reactive chemicals are involved in many industrial incidents every year harming people, property, and the environment.

Some reactions require very little activation energy to be initiated. If the reaction is exothermic, the energy initially produced may accelerate a continued reaction and release energy too rapidly to be controlled. Temperature, shock, static, and light may trigger an uncontrollable reaction. In some combinations, a chemical contaminant may act as a catalyst to reduce the activation energy needed to initiate or sustain a reaction.

Much of the traditional approach to process safety is based on controlling the hazards associated with chemical processes and plants. This is done through the improving procedures, installing additional safety interlocks and systems, and improving emergency response. Such control measures aim to reduce the risk. However until the hazard is identified, it is not possible to assess the risk.

Identifying reactive chemical hazards is still the ultimate goal. The primary difficulty in this identification stems from the variety of conditions under which chemicals can

undergo an uncontrollable reaction. Some chemicals are unstable and can vigorously polymerize, decompose, condense, or become self-reactive. Other chemicals can react violently when exposed to common environment chemicals or conditions. A major difficulty, which arises when one considers the problem as a whole, is that reactive chemical hazards are seldom a unique characteristic of the chemical but highly depend on the process conditions and mode of operation. Therefore, the identification of a reactive hazard requires a detailed evaluation of both the properties of the substances used and the operating conditions. The dilemma is that many so-called “benign” reactions can become highly reactive or undergo runaway reactions under slightly different conditions or with the introduction of minute impurities.

The aim of this research is to facilitate an understanding of the philosophies and stages that should be followed to evaluate chemical reactivity through an effective and practical systematic approach. The primary goal of applying this approach is to provide the required information for safer process design and operation based on a thorough understanding of process chemistry, thermodynamic, and kinetic behavior.

Objectives of this research also include proving better understanding of the existing experimental and computational methods, potentials and limitations, and introduction of new screening methods that allow the cost of chemical reactivity procedures to be reduced without compromising process safety principles.

In this research the background of reactive chemicals evaluation methods are reviewed in Chapter II. Based on the extent of the problem, a systematic approach for reactive chemicals analysis is developed in Chapter III. This approach is a tiered

framework in which one starts with simple screening tools based on thermophysical properties and thermodynamic analysis, use of quantum mechanics calculation and thermodynamic-energy correlations, and finally employs additional screening and experimental measurements. The applied research methodology and procedures are presented in Chapter IV.

Three highly reactive systems were investigated using this systematic approach for evaluating chemical reactivity to test the validity of the approach. The decomposition of *di-tert*-butyl peroxide in toluene is the first system evaluated and is presented in Chapter V. In Chapter VI, the copolymerization of styrene acrylonitrile monomers is presented. This system represents an important class of chemical reactions that are widely applied in the manufacturing of polymeric materials. The third reactive system, presented in Chapter VII, is the polymerization of 1,3-butadiene in the presence and absence of oxygen. This system represents highly complicated reaction mechanisms for a highly toxic substance.

The Evaluation of these three systems will show the uncontestable need for a systematic approach for chemical reactivity assessment especially in providing the necessary stoichiometric, thermodynamic, and kinetic parameters.

CHAPTER II

APPROACHES IN CHEMICAL REACTIVITY

1. Précis

Although it is generally accepted that reactive chemical incidents pose a significant safety problem, there is very little agreement on how to identify and implement an evaluation approach for reactive hazards. Many procedures have been suggested in the recent literature to identify, categorize, and evaluate reactive chemicals. However, because the needs for an assessment procedure vary from one chemical process to another, much effort has been devoted to provide specific-case assessment approaches. This resulted in many methodologies that cannot be generalized to other hazardous reactivity scenarios.

The U.S. Chemical safety Board (CSB) in its recent study [1] identified 167 reactive chemical incidents since 1980 that caused 108 deaths to workers and the public. More than 25 per cent of these incidents involved process chemistry that was not well understood, although general reactivity hazards did exist.

In this chapter, some of the relevant work during the last few years is addressed. The aim is to present the most applied procedures in chemical reactivity evaluations. The detailed description of these procedures is available in the cited references.

2. Traditional Approaches of Evaluation

Effective identification, understanding, and evaluation of reactive chemical hazards in process chemistry are critical components for optimal and safe process operation. These components are often among the first activities in the design and development of chemical processes. Ineffective reactivity evaluation is cited as a major cause of chemical industry incidents.

This fact and the losses in lives, properties, and environment caused by reactivity-related incidents have motivated researchers and various process safety organizations to suggest a variety of chemical reactivity evaluation approaches [2–13]. These recent approaches constitute an attempt to raise the awareness of reactivity hazards and provide information about existing qualitative and quantitative techniques. However, a comprehensive approach to address all circumstances has not been realized [1].

Some of these approaches provided valuable information; however, no coherence among the suggested techniques exists. The need for a systematic method to define the links among the various evaluation levels and the best approach was always undeniable.

Searching the literature for chemical reactivity evaluation techniques provides a large number of methods that can be classified as qualitative and quantitative. Qualitative methods are considered the simplest level of evaluation whereas experimental thermal analysis represents the most advanced level quantitative evaluation. In the following sections, the most applied methods are reviewed.

2.1. Qualitative Methods

Several qualitative chemical reactivity evaluation methods are widely applied among the process safety community including chemical listing, databases, molecular structure considerations, incompatibility, and experience-based review.

Experience-based review is usually based on experience with conducting chemical reactivity hazards evaluation procedures or on the ability to learn lessons from previous reactivity-related incidents.

These qualitative methods can be useful in identifying reactive scenarios; however none of them are designed specifically to address reactive hazards. Many of the existing chemical reactivity evaluation approaches [2,5,7] do not adequately address how to manage the unique aspects of reactive hazards when performing these methods.

2.1.1. Reactive Chemical Listing

Reactive chemical lists were originally developed based on previous experience or related incidents due to the chemical intrinsic reactivity. The U.S. Occupational Safety and Health Administration (OSHA) promulgated the Process Safety Management (PSM) standards covering highly hazardous chemicals that included toxic, flammable, highly reactive, and explosive substances. This list was based on several other lists of potentially hazardous chemicals [1]. The National Fire Protection Association (NFPA) had also developed a list based on the flammability and reactivity behavior of the chemicals. These limited lists, and the list approach in general, has failed dramatically

to provide the help needed to minimize reactive chemical hazards or to regulate chemical reactivity.

The absence or presence of a chemical in these lists does not provide the appropriate information to predict the chemical behavior under various process scenarios.

2.1.2. Molecular Structure Considerations

The molecular structure of a chemical substance has traditionally been used as a screening tool to identify potential reactivity hazards. Some typical structural characteristics in high-energy substances such as the relative degree of unsaturation, high proportion or high local concentration of nitrogen in the molecular structure, and nitrogen-to-hydrogen bonds have in the past been used to identify reactive chemicals [14].

The existence of certain functional groups within the molecular structure of a substance was considered a clear indication of structure thermal instability. Several functional groups such as peroxide groups, nitro groups, azo groups, and double and triple bonds were considered reactive. Although this conclusion may be true for many compounds, it is not guaranteed. For example, the presence of a nitro group attached to a long aliphatic chain does not show a thermal hazard potential, even though the nitro group is considered to be an unstable structure. On the other hand, the initial absence of unstable groups is no guarantee of long-term stability of the compound. For example, some aldehydes and ethers are easily converted to peroxides by reaction with oxygen from air [2].

Greuer [8,15] studied the correlation between decomposition energies and functional groups of organic and inorganic compounds. A significant effect of molecular structure on the decomposition energy of molecules was identified; however, when these correlations were extended to include other kinetic properties such as onset temperature of the decomposition reaction, this correlation failed.

2.1.3. *Chemical Incompatibility*

The hazards resulting from inadvertent mixing of chemicals such as explosion, fire, excessive increase in pressure or temperature, or the release of toxic vapors is referred to as chemical incompatibility, which is a well-recognized problem. Much effort is required for the development of chemicals incompatibility charts and tables. A significant amount of compatibility information is accessible through many sources [16–18].

Recently, Winder and Zarie [19] combined major chemical incompatibility approaches to a more comprehensive one that enabled better decision-making of chemical usage and storage. In a different study [20], chemical incompatibility was suggested as a screening tool for chemical reactivity evaluation.

Incompatibility is a matter of degree, however, and many parameters such as temperature, amount of material, maximum process pressure, and time of mixing may affect the degree of hazard. Hence, when using the available incompatibility charts and tables, system conditions must be specified. In cases where chemicals of interest are not tabulated, a simple mixing test may help provide an indication of incompatibility, which

may require additional testing. More advanced compatibility analysis evaluation methods are available [21–23].

2.2. *Quantitative Methods*

To specify safe design and operating requirements, identified hazards must be evaluated to understand the potential consequences of uncontrolled chemical reactions. Quantitative analysis of reactivity hazards of a specific chemical process is a complicated process. This information is obtainable through theoretical thermodynamic calculations and experimental data modeling. Experimental methods have advanced significantly to meet the needs of chemical reactivity evaluation, which led to more expensive experimental procedures. However, the application of thermodynamic calculations for chemical reactivity evaluation is still under development. In the following two sections, these techniques are reviewed.

2.2.1. *Thermodynamic Calculations*

The molecular structure of each compound in the system may be used for calculating the potential for exothermic behavior. Various methods have been used to calculate heat of reaction, such as heat of formation method [2]. Although high accuracy may be difficult to achieve using this method, preliminary evaluations and possible indications of reactivity hazards are useful for screening purposes.

The heat of reaction has been used to estimate the possible maximum adiabatic temperature rise, ΔT_{ad} , and maximum system temperature, T_{max} , as follows

$$\Delta T_{\text{ad}} = \frac{\Delta H_r}{m C_s} \quad (2.1)$$

$$T_{\text{max}} = \Delta T_{\text{ad}} + T_{\text{process}} \quad (2.2)$$

where ΔH_r is heat of reaction, m is the reacting substance mass, C_s is heat capacity of the reaction mixture, and T_{process} is the process normal operating temperature. If this adiabatic temperature increase is not major, and if the system maximum temperature is not above its boiling point, the potential hazard of this system may be minimal.

The ΔT_{ad} value can be used to investigate whether unwanted exothermic reaction initiation temperature is within or overlapping the process operating temperature range. This value may determine whether a more detailed investigation is required. There are several values of ΔT_{ad} used as a rule of thumb; the most common ones are 50 K [24,25] and 100 K [26,27] for normal activation energies. In general, the disadvantage of this technique is that the accuracy of the calculated temperatures depends on the quality of the calculated heat of reaction.

To enhance the quality of calculated thermodynamic parameters of reactions, the Benson's molecular group contribution method [28–30] has been used in many approaches. Verevkin [31] predicted thermochemistry of nitro compounds using improved group contribution values. This method was incorporated into the ASTM CHETAH™ program [32], which can provide significant reactivity hazard calculations. The CHETAH™ program has been reviewed by various researchers [2,33–35]. This

method, however, is limited to the available information of contributing groups' thermodynamic data. Some other limitations are discussed in Chapter III.

Other methods, such as the average bond energy summation [36], have been used to predict thermodynamic parameters.

The molecular structure of different reactive system components is used to conduct oxygen balance, OB, calculations. OB is the amount of oxygen, expressed as weight percent, liberated as a result of complete conversion of the material to relatively simple oxidized molecules. This balance considers the number of oxygen and reducing atoms in the substance itself. If all reducing atoms can be oxidized completely without excess oxygen, the oxygen balance is zero, and the energy generation of the substance is maximum and is independent of the external oxygen concentration. For molecules containing the elements carbon, hydrogen, and oxygen, oxygen balance is expressed by

$$OB = \frac{-1600 \left[2x + \left(\frac{y}{2} \right) - z \right]}{\text{Molecular Weight}} \quad (2.3)$$

where x is the number of carbon atoms, y is the number of hydrogen atoms, and z is the number of oxygen atoms.

A criterion for the value of this balance has been proposed [2]. However, in some cases the results of this simple tool may be misleading in that it may not bear any direct relationship to hazard potential. Shanley and Melhem [37] studied some familiar compounds of known hazard potential, and found that oxygen balance values do not correlate well with the known hazard potential of these compounds.

To enhance the ability to predict reaction thermodynamic parameters to be used in reactivity evaluation, some researchers investigated the applicability of computational quantum chemistry methods [38,39]. These methods were primarily used to predict the Gibbs free energy and enthalpy of a reaction. A more advanced application was to predict missing data points in the group contribution method database [40].

2.2.2. *Experimental Analysis*

The applications of reaction calorimetry (thermal analysis) techniques have expanded dramatically in the last 30 years to include various applications of science and engineering including process safety and reactive hazard evaluation [41–44]. Calorimetric studies have been able to answer some significant needs related to reactivity hazards evaluation, such as the overall thermodynamic and kinetic parameters for reactive systems. Thermal analysis techniques have been a primary source of experimental data in the design of emergency relief systems [45,46].

Calorimeters can be operated under various principles. However, four major operating principles have been used in chemical reactivity evaluation procedure including isothermal, isoperibolic, adiabatic, and temperature-programmed calorimeters. Singh [47] discusses the recent advances of reaction calorimetry. A comparison of these calorimetric operation principles is discussed extensively in the literature [2,7,48].

Due to the specific conditions of heat transfer, the heat of an exothermic process is almost totally retained, hence, near-adiabatic conditions are maintained during runaway reactions. Adiabatic calorimeters are considered the most representative of the behavior

of real processes. Application of adiabatic thermal analysis techniques to evaluate reactive chemical hazards has motivated researchers to develop specifically designed adiabatic calorimeters for chemical reactivity hazards assessment. Adiabatic Dewar Calorimeter, Accelerated Rate Calorimeter (ARCTM), Automatic Pressure Tracking Adiabatic Calorimeter (APTACTM), Advanced Reactive System Screening Tool (ARSSTTM), and Vent Sizing Package (VSPTM) are among the several commercially available adiabatic calorimeters. Sempere et al. [49] investigated the suitability of various adiabatic apparatus to evaluate exothermic reaction hazards such as decomposition reactions. Heldt and Anderson [50] discussed the application of modified adiabatic calorimeters to perform chemical reactivity analysis.

Temperature-programmed differential-scanning calorimeter (DSC) and heat-flux calorimeters were used to screen reactive systems. The main applications were to detect reaction onset temperature, measure heat of reaction, self-accelerating decomposition temperature, and time to maximum rate [25,51,52].

The experimental results of these calorimeters vary based on the operating mode, sample size, precision, and sensitivity. Comparisons of the various calorimetric methods are available in the literature [2,53–55].

Experimental data analysis and modeling is another significant approach that may affect the evaluation of chemical reactivity. Several researchers addressed the effect of thermal inertia as a source of heat losses [56], scale-up [24,57,58], and calorimeter sensitivity [59] on the modeling of reactive systems [60–62].

3. Conclusions

Although there have been many approaches and methods in the literature to evaluate chemical reactivity hazards, nevertheless, these efforts are focused on addressing one system at a time. There is a lack of consistency among the various techniques that made the results insufficient to provide the chemical understanding required for safer process design and operation.

The huge number of chemicals and variety of operating conditions makes the dependence on experimental analysis alone quite expensive. The need to introduce a theoretical approach is clear in the literature, but with insufficient guidelines for implementation. In the following chapter these literature review findings are used to establish a systematic approach for evaluating chemical reactivity.

CHAPTER III

SYSTEMATIC APPROACH FOR CHEMICAL REACTIVITY

EVALUATION*

1. Précis

As discussed earlier, thermal stability of reactants, intermediates, and products is of significant interest to the chemical industry. The engineering design of equipment to prevent, control, or withstand runaway reactions is of great concern from a safety viewpoint, and many procedures have been suggested for categorizing reactive chemicals. Because the need for an assessment procedure varies from one industry to another, generally, researchers have addressed this issue from a specific case or a specific chemical viewpoint. However, a generalized approach still is an ultimate goal. For an approach to be effective, it should be based on the understanding of the stoichiometry, thermodynamics, and kinetics of the reactive system and should require minimum time and inexpensive procedures to implement.

The aim of this research is to develop a systematic approach for evaluating reactive systems. This approach is a combination of theoretical and experimental levels of evaluation to identify reaction stoichiometries and estimate thermodynamic and kinetic

* This chapter contains material reprinted from the Transactions of the Institution of Chemical Engineers: Part B, 80 (3), A. A. Aldeeb, W. J. Rogers, and M. S. Mannan, Theoretical and experimental methods for the evaluation of reactive chemical hazards, 141-149, Copyright (2002).

parameters of potentially hazardous reactions. In this chapter, the required parameters for evaluating chemical reactivity are presented and the various levels of evaluation for these parameters are discussed.

2. Characterization of Chemical Reactivity

An evaluation of chemical reactivity depends on essential information, which includes process operating conditions, process chemistry, conditions under which chemical reactive hazards can appear, and parameters for quantifying reactivity hazards.

Defining these conditions and parameters helps simulate the chemical process for optimum, safe, and economical operating conditions. Evaluating this information is not easy. Laboratory testing has been the traditional approach for evaluating chemical reactivity. This approach is practical for simple systems, but may not be applicable for more complex systems or more energetic or toxic materials. Because of the large number of chemical compounds and reaction scenarios in chemical production and storage facilities, experimental analysis alone can be very expensive and time consuming. Moreover, in case of a complex reactive system, experimental procedures provide an overall evaluation of system thermodynamic and kinetic data but do not explain reaction stoichiometry. In fact, system analysis is often required beyond laboratory measurements.

To characterize the reactivity hazards of a system, a number of parameters should first be identified. Those parameters describe the severity of the exothermic behavior of a reactive system. Such parameters may include temperature at which significant

exothermic behavior is initiated, T_o , maximum adiabatic temperature rise, ΔT_{ad} , heat of reaction under adiabatic conditions, ΔH_r , boiling point of the reaction mixture, T_{bp} , maximum temperature attained by runaway of the reaction, T_{max} , required time to reach maximum reaction rate under adiabatic conditions, TMR_{ad} , temperature of no return, T_{NR} , maximum reaction self-heating rate, $(dT/dt)_{max}$, and maximum pressurization rate, $(dP/dt)_{max}$.

Calculation of these parameters depends on the availability of thermodynamic and kinetic data. The accuracy of this reactivity evaluation depends directly on the quality of the measured parameters. It should be noted that for simple systems (single reaction systems) this evaluation is acceptable when using approximate thermal analysis techniques. But for complex (multi reaction) systems, this evaluation is based on the overall thermodynamic and kinetic measurement, which provides poor or no description of the reaction mechanism (stoichiometry). Understanding reaction mechanisms is of great importance when addressing reactivity hazard evaluation. Understanding the reaction chemistry helps focus the attention on the most reactive components (reactants, intermediates or products), and it helps explain the pressure behavior through knowledge of the main system components that may contribute to the pressure increase.

3. Description of the Approach

This approach consists of three levels, as shown in Figure 3.1. In each level, the reactive system is evaluated to understand the reaction chemistry, identify the possibility of exothermal activity, and quantify the reactive chemical hazards. Each of these levels

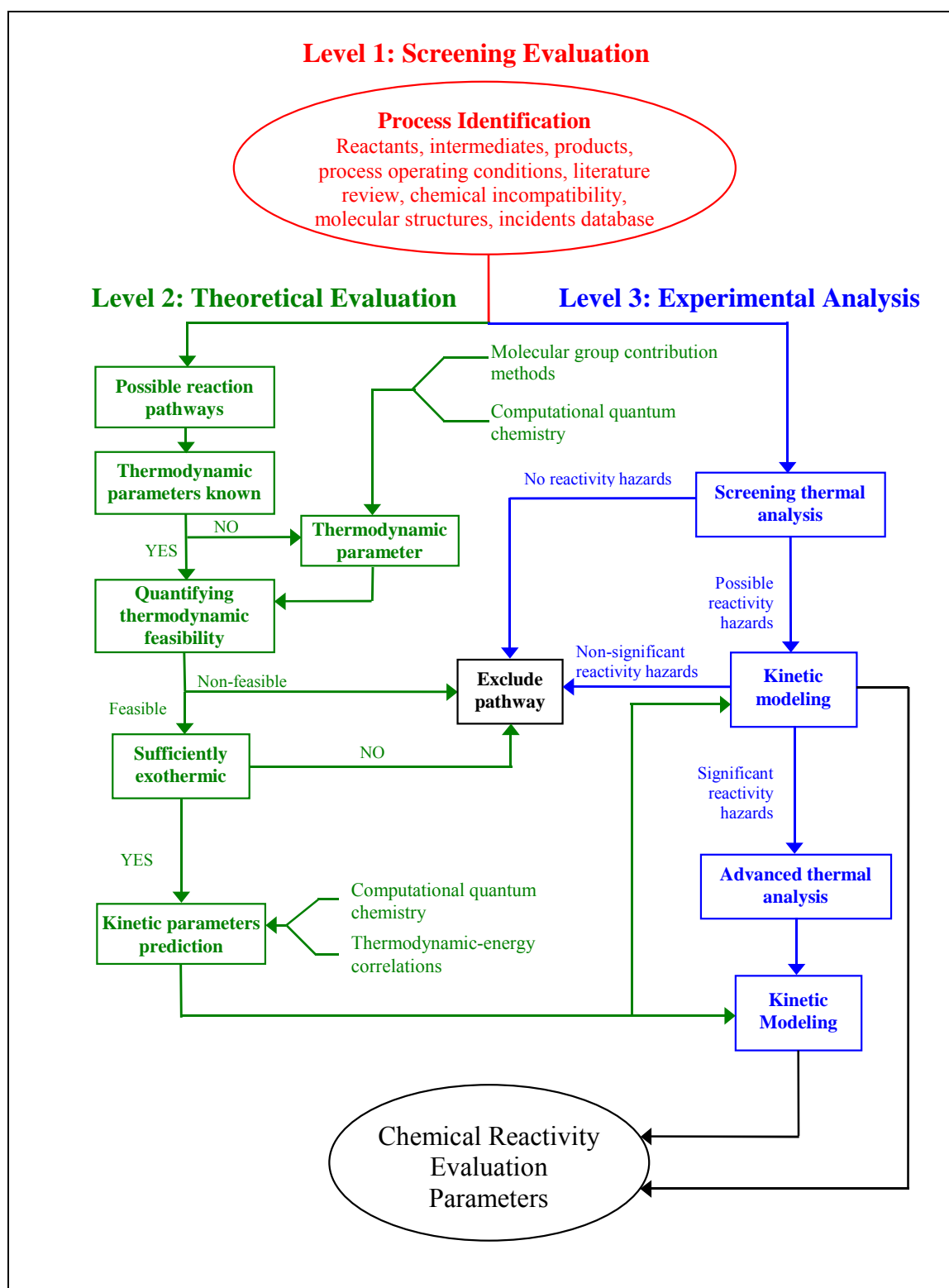


Figure 3.1. Systematic approach for chemical reactivity evaluation

is discussed in the following sections. This systematic approach allows one to focus the advanced experimental analysis on the most hazardous reactions. In each of the three evaluation levels, predicting or calculating stoichiometric, thermodynamic, and kinetic parameters is the main objective, and many reaction stoichiometries can thereby be excluded from the need for expensive experimental analysis.

3.1. Level 1: Screening Evaluation

In the data screening evaluation level, reactants, products, and operating conditions are identified. Literature and databases are searched for information about substances in the chemical system. Relevant data include physical and chemical properties, thermodynamics, kinetics, incidents, and case studies.

Many of the popular reactivity screening tools are applied in this level of evaluation. Oxygen balance, molecular structure considerations, and chemical compatibility are among these tools.

In this evaluation level, some chemicals or identified reactions that clearly present no hazardous potential, such as endothermic reactions, may be excluded from further testing. Other cases require more detailed analysis for potential hazard assessment.

3.2. Level 2: Theoretical Evaluation

In this level of evaluation, theoretical methods are used to predict reaction pathways, and to calculate thermodynamic and kinetic parameters for these pathways.

The first step in this level is to postulate potential reaction pathway scenarios. This is done based on available information in the literature or based on similar behavior of the other known systems. To predict thermodynamics and kinetics of the selected reaction pathways, three levels of theoretical techniques are employed: (1) molecular group contribution methods, (2) computational quantum chemistry methods, and (3) correlations based on thermodynamic energy relationships.

3.2.1. Molecular Group Contribution Methods

Chemists and physicists have known for over 60 years that most molecular properties of larger molecules can be considered, roughly, as being made up of additive contributions of the individual atoms or bonds in the molecule. This idea was expanded to show that adding up the contributions of all of the bonds in the molecule, and then correcting for the influence of various side chains could estimate a wide variety of thermodynamic properties of molecules.

These methods are based on correlations obtained from a large number of experimental values of thermodynamic properties for common molecules. These methods have the advantage of simplicity, acceptable level of accuracy for some organic molecules, and low cost. However, implementation of these methods is very limited to the available experimental database [40]. Moreover, these methods are unable to differentiate between the various molecular configurations such as isomers, leading to large deviations in the calculated enthalpies [38].

In this approach, molecular group contribution methods are preliminary screening tools to detect sufficiently unstable molecules by predicting thermodynamic parameters. The indication of potential exothermic reaction requires evaluation through more advanced theoretical and experimental techniques. Commercially available software that applies molecular group contribution methods is discussed in Chapter IV.

3.2.2. *Computational Quantum Chemistry Methods*

In the last several years, the computational quantum chemistry methods have been developed in a way that allows estimations of thermodynamic properties for gas-phase species. Whereas these methods are still too complex for the ordinary user, it is believed that these methods will become more widely used in the field of thermochemistry as the methods becomes less sophisticated, accurate, and the computer tools become more powerful.

Computational quantum chemistry methods are based on molecular quantum theory when the motion and distribution of electrons is described in terms of electron probability distributions or molecular orbitals [38]. It is basically a correct mathematical description of the behavior of electrons, and thus of chemistry. The Schrödinger equation was the mathematical description for these behaviors.

Numerical techniques have been developed to perform the quantum chemistry calculations. Among the most known techniques are *ab initio*, Density Functional Theory (DFT), and semi-empirical methods.

The *ab initio* methods are computations that are derived directly from theoretical principles without including experimental data. These computations are approximate quantum calculations due to the mathematical approximations used.

Hartree-Fock (HF) [63] is the most common *ab initio* method. Its primary approximation considers average Columbic electron-electron repulsion instead of the explicit repulsion interaction. The complete basis set (CBS) [64] is another *ab initio* method, however this method is more advanced than the HF method due to the application of different numbers of basis functions and levels of theory as an extrapolation of *ab initio* methods to provide a more acceptable approximations.

Gaussian theory is another extrapolating form of *ab initio* results, which estimates exact energies. The G2 [65] method is one of the most common levels of this theory with high computational cost.

DFT, a recent theory compared to *ab initio* methods, is a computational theory that uses electron density instead of a wave functions to calculate the molecular energy. Several functionals are available to perform this calculation and B3LYP [66,67] is the one most frequently used.

Semi-empirical methods are set up with the same general structure as a HF calculation. However some approximations are introduced by fitting the results to experimental data. The approximations reduce the calculation cost significantly, however the quality of results is reduced as well. The Austin Model 1 (AM1) [68] is a very common application of these semi-empirical calculations.

These various computational levels of theory are used to predict thermodynamic properties of reactive systems. These properties include, but are not limited to, enthalpy and entropy of formation of the reactants and products, enthalpy and entropy of the reaction, Gibbs free energy of the ideal gas reaction, and Gibbs free energy of mixing of the reaction.

Because there is no single quantum chemistry method that yields satisfactory results for all chemical systems, in this work, various levels of theory were applied when performing these calculations to evaluate the effect of theory on the thermochemistry calculations.

Once the thermodynamic properties were predicted or estimated for each possible reactant, intermediate, and product in the suggested reaction pathways, enthalpy and Gibbs free energy calculations were performed to select plausible stoichiometries from the suggested pathway scenarios. Plausible stoichiometries are thermodynamically feasible and sufficiently exothermic. For a thermodynamically feasible reaction, the corresponding Gibbs free energy change, ΔG_r , is negative.

The Gibbs free energy of reaction at constant temperature, T , is given by

$$\Delta G_r = \Delta H_r - T \Delta S_r \quad (3.1)$$

The enthalpy of reaction, ΔH_r , is given by

$$\Delta H_r = \Delta H_r^{\text{idg}} - \sum_i^N \nu_i \Delta H_{\text{vap},i} + \Delta H_r^{\text{mix}} + \Delta H_r^{\text{press}} \quad (3.2)$$

where, ΔH_r^{idg} : enthalpy of reaction calculated in the ideal gas phase

$\Delta H_{\text{vap},i}$: enthalpy of vaporization or sublimation for N condensed species

ΔH_r^{mix} : mixing and solvent enthalpic effects

$\Delta H_r^{\text{press}}$: pressure enthalpic effects

Δv_i : stoichiometric coefficient of species i

The entropy of reaction, ΔS_r , is given by

$$\Delta S_r = \Delta S_r^{\text{idg}} - \sum_i^N v_i \frac{\Delta H_{\text{vap},i}}{T} + \Delta S_r^{\text{mix}} + \Delta S_r^{\text{press}} \quad (3.3)$$

where, ΔS_r^{idg} : entropy of reaction calculated in the ideal gas phase

ΔS_r^{mix} : mixing and solvent entropic effects

$\Delta S_r^{\text{press}}$: pressure entropic effects

Therefore, the Gibbs free energy change on reaction can be defined by the following equation

$$\Delta G_r = \Delta G_r^{\text{idg}} + \Delta G_r^{\text{mix}} + \Delta G_r^{\text{press}} \quad (3.4)$$

Some assumptions were made to simplify these relationships. The pressure effects on the enthalpy and entropy of reaction are usually insignificant compared to the other contributions, thus they can be neglected. The solvent and mixture interaction enthalpy and entropy contributions are usually small when compared to the enthalpy and entropy of the reaction. It is only when the solvent has particularly strong affinities with the solutes, such as polar interactions or formation of hydrogen bonds, that these terms can be significant [39].

The thermodynamically non-feasible ($\Delta G_r > 0$) and non-hazardous (low ΔH_r or $\Delta H_r > 0$) reaction pathways were generally excluded and the remaining ones are considered for further evaluations.

High exothermic ΔH_r is considered as an indication of hazard, but such an indication is not enough in assessing the potential of a reactivity hazard. A more thorough evaluation should be based also on the kinetics of the reaction pathways (i.e., the reaction rate). Predicting system kinetics is possible using computational quantum chemistry and transition state theory (TST) [69]. To predict primary feasible and hazardous pathways, the concept of intrinsic activation barriers is applied as discussed in the following section.

3.2.3. Correlations Based on Thermodynamic-Energy Relationships

Evans and Polanyi [70,71] examined the relationship between the thermodynamics of a reaction and the activation barrier (activation energy E_A). They showed empirically that as a reaction type becomes more exothermic, its activation barrier generally decreases. Evans and Polanyi also noted that in many cases the activation barrier, E_A , for a given reaction is related to the heat of reaction, ΔH_r , via what is now called the Polanyi relationship

$$E_A = E_A^o + \gamma_P \Delta H_r \quad (3.5)$$

where, E_A^o is the intrinsic barrier of the reaction and γ_P is the transfer coefficient. A detailed derivation of this equation is given in [72] and [73] and the procedure to find a

γ_p constant is given in [72] and [74]. Physically, the intrinsic activation barrier is the energy to distort the reactant orbitals to the transition-state geometry. It was noted that the intrinsic barriers can be a way to quantify the idea that some elementary reactions are more difficult than others. Also intrinsic barriers to reaction allow one to predict whether one reaction pathway is favored over another reaction pathway [75].

In this research, the activation energy barriers from Equation 3.5 were calculated using the heats of reaction that were predicted using the various levels of computational quantum calculations discussed in the previous section.

Masel and Lee [75] suggested that the intrinsic barrier and transfer coefficient are to a great extent a function of the reaction mechanism type and not the detailed molecular structures of reacting substances. In fact, for some reaction mechanisms, the intrinsic energy barrier and transport factor values are available in the literature [72]. This means that where the reaction mechanism is defined, the activation energy can be estimated without the need for detailed transition state calculations. This approach was used in this research to predict dominant reaction pathways.

In a different study [76], validation of the Polanyi equation was conducted on 45 homolytic cleavage reactions having the general equation



where X is H, CH₃, and NO₂, and R-X are a wide range of molecules. Enthalpies of reaction were calculated using the B3P86 level of theory [77] with the cc-pVDZ basis set and experimental activation energies. The resulting correlation was

$$E_A = (0.92 \pm 0.06) \Delta H_r \quad (3.7)$$

This correlation has a linear regression coefficient of 0.922 and is presented in Figure 3.2. There is a clear indication of a significant correlation that may be used to predict the activation energy of a homolytic cleavage correlation. According to Equation 3.7, the E_A^o is 0 and the γ_P is about 0.92. These results consent with E_A^o the γ_P literature values of 0 and 1, respectively, for simple bond-scission reactions [72].

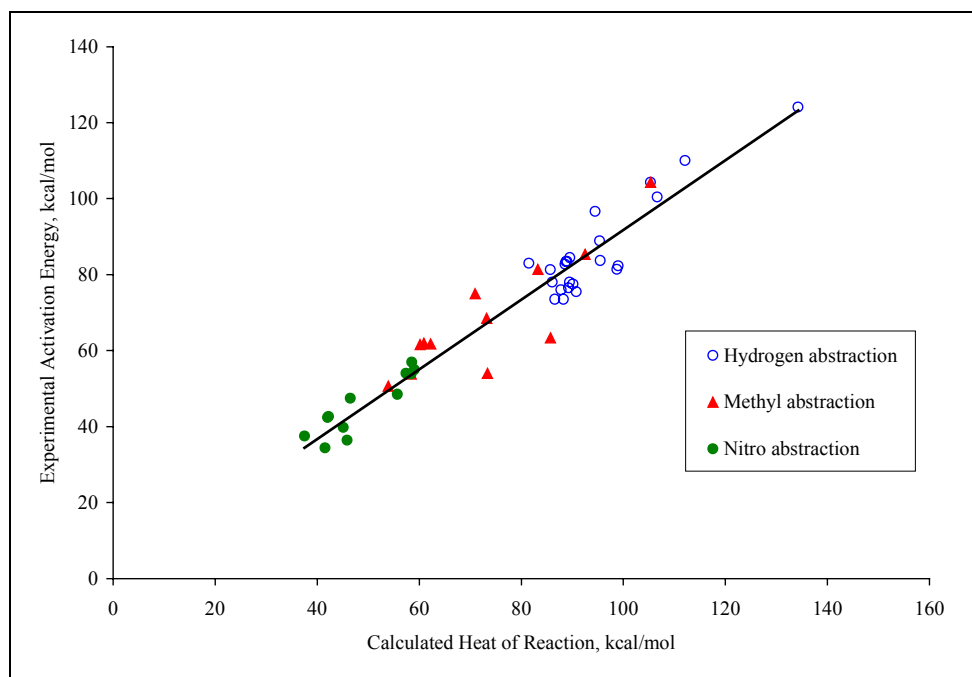


Figure 3.2. Validation of Polanyi equation for 45 homolytic cleavage reactions [76]

The Polanyi equation may not work for all cases. For highly exothermic reactions, this equation can result in a negative activation energy, which is physically unacceptable or it may start showing some deviation from its linear nature. In this case the Marcus equation [78,79] can be applied, which is a quadratic extension of Polanyi equation

$$E_A = \left(1 + \frac{\Delta H_r}{4 E_A^o} \right)^2 E_A^o \quad (3.8)$$

A derivation of Equation 3.8 is presented in the literature [72,73].

To make both Polanyi and Marcus equations most efficient, it is recommended that the constants of intrinsic barriers and transfer coefficients be predicted over similar groups of compounds to minimize the effects of ligand differences on the predicted energies.

An overall reactivity evaluation was developed based on this pathway prediction approach. Experimental analyses were then performed to obtain more accurate overall kinetic measurements, for determining missing parameters, and to test results of the theoretical methods.

3.3. Level 3: Experimental Analysis

Safety and thermal reaction risk evaluations are based on the exact characterization of reactive systems, including knowledge of the reaction stoichiometry, thermodynamic, and kinetic parameters. An exact determination of the reaction parameters by traditional means requires extensive and time-consuming laboratory investigations, which may not be cost-effective for many specialty chemicals. Also, it may not be immediately

applicable to large-scale production purposes due to the variability in raw materials and operating conditions [80]. However, as shown in the previous section, the results using theoretical computational thermodynamic and kinetic approaches are quite dependent on the initial assumptions of reaction pathways and process conditions used in the evaluation process. Incorrect assumptions may result in the hazards of the system being greatly over- or under-estimated. As a result, the parameter prediction process is not generally accurate enough to be used alone for reactivity evaluation of the most energetic reactions within the system, but it is of great importance in guiding the experimental work. Therefore, experimental thermal analysis is the most acceptable level of evaluation to model reactive systems for safer process design and operation. The experimental analysis is more effective when coupled with the previously discussed theoretical level of evaluation.

Mainly, there are four common thermal analysis techniques including temperature differential scanning, isoperibolic, isothermal, and adiabatic calorimetry. Experimental techniques for chemical reactivity evaluations produce data of varying quality. In this research, these techniques are divided into two levels: (1) screening analysis techniques, and (2) advanced analysis techniques. This classification helps to provide the necessary chemical reactivity evaluation information with the fewest number of expensive and time-consuming experimental analyses.

The objectives of conducting screening and advanced thermal analysis are not quite the same. For screening thermal analysis techniques, the objectives are to detect the exothermic behavior and to provide an approximate overall temperature and heat of

reaction. However, the objectives of conducting advanced thermal analysis techniques are to obtain more accurate thermodynamic and kinetic parameters with pressure behavior scenarios with thermal inertia and scale-up effects evaluation.

Adiabatic analysis is a technique used in advanced thermal analysis and considered as the most favored technique particularly for large reacting masses. In industrial plant situations of thermal runaway, neither the process cooling system, nor the reaction container will be able to dissipate the huge amounts of energy released. The increasing reactant mass temperature will increase the rate of reaction exponentially, leading to more heat production while near-adiabatic conditions are maintained. Because of that, adiabatic thermal analysis is considered a significant requirement for comprehensive reactivity evaluation.

The generated time-temperature-pressure data are used to calculate the thermodynamic and kinetic parameters of the system and then reactivity evaluation parameters. Generally, it is difficult to maintain perfect adiabatic conditions and it is reflected in the results. Therefore, data adjustment should be considered during parameter calculations and reactivity hazard evaluation. The detailed experimental data analysis is presented in Chapter IV.

4. Reactive Systems Under Investigation

Three reactive systems were studied in this work for evaluating their reactivity hazards. Selection of these systems was based on the fact that they represent different chemical groups and may follow different reaction mechanisms. Also, these reactive

systems were involved in incidents due to their inherent reactivity hazards. Applying the proposed approach for chemical reactivity evaluation to these systems has showed the degree of success of this approach. Available data in the literature for these systems were used in evaluating our research findings.

Systems that were investigated included the decomposition of *di-tert*-butyl peroxide (DTBP) in toluene, copolymerization of styrene-acrylonitrile (SAN), and polymerization of 1,3-butadiene (BD).

A detailed evaluation of the decomposition of DTBP in toluene was performed to provide better understanding to the stoichiometric and thermokinetic behavior of this reaction. Although this system represents a clear chemistry mechanism, it provided a great opportunity to study the limitations of each level of this approach.

Copolymerization of SAN represented a more complicated reactive system to be evaluated. Limited literature information is available on this system, although it represents a significant reaction mechanism with wide industrial applications. In this study, the copolymerization and decomposition scenarios of SAN were evaluated at different inhibited styrene-to-acrylonitrile feed ratios.

The last system studied is thermal polymerization of 1,3-butadiene in the presence and absence of oxygen. This system has been involved in several catastrophic incidents. Although several research studies have been conducted on this system, a more fundamental evaluation approach is still needed. The hazardous nature of reactivity and toxicity made the experimental evaluation of this system the most difficult.

5. Conclusions

The combination of computational methods and experimental thermal analysis techniques in a systematic approach for chemical reactivity evaluation will focus the attention on the most possible and most hazardous reaction stoichiometry and hence reduce the need for detailed experimental analysis. More detailed and advanced experimental analyses may still be required for more complex systems.

In general, this approach for evaluating chemical reactivity can be applied to a variety of systems. The degree of success in applying this approach depends on the system complexity and on the appropriate levels of experimental analysis and theory to measure and predict the thermodynamic and kinetic parameters.

This approach is not intended to be applied in parts. In fact, the parallel implementation of the theoretical and experimental analysis levels enhances the reactivity evaluation conclusions and reduces the associated cost associated. The comprehensive application of the various levels of evaluation is the primary strength of this approach.

CHAPTER IV

RESEARCH METHODOLOGY AND PROCEDURES

1. Précis

In Chapter III, a systematic approach for chemical reactivity evaluation is presented. Clearly, the applied techniques in that approach are, mainly, classified into theoretical and experimental techniques. In this chapter, theoretical evaluation methods and experimental thermal analysis techniques performed in this research are presented. The experimental data analysis methodology is also discussed in the last section to provide a mathematical approach for analyzing the calorimetric data.

2. Theoretical Evaluation Methods

Various theoretical calculation methods were applied in this research to predict thermodynamic and kinetic parameters of reactive system pathways. The selection of these methods was intended to provide a variety of approaches that may help address specific problems in each reactive system. The applied methods in this research are described in the following sections. The focus in this chapter was not to provide detailed discussion of theory behind these methods; other sources may provide more specific information [28,40,69,72].

2.1. Molecular Group Contribution Methods

Molecular group contribution methods were expanded by Benson [28] to show that adding the contributions of all bonds in the molecule, then correcting for the influence of various side chains can predict a wide variety of thermodynamic properties of molecules. In 1974, the American Society for Testing and Materials (ASTM) Committee E-27 introduced this software package known as the ASTM Computer Program for Chemical Thermodynamic and Energy Release Evaluation (CHETAH™). The CHETAH™ program (version 7.2) [32] applies molecular group contribution method for thermodynamic property calculations.

In this research, CHETAH™ was utilized to calculate a range of thermodynamic properties for the reactive systems under investigation such as, entropy, S , enthalpy of formation, ΔH_f , Gibbs free energy of formation, ΔG_f , enthalpy of reaction, ΔH_r , entropy of reaction, ΔS_r , and Gibbs free energy of reaction, ΔG_r .

These calculations were applied to the overall reaction pathway. Reactants and products are identified either through available literature information or through advanced calculations. For each compound, the contributing groups were identified in the CHETAH™ database and selected to build the molecule. The reaction stoichiometry was also balanced and reaction thermodynamic properties were calculated.

As discussed in Chapter III, there are limitations to the CHETAH™ software capabilities, which include thermodynamic calculations of radicals and liquids, and the limitation of its molecular group database. Hence, in this research, CHETAH™ was

primarily used as a screening tool and to compare the calculated values with those obtained through higher-level calculations.

The error associated with the CHETAH™'s thermodynamic calculations depends on the quality of contributed groups thermodynamic values and the reaction stoichiometry assumptions.

2.2. Computational Quantum Chemistry Methods

Compared to group contribution methods, computational quantum chemistry methods are more advanced techniques and require more knowledge and experience. Because there is no single quantum chemistry method that yields satisfactory results for all chemical systems, several levels of theory were applied in this research to predict thermochemistry parameters for proposed reaction pathways of the reactive systems under investigation. This approach provides the ability to compare between the significance of final conclusions and calculation cost. The usefulness of the various methods depends on the system size, the property that is calculated, and the calculation costs.

The applied computational levels included the semi-empirical method Austin Model 1 (AM1), *ab initio* methods of Hartree-Fock (HF), Complete Basis Set (CBS-4M), and the Gaussian Theory method (G2), and Density Functional Theory (DFT) method (B3LYP).

The AM1 method is an inexpensive popular level of theory for modeling organic compounds. AM1 employs an approximate form of Schrödinger equation with

appropriate parameters derived from experimental data for the type of chemical system under investigation [81]. AM1 was applied as a qualitative reaction evaluation tool and to predict general trends of thermochemical parameters.

The HF method is the most common *ab initio* calculation [69]. This method is a simple and inexpensive level of calculation, because some exchange correlation effects among electrons are ignored [38]. This level of calculation was conducted with the 6-31G(d) basis set [82] that describes a wave function.

Another *ab initio* calculation was performed using a higher level of theory of the CBS-4M method. The CBS method involves a set of calculations with various numbers of basis functions and levels of theory. The CBS extrapolation models employ asymptotic extrapolation of second-order energy and relatively small basis sets for the higher-order correlation energy [64]. This new version, CBS-4M, became available recently and allows calculations of molecular properties with a reasonable degree of accuracy for molecules of relatively large molecular size [83].

The Gaussian theory method G2 is considered a high-level method, and it was used to predict high-accuracy thermochemical parameters. This method started from the observation that certain *ab initio* methods show a systematic error for predicting the energies of the ground states of organic molecules. This observation led to the development of a correction equation that uses energies from several different *ab initio* calculations to extrapolate a high-accuracy result.

The DFT method B3LYP was applied for more accurate thermochemical parameter predictions. The DFT states that the ground state energy of a system of electrons is a

function of the electron density and correlation effects using functionals, which include terms for exchange and correlation energy that depend on the electron density and density gradient. The 6-31G(d) basis set was used to provide an acceptable degree of accuracy.

Initially, for all these calculations, the molecular structures of possible reactants, intermediates, and products were optimized for minimum energy geometry, and then frequency calculations were applied to determine the thermochemical parameters of these structures. All of these calculations were performed using the GUASSIAN 98 [84] software available through the supercomputers K2 and Titan at Texas A&M University supercomputing facilities.

2.3. *Thermodynamic-Energy Correlations*

Predicting primary reaction pathways was possible by applying of the Polanyi and Marcus equations as discussed in Chapter III. These equations showed empirically that as a reaction type becomes more exothermic, its activation barrier decreases. From Chapter III, the Polanyi equation

$$E_A = E_A^o + \gamma_p \Delta H_r \quad (3.5)$$

and the Marcus equation

$$E_A = \left(1 + \frac{\Delta H_r}{4 E_A^o}\right)^2 E_A^o \quad (3.8)$$

were specified to provide a relationship between thermodynamic and kinetic parameters of an elementary reaction. In this research, they were used to predict activation energy, E_A , of an elementary reaction via the knowledge of its heat of reaction, ΔH_r , intrinsic barrier of the reaction, E_A° , and the transfer coefficient, γ_p .

The heat of reaction is calculated using the various computational quantum chemistry methods discussed in the previous section. The intrinsic barrier and transfer coefficient of many reaction mechanisms are available in the literature [72]. Those values are used to predict activation energies and hence the most dominant reaction pathways.

An overall reactivity evaluation was developed based on this prediction approach. Finally, the overall experimental analysis results were compared to the theoretical findings for reactivity evaluation conclusions.

3. Experimental Thermal Analysis

Calorimetric analysis is a fundamental procedure that provides overall thermodynamic and kinetic parameters for chemical reactivity thermal hazards evaluation. There are many commercially available calorimeters applying various thermal analyses operating principles and providing varying quality data. Although adiabatic calorimetry is the most frequently recommended technique, other techniques can also be applied for reactivity hazards evaluation.

In this study, three calorimeters were used for experimental thermal analysis of the proposed reactive systems. Apparatus description, operating modes, procedures, and

data quality for each of these calorimeters are discussed in the following sections of this chapter.

3.1. Reactive System Screening Tool

The Reactive System Screening Tool (RSST™) is an open-cell calorimeter that was developed in 1993 by Fauske and Associates, Inc. [85] to evaluate emergency relief vent requirements.

The RSST™ can quickly and safely determine potential for runaway reactions. It measures the rate of temperature and, for gas-producing reactions, pressure increase for determining energy and gas release rates. This information helps to identify possible runaway reaction conditions, and can be used with simple methods to size reactor relief vents. This information is useful in industry when a large number of chemicals and processes must be screened.

The RSST™ applies the principle of ramping temperature to measure potential reactivity thermal and pressure hazards. In RSST™ test, a linear heating energy is added to the reactive sample to initiate the exothermic reaction of the system. Because of this linear heating energy addition to the reaction energy, the effects on the measurement of chemical energy release due to heat losses from the test cell to the surroundings are reduced. Figure 4.1 illustrates the principle of ramping temperature applied in the RSST™.

By computer control, the imposed linear heating rate can be varied from about 0.1°C/min to ramp rates approaching those required to simulate fire exposure by using

the immersion heater option. This heating rate can be held at a fixed level or varied during a test run. The RSST™ can operate with temperatures up to 500°C and pressures up to 500 psig.

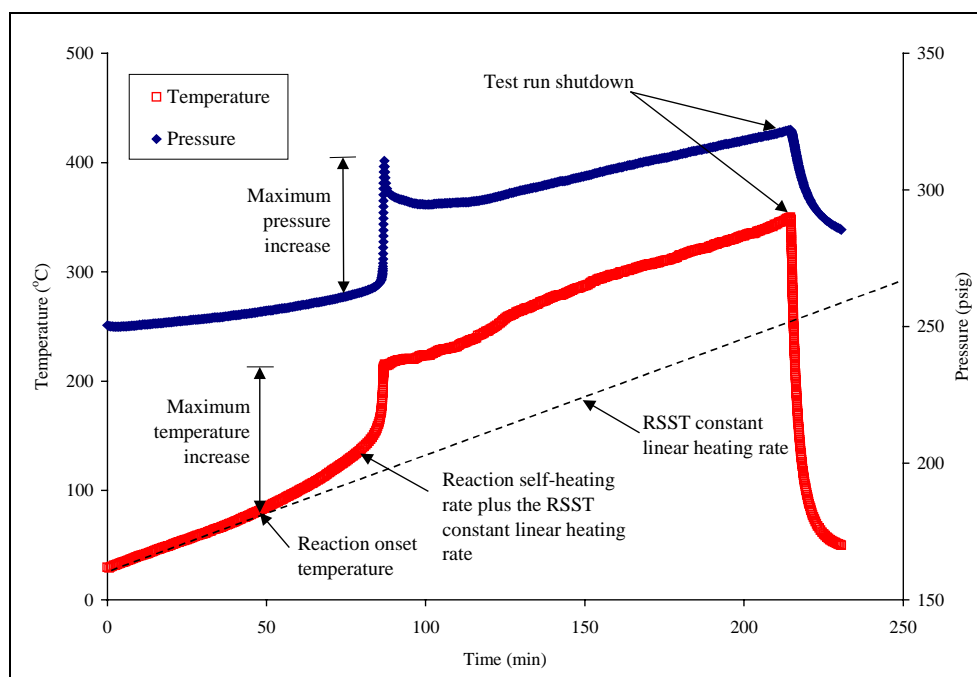


Figure 4.1. Typical temperature and pressure profiles of the RSST™ test

3.1.1. Apparatus Description

The RSST™ consists of three major components: a stainless steel containment vessel, control box, and computer control software. The containment vessel, as presented in Figure 4.2, houses the small (10 cm³) open spherical glass test cell (reaction

vessel), the heater, thermocouple, pressure transducer, and the insulation assembly. This containment vessel maintains the chemical sample under a pre-set pressure and safety vessel that is provided with a 500-psig rupture disk. The containment vessel is connected to a control box by a wire cable set. This wire cable set provides transfer of thermocouple and pressure signals to the control box and supplies the heater with power. A magnetic stirrer base is located beneath the containment vessel to provide a magnetic field for a stirrer bar element inside the test cell for continuous mixing of the sample. The sample cell volume is 10 mL and the containment volume is 350 mL. The RSST™ containment vessel allows for reagents to be added during a test.

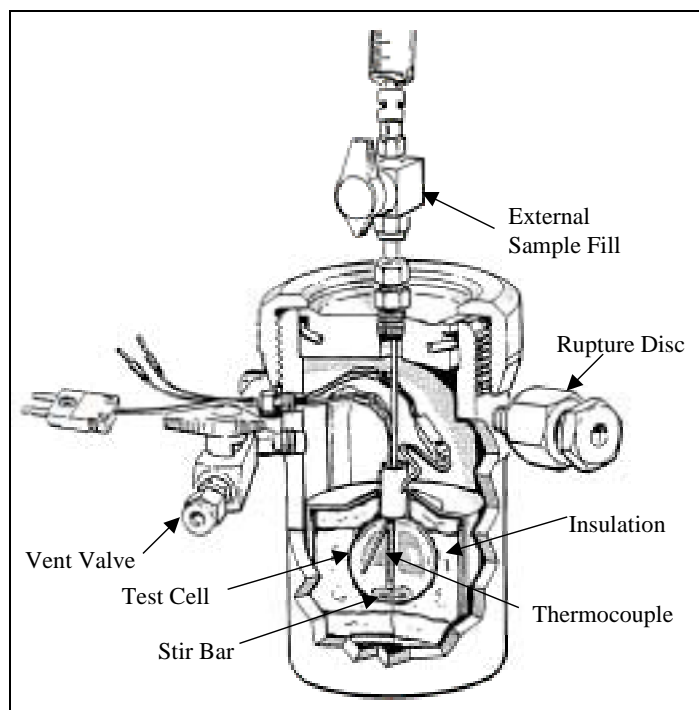


Figure 4.2. Overall schematic of the RSST™ test cell and containment vessel [with permission from Fauske & Associates, Inc.]

A key feature of the apparatus is its low effective heat capacity relative to that of the sample, which results in a thermal inertia factor, ϕ , of approximately 1.04. This feature allows the measured data to be directly applied to process scale [86].

The control box contains the heat power supply, temperature/pressure amplifiers, and data acquisition, and control panel. The heater surrounding the test cell is controlled by feed back from the sample measurement to supply enough heater power to overcome heat losses and to assure a pre-specified linear temperature rise rate.

The RSST™ measures and records sample temperature, pressure, rate of temperature, and rate of pressure in the test vessel as a function of time during the sample reaction.

3.1.2. Operating Modes and Procedures

In this research, samples were tested with the RSST™ in the presence of air (as with the DTBP analysis) or in the absence of air, under nitrogen environment, as with SAN analysis. In the case of the DTBP analysis, the sample and test cell were weighed and then loaded into the containment vessel. However, for the SAN analysis, the empty test cell was loaded into the containment vessel and then evacuated of air to a pressure of about -10 psig using a vacuum pump connected to the containment vessel. A series of nitrogen purging and evacuating steps were applied to assure the absence of air from the containment vessel. The vessel was kept under a pressure of about -10 psig, and the SAN sample was injected into the test cell using the special external sample fill arrangement.

Typically, a sample size of about 9 – 10 g was loaded in every test run. A constant stirring was applied for all samples along the test run time. The containment vessel was pressurized with nitrogen to about 250-300 psig to reduce the samples' boil-off and material losses from the test cell to the containment vessel. Samples were then heated to a constant linear rate. To determine exothermal reactivity, various constant linear heating rates ranging from 0.7 to 3.3 °C/min were applied to evaluate the effect of linear heating rates on the RSST™ performance. Experiment shutdown criteria were selected for each run based either on the maximum reached temperature or on the total test run time.

The sample temperature and pressure vs. time profiles were measured and recorded. Self-heating and pressurization rates were found as functions of sample temperature.

3.1.3. Data Quality

To maintain high RSST™ data quality, several steps were taken frequently. Calibration of the thermocouple was performed every time a new thermocouple was installed. A thermocouple single-point calibration (0°C) was performed frequently. Output voltage levels for the temperature signals were evaluated by the RSST™ software to detect any significant deviation. This output voltage is an approximate linear 0 – 5 V for 0 – 500 °C. The manufacturer specifies a thermocouple measurement error of $\pm 0.1^\circ\text{C}$.

Similarly, a calibrated pressure transducer produces a voltage signal of about 0 – 2.5 V (direct current) that is proportional to the pressure level of about 0 – 500 psig. The

RSST™ software periodically evaluated this performance. A single-point calibration (0 psig) was performed for every test run.

Prior to each run, a leak test was performed in which the containment vessel was pressurized to about 350 psig and monitored over a 2- to 4-hour period. Any leaks detected using a water-soap solution were eliminated.

Heater resistance was measured using a volt/ohm meter for typical values of 11 – 13 ohms for every test run. When these typical resistances were not maintained, the heater was replaced.

Every sample test was at least repeated for three measurements to assure acceptable experimental reproducibility.

3.2. Heat Flux Calorimeter

The Setaram heat flux calorimeter, C80D, was utilized to evaluate the DTBP in the toluene decomposition reaction. This analysis was performed at the National Research Institute for Fire and Disaster (NRIFD) in Tokyo, Japan.

The C80D calorimeter applies the Calvet principle where the difference of the heat flux between a sample and a reference is measured. The flux meters are thermopiles that completely enclose the sample or the reference material. They can be used in isotherm or temperature-scanning mode. This calorimeter can measure temperature, pressure, and heat of reaction. It has a temperature operating range of 25 to 300 °C and a pressure up to 350 bars. The C80D can apply temperature-scanning rate between 0.01 to 2 °C/min with a sample size up to 10 mL in a glass vessel.

3.2.1. Apparatus Description

The C80D calorimeter consists of a conducting calorimetric block surrounding the heat transducers. This block is itself surrounded by the heating element and arranged in an insulated chamber. The sample contained in an experimental vessel is introduced into the chamber through a hole and rests in a sensing space, entirely surrounded by the heat transducers. An identical vessel without a sample is arranged in a second hole. The differential arrangement of the heat transducers provides a signal proportional to the heat exchanged by the sample as a result of canceling out the interference associated with temperature control of the calorimetric block.

3.2.2. Operating Modes and Procedures

The temperature-scanning mode of C80D operation was applied at a rate of 0.1°C/min in this study to measure the heat of reaction of 0.1 g samples.

3.2.3. Data Quality

The C80D calorimeter was calibrated for the experimental temperature range using a resistance vessel which simulates the experimental vessel and which delivers calibrated electrical power. The calorimetric resolution of the C80D is 0.1 μ W.

3.3. Automatic Pressure Tracking Adiabatic Calorimeter

In real chemical processes under a thermal runaway scenario, near-adiabatic conditions are maintained. To maximize process design safety, adiabatic reaction

calorimetry has proven to be extremely useful in simulating real chemical process runaway scenarios.

The Automatic Pressure Tracking Adiabatic Calorimeter (APTAC™) by Arthur D. Little is an adiabatic closed-cell reaction calorimeter that can operate at pressures up to 2,000 psia and temperatures up to 500°C. The machine is fully automated and is operated by an easy-to-use control program operating under Microsoft Windows. Reactions are performed in a small spherical flask of about 130 mL, which can be constructed of various materials including glass, titanium, stainless steel, and tantalum. Thermal inertia factors, ϕ , down to about 1.1 are attainable. The reaction vessel can vary in volume and mass, depending on the chemical reaction under study, and the expected maximum rates of self-heating and pressure generation. Generally, most reactions are performed in a 2.5-in-diameter titanium vessel with a wall thickness of about 0.02 in and a mass of about 30 g.

3.3.1. Apparatus Description

The APTAC™ consists of four main heaters: bottom, top, side, and tube heaters. These heaters and the reaction vessel are surrounded by insulation and placed in a 500-mL pressure vessel that can operate with pressures up to 2,000 psig. A magnetic stirrer bar element mixes the reactants. The reaction vessel as presented in Figure 4.3 is suspended from the top heater. A more detailed schematic of the APTAC™ is discussed in the literature [87]. Seven type-N thermocouples continuously measure the sample and reaction vessel wall temperature, nitrogen gas in the pressure vessel, and the four

heaters. This arrangement of temperature measurement assures the continuous monitoring and control of adiabatic conditions.

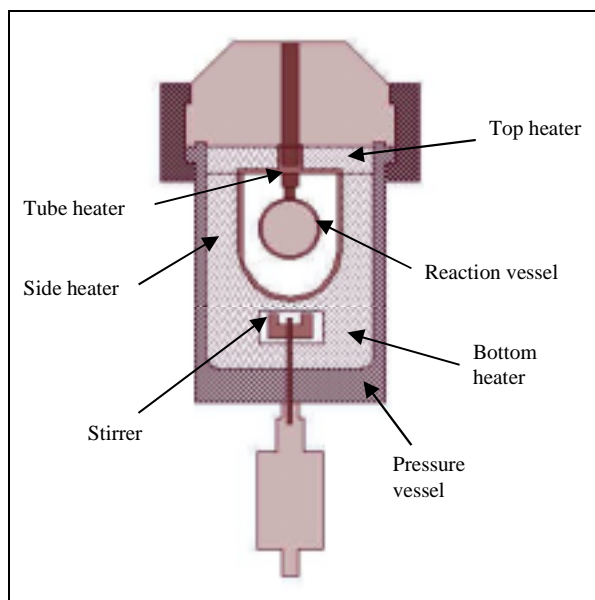


Figure 4.3. Schematic of APTAC™ reaction and pressure vessels

Under reaction runaway conditions, the reaction vessel is prevented from bursting due to internal pressure generation by injecting nitrogen gas around the vessel at a rate (up to 20,000 psi/min) sufficient to keep the pressure differential across the wall of the reaction vessel less than ~10 psi. The adiabatic conditions are maintained through the heater capability to match the reaction temperature up to 400°C/min.

A sample may be loaded directly to the reaction vessel at the beginning of the experiment, or they may be injected at specified time of the test run using the single-shot

injection bomb or a high-pressure syringe pump. Venting the reaction vessel is possible through complete automated operation to an internal condensation vessel or to an external containment vessel.

Control of the heaters and nitrogen flow to the reaction and pressure vessels, data recording, sample injection, reaction vessel venting, and most of the safety features of the calorimeter are controlled by an IBM-compatible PC running under Microsoft Windows NT. Signals from the thermocouples and pressure transducers are processed using the National Instruments SCXI units of signal conditioning and a 16-bit A/D board. Control signals to the heaters, flow valves, and stirring are processed using a 12-bit A/D board.

The APTAC™ is provided with several control and safety features to minimize hazards associated with any highly reactive system. Heaters are protected from high power input (5 kW). Maximum temperature and heating rate cannot be exceeded. Failure of any thermocouple to provide signal causes the heaters to shut down. The cabinet doors are provided with locks that cannot be opened under normal operation to minimize exposure to high temperatures, pressures, and toxic chemicals.

Pressure hazards associated with high-pressure differences between the reaction vessel and the pressure vessel will cause an automatic shutdown. The control system will not allow the maximum pressure and pressurization rate to be exceeded. Other protection barriers are also provided. The pressure vessel is equipped with a 2,000-psig rupture disk. The pressure vessel cannot be opened manually when pressurized. Any spills and leaks are safely contained or vented to external vessels.

3.3.2. *Operating Modes and Procedures*

Several APTACTM operating modes are available including heat-soak-search, heat ramp, isothermal, and heat-wait-search. The APTACTM can also conduct closed or vented reaction vessel experiments.

In the heat-soak-search mode, the sample is held at specified elevated temperature until either an exotherm is detected or a pre-set time limit is exceeded. The heat ramp mode is similar to the RSSTTM operating mode discussed earlier, where the sample is heated at a specified rate until an end temperature is reached. For the isothermal mode, the sample is heated to the required temperature at the stated heating rate and held there until the time limit is exceeded. The sample is then allowed to cool.

In this research the focus was on the fourth operating mode, heat-wait-search. In this mode the sample is heated in small steps with an exotherm search at each step, as illustrated in Figure 4.4. If an exotherm is detected at a reaction onset temperature, the heating mode shifts to adiabatic. After reaching the reaction maximum temperature, the heat-wait-search resumes for further exotherms search until time or temperature limits are exceeded where the sample is then allowed to cool. The pressure follows similar behavior as presented in Figure 4.5.

A combination of different operating modes is possible. All these operating modes may also be subdivided depending on whether or not a liquid or gas sample is to be injected into the reaction vessel at some point in the experiment.

In this research, three reactive systems were tested with the APTACTM. There were no significant differences in the experimental procedures among these systems except

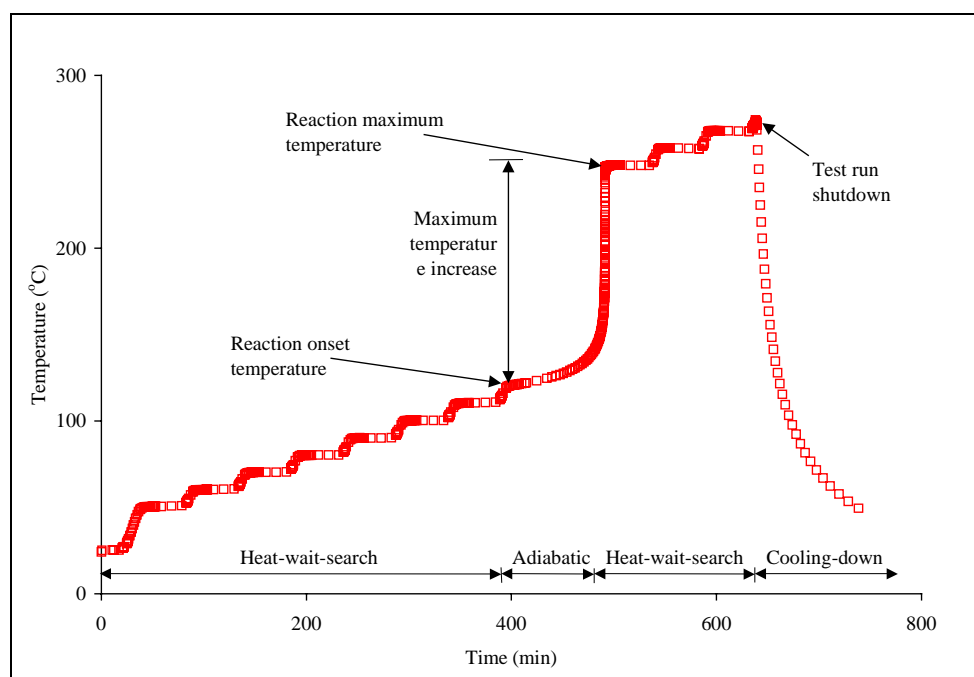


Figure 4.4. Typical heat-wait-search operation mode of the APTAC™

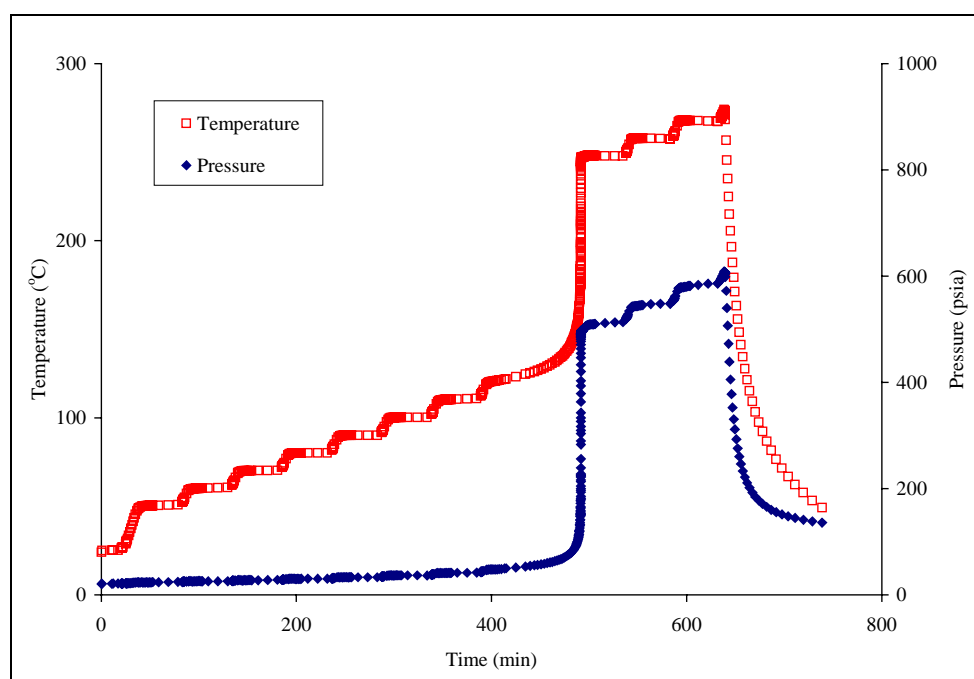


Figure 4.5. Temperature-pressure profiles of the APTAC™ heat-wait-search mode

for the sample preparation steps. Sample preparation procedures are discussed here and later in Chapters V, VI, and VII.

The DTBP reactive system samples were prepared by mixing the DTBP with a solvent. The tested sample and reaction vessel were weighed and then loaded into the pressure vessel.

In the SAN analysis, styrene and acrylonitrile monomers were mixed and transferred to the reaction vessel, which was then loaded into the pressure vessel. Each SAN sample inside the reaction vessel was frozen using a liquid nitrogen bath at -102°C that surrounded the reaction vessel. Air in the reaction vessel was then evacuated to a pressure of about 2 psia using a vacuum pump connected to vessel. A series of nitrogen purging and evacuating cycles were applied to assure the absence of air from the containment vessel. After evacuation, the vessel was kept under a nitrogen pressure of about 15 psia and left to warm-up to room temperature.

Because 1,3-butadiene is a gas at room temperature, the normal procedure for external sample loading to the reaction vessel was not applicable. Therefore, a special tubing arrangement was applied to transfer the butadiene into the reaction vessel. This special arrangement is discussed in Chapter VII.

The 1,3-butadiene was tested in the presence and absence of oxygen. The empty reaction vessel was first attached to the pressure vessel and then evacuated of air to a pressure of 5 psia using a vacuum pump connected to the reaction vessel. This concentration of air in the reaction vessel was used for all the analysis involving 1,3-butadiene in the presence of oxygen. After that, the 1,3-butadiene sample was

transferred from a pressurized cylinder. For the analysis in the absence of oxygen, a series of nitrogen purge and evacuation cycles were applied after the first air evacuation to assure the absence of air from the reaction vessel. After that, the vessel was kept under a nitrogen pressure of about 5 psia, and the 1,3-butadiene sample was transferred into the reaction vessel. In all cases, a liquid nitrogen bath at -102°C that surrounded the reaction vessel was used to enhance the 1,3-butadiene transport process. The sample and reaction vessel were left to warm to room temperature.

As soon as the loaded sample and reaction vessel reached room temperature, the pressure vessel was closed. Closed-cell heat-wait-search mode of operation was applied for all of the tested samples in this study. Samples were initially heated to 50 or 80°C depending on the expected reaction onset temperature. Heating steps of 10°C were conducted at a rate of $2^{\circ}\text{C}/\text{min}$. A waiting period of 45 minutes after each heating step was applied. The self-heating rate threshold limit was selected to be 0.05 or $0.1^{\circ}\text{C}/\text{min}$ to detect reaction onset temperature and start the adiabatic mode of operation. Shut down criteria were selected not to exceed a specified maximum temperature or the maximum heating and pressurization rates of the APTACTM.

At the end of each run, the sample was cooled to room temperature and the final weight of the sample was recorded.

The sample temperature and pressure vs. time profiles were measured and recorded. Self-heating and pressurization rates were determined as functions of sample temperature.

3.3.3. *Data Quality*

The APTAC™ is known for the high quality of measured data. To maintain this high quality several procedures were applied frequently to assure the accuracy and reproducibility of the calorimeter including leak detection, thermocouple calibration, and ice point check.

Leak detection was performed frequently and every time a tubing or thermocouple was replaced. Leak detection from the reaction vessel was performed automatically by the APTAC™ at the start of every run. The reaction vessel was pressurized to 50 – 100 psia and the pressure changes were monitored for a 20-min period. When the pressure changes were between –0.01 to 0.01 psi/min, the apparatus was judged to be leak tight. Manual leak detection tests were also performed. The reaction and pressure vessels were pressurized to 150 psia with nitrogen and pressure change rates were monitored for 4 – 6 h for changes larger than 0.01 psi/min. Leaks were identified using water soap solution.

Calibration of the sample thermocouple was performed every time a new thermocouple was installed. A thermocouple re-calibration was performed frequently (every 10 runs). Both relative and absolute thermocouple calibrations were conducted.

A relative calibration is performed to ensure that the sample, reaction vessel wall, and nitrogen thermocouples all provide the same output to the data logging system when they are at the same temperature. This calibration reduces the potential for either positive or negative drifts that may cause loss of the adiabatic conditions or the detection of false onset temperatures. This relative calibration was conducted automatically and overnight

for a temperature range of 25 – 350 °C. Following this calibration the temperature relative measurement error of the thermocouples was around $\pm 0.1^\circ\text{C}$. Typical relative calibration curves are presented in Figure 4.6. Also, relative calibration was applied to detect leaks through the plotting of reaction vessel pressure vs. temperature as presented in Figure 4.7. In this plot the pressure during the heating and cooling stages followed the pressure path and suggested a leak-tight vessel.

Absolute calibration of thermocouples was achieved through the ice point (0°C) check. Every new thermocouple was placed in ice water and the offset from 0°C was adjusted through the software.

Pressure transducers were frequently tested for their readings by measuring the vapor pressure of Aldrich 99+% water. The curve of vapor pressure vs. temperature is compared to experimental steam tables [88] vapor pressure-temperature plot of water as presented in Figure 4.8. The reaction and pressure vessels transducers have a range of 3,000 psi and an accuracy of $\pm 0.1\%$ of range.

To assure the reproducibility of APTACTM data, every sample test was repeated at least for three determinations. Moreover, the 30 wt% DTBP in toluene was tested over a long period of time (8 months), as presented in Figure 4.9, to assure acceptable experimental reproducibility.

4. Experimental Data Analysis

The accuracy of predicted reaction runaway behavior and the adjustment for different critical factors affecting the experiment is only as precise as the data obtained

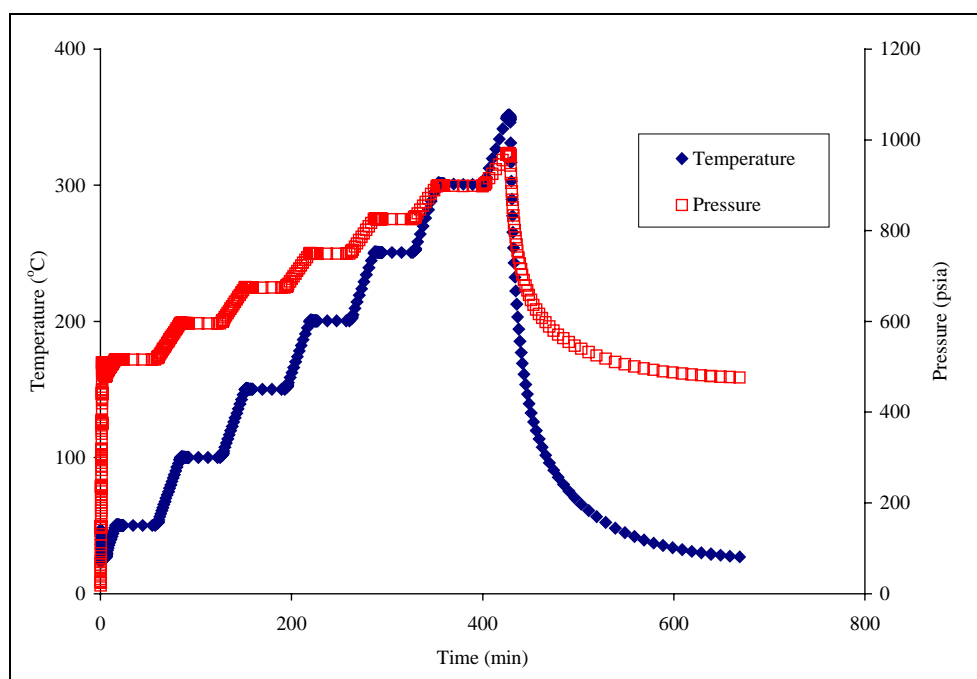


Figure 4.6. Temperature and pressure profiles during APTAC™ relative calibration

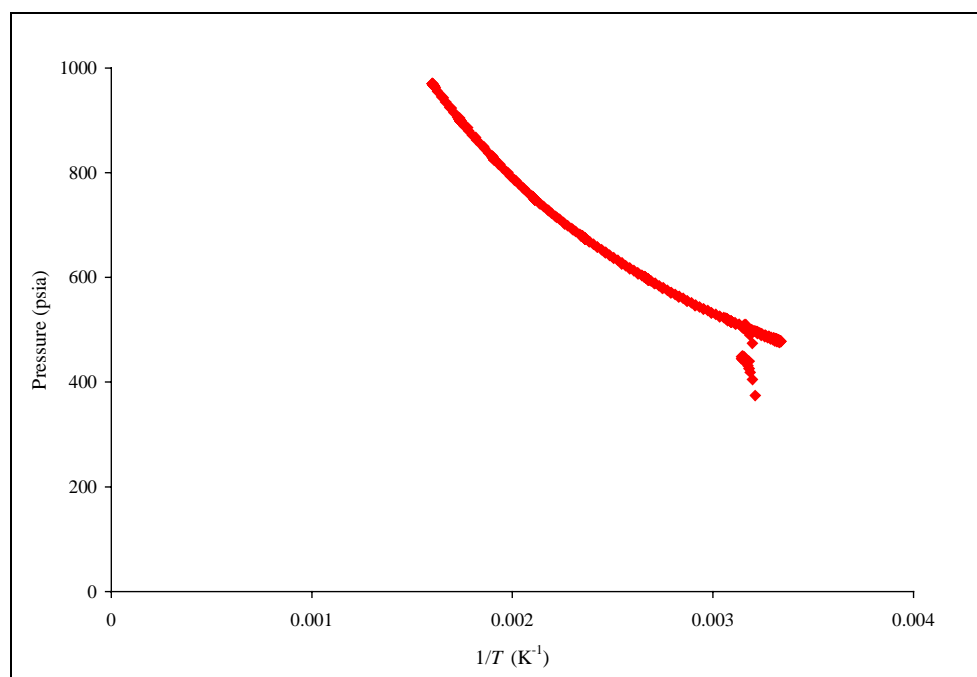


Figure 4.7. Pressure data during relative calibration of APTAC™ thermocouples

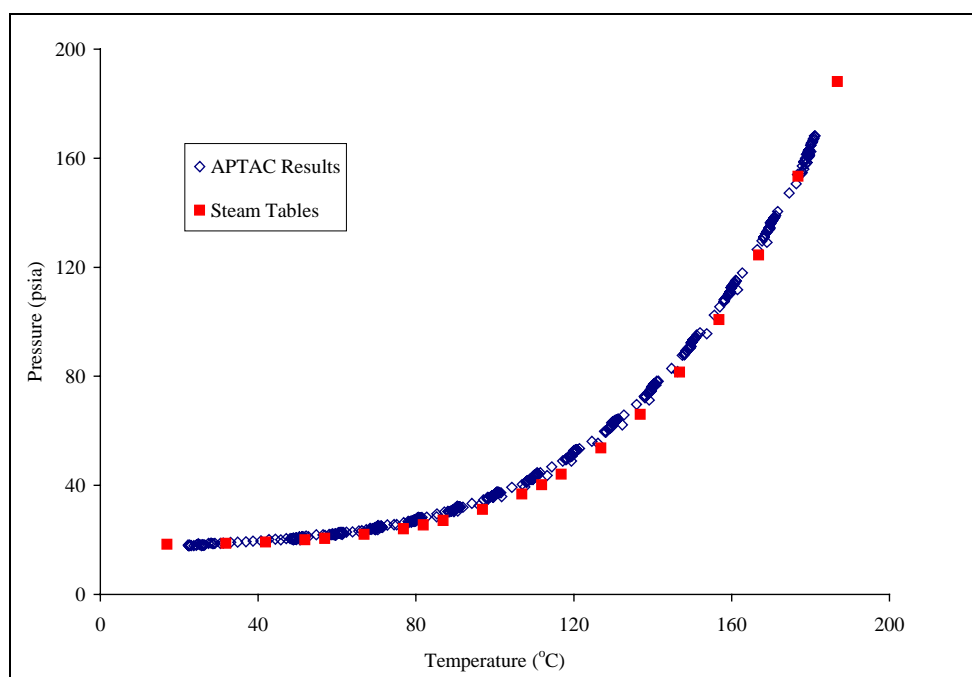


Figure 4.8. Water vapor pressure of the APTAC™ and steam tables

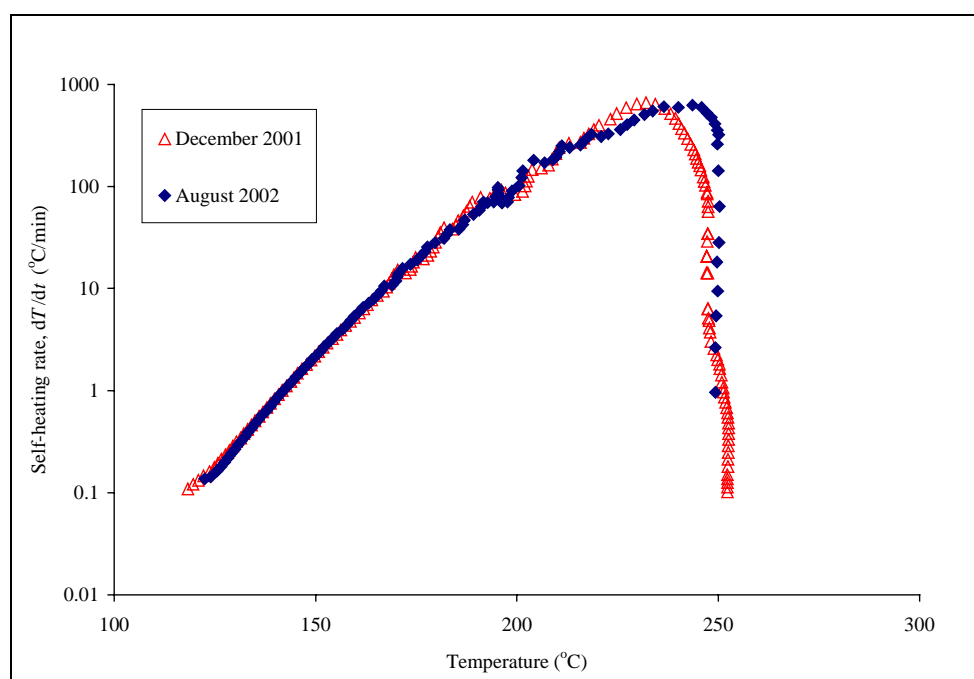


Figure 4.9. Self-heating rate of 30 wt% DTBP in toluene over 9 months

to describe the reaction. As discussed earlier, information characterizing a runaway reaction is usually obtained using one or more of several experimental methods. Of particular importance is the accurate calculation and modeling of the reaction kinetics. Common methods for obtaining reaction kinetics from thermal analysis experimental data are described in the literature [49,58,60,62,89,90].

The generated time-temperature data from the RSST™ and APTAC™ are analyzed to determine reactivity hazard parameters discussed in Chapter III. In this section, the focus is on the mathematical derivation of reaction kinetic models and on the thermal inertia adjustment. Although there are heat losses associated with experimental measurements, especially with the RSST™, these heat losses were ignored for simplicity.

4.1. Kinetic Modeling

The adiabatic (or semi adiabatic) calorimetric data, and material and energy balances are coupled in this analysis to provide an acceptable kinetic model that describes the runaway behavior of the reactive system.

General material balance of calorimetric analysis can be reduced with proper assumptions of closed system with uniform temperature and concentration distribution to

$$\frac{dN}{dt} = r V \quad (4.1)$$

where N is number of moles of material, r is reaction rate, t is time, and V is reacting volume.

The general energy balance based on the first law of thermodynamics can also be simplified with proper assumptions of closed system, constant volume, negligible changes in kinetic and potential energies, ideal solutions, and negligible pressure effects to yield

$$\frac{dT}{dt} = \frac{(-\Delta H_r)(-rV)}{N_o C_s} \quad (4.2)$$

where T is the reacting system temperature, ΔH_r is heat of reaction, N_o is the initial number of moles of material, and C_s is the heat capacity of reacting material.

Combining and then integrating Equations 4.1 and 4.2 gives

$$T - T_o = \frac{(-\Delta H_r)(N - N_o)}{N_o C_s} \quad (4.3)$$

In Equation 4.3 it is assumed that ΔH_r is not a function of temperature.

For a single reactant with n^{th} order kinetics and constant volume the reaction rate can be described as follows

$$\frac{dC}{dt} = r = -k C^n \quad (4.4)$$

where k is the reaction rate constant, C is the single reactant concentration at any time, t , and n is the reaction order. For an exothermic reaction at adiabatic conditions, the rate of the reaction with dissipation of reactants is expected to decrease after reaching its maximum value and finally diminishes to zero after completing the reaction at temperature, T_{max} . So at any time, the following relation approximately expresses the concentration of the reactant, C , in terms of the temperature, T

$$C = \frac{T_{\max} - T}{T_{\max} - T_o} C_o \quad (4.5)$$

where C_o is the initial reactant concentration and T_o is the initial temperature at which exothermic reaction is detected. The adiabatic temperature rise, ΔT_{ad} , is then defined as

$$\Delta T_{\text{ad}} = T_{\max} - T_o \quad (4.6)$$

The heat of reaction, ΔH_r , can be evaluated using Equations 4.3 and 4.6 when the reaction reaches completion and the reactant number of moles is zero as follows

$$\Delta H_r = m C_s \Delta T_{\text{ad}} \quad (4.7)$$

In Equation 4.7, the heat capacity of the reaction mixture, C_s , is assumed independent of T over ΔT_{ad} and m is the mass of the reactant. Differentiating Equation 4.5 with respect to time and substituting into Equation 4.4, the following equation is derived

$$\frac{dT}{dt} = k \left(\frac{T_{\max} - T}{\Delta T_{\text{ad}}} \right)^n \Delta T_{\text{ad}} C_o^{n-1} \quad (4.8)$$

where $\left(\frac{dT}{dt}\right)$ is the self-heating rate at any temperature and time. This equation relates the measured temperature to the kinetic behavior of the system. For simplicity, Equation 4.8 can be rearranged as follows

$$k^* = k C_o^{n-1} = \frac{dT}{dt} \frac{(\Delta T_{\text{ad}})^{n-1}}{(T_{\max} - T)^n} \quad (4.9)$$

where k^* is a pseudo zero-order rate constant. This rearrangement utilizes the calorimetric thermal data of T , T_o , T_{\max} , dT/dt , and the reaction order to calculate a reaction rate. It is assumed that C_o , which is the reactant concentration at T_o , is almost the initial concentration. Also, it can be assumed that the reaction rate constant is consistent with the Arrhenius equation

$$k = A \exp\left(\frac{-E_A}{RT}\right) \quad (4.10)$$

where A is the constant frequency factor, E_A is activation energy (assumed independent of T), and R is the gas constant. Substituting Equation 4.10 into Equation 4.9, the following is derived

$$\log(k^*) = \log(A C_o^{n-1}) - \frac{E_A}{2.303 R T} \quad (4.11)$$

From this equation the Arrhenius parameters A and E_A , can be determined for the overall reaction. The plot of $\log(k^*)$ vs. $1/T$ yields a straight line where the slope is E_A and intercept is A .

Equation 4.9 can be integrated to calculate the adiabatic time to maximum rate of the exothermic reaction, TMR_{ad} . Applying the boundary conditions of time changing from any time, t , to the time at the maximum rate, t_{MR} , and the temperature changing from any temperature, T , to the temperature of the maximum self-heating rate, T_{MR} , will yield the following equation

$$\int_t^{t_{MR}} dt = \int_T^{T_{MR}} \frac{1}{k \Delta T_{ad}} C_o^{1-n} \left(\frac{\Delta T_{ad}}{T_{max} - T} \right) dT \quad (4.12)$$

Equation 4.12 can be integrated numerically, however, Townsend and Tou [60] showed that an approximate analytical solution could be achieved for any n^{th} order of reaction to yield the following equation

$$TMR_{ad} = \frac{R T^2}{\left(\frac{dT}{dt} \right)_T E_A} - \frac{R T_{MR}^2}{\left(\frac{dT}{dt} \right)_{T_{MR}} E_A} \quad (4.13)$$

In most cases, TMR_{ad} is used to calculate the time between the reaction onset temperature, T_o , and the maximum self-heating rate temperature, T_{MR} .

4.2. Thermal Inertia

Initially, we assumed that adiabatic conditions are maintained in these experiments; however, some of the heat generated will be lost due to heating the test cell. In this case, the system heat balance follows

$$m_s C_s \Delta T_{ad,adj} = (m_s C_s + m_c C_c) \Delta T_{ad,meas} \quad (4.14)$$

where m_s and C_s are the sample mass and heat capacity, m_c and C_c are the cell mass and heat capacity, $\Delta T_{ad,meas}$ is the overall system measured adiabatic temperature rise, and $\Delta T_{ad,adj}$ is the adjusted adiabatic temperature rise. From Equation 4.14 the thermal inertia factor, ϕ , is defined as

$$\phi = \frac{(m_s C_s) + (m_c C_c)}{(m_s C_s)} \quad (4.15)$$

and Equation 4.14 can be written as

$$\Delta T_{\text{ad,adj}} = \phi \Delta T_{\text{ad,meas}} \quad (4.16)$$

This factor is used to correct the thermodynamic measured and calculated parameters [56,60]. Under perfect adiabatic conditions ϕ has the value of 1. The inverse of thermal inertia, $1/\phi$, is commonly known as the degree of adiabaticity.

System temperatures are adjusted to new ϕ factors by equating the corrected adiabatic temperature rise of two different ϕ factors using Equation 4.16. This yields the following

$$T_2 = T_{o,2} + \left(\frac{\phi_1}{\phi_2} \right) (T_1 - T_{o,1}) \quad (4.17)$$

The measured values of temperature and self-heating rates are corrected for perfect adiabatic conditions using the calculated ϕ . At similar self-heating rates, there could be various system temperatures depending on the value of ϕ . The onset temperature of the reaction measured at any ϕ factor is adjusted to a new value at any ϕ using Equations 4.8 and 4.9 as follows

$$\left. \frac{dT}{dt} \right|_{\phi_1} = \left. \frac{dT}{dt} \right|_{\phi_2} \quad (4.18)$$

$$A \exp\left(\frac{-E_A}{RT_{\phi_1}}\right) \left(\frac{T_{\text{max},\phi_1} - T_{\phi_1}}{\Delta T_{\text{ad},\phi_1}}\right)^n \Delta T_{\text{ad},\phi_1} C_o^{n-1} = A \exp\left(\frac{-E_A}{RT_{\phi_2}}\right) \left(\frac{T_{\text{max},\phi_2} - T_{\phi_2}}{\Delta T_{\text{ad},\phi_2}}\right)^n \Delta T_{\text{ad},\phi_2} C_o^{n-1} \quad (4.19)$$

Substituting Equations 4.6 and 4.16 into Equation 4.19 yields an equation to adjust the reaction onset temperature at any ϕ

$$\frac{1}{T_{o,2}} = \frac{1}{T_{o,1}} + \frac{R}{E_A} \ln\left(\frac{\phi_1}{\phi_2}\right) \quad (4.20)$$

The self-heating rate can be adjusted to new ϕ factors by using the following equation

$$\left.\frac{dT}{dt}\right|_{\phi_2} = \left(\frac{\phi_1}{\phi_2}\right) \exp\left[\frac{E}{R}\left(\frac{1}{T_{\phi_1}} - \frac{1}{T_{\phi_2}}\right)\right] \left.\frac{dT}{dt}\right|_{\phi_1} \quad (4.21)$$

This equation is primarily used to adjust the measured maximum self-heating rates of reactions.

The maximum temperature reached and the overall heat of reaction are also corrected using this ϕ as follows

$$T_{\max} = T_{o,\text{adj}} + \phi \Delta T_{\text{ad,meas}} \quad (4.22)$$

$$\Delta H_r = m C_c \phi \Delta T_{\text{ad,meas}} \quad (4.23)$$

Finally the time to maximum reaction rate under adiabatic conditions is corrected. Wilcock and Rogers [56] suggests the following TMR_{ad} at $\phi = 1$ correction

$$TMR_{\text{ad,adj}} = \frac{TMR_{\text{ad,meas}}}{\phi} \quad (4.24)$$

CHAPTER V

THERMAL DECOMPOSITION OF DI-TERT-BUTYL PEROXIDE IN TOLUENE*

1. Précis

Organic peroxides are widely used in the chemical industry, especially the plastic industry, in processes for the manufacture of high polymers, polyesters, and natural rubbers. Generally, organic peroxides are used to initiate free radical reactions for performing polymerization, curing, and cross-linking reactions. Only low concentrations of peroxide in a monomer, resin, or compound are needed in these chemical processes to start a chain of free radical reactions.

The decomposition of peroxides into free radicals generally proceeds by thermally activated first-order unimolecular reaction due to the superficial cleavage of the weak oxygen-oxygen bond [91]. The thermal instability of the peroxides can cause safety problems. Peroxides decomposition reactions are highly exothermic with extreme self-heating rates. Such self-accelerating decomposition is accompanied by the formation of hot gaseous decomposition products and that can lead to thermal runaway [92].

* This chapter contains material reprinted from the Transactions of the Institution of Chemical Engineers: Part B, 80 (3), A. A. Aldeeb, W. J. Rogers, and M. S. Mannan, Theoretical and experimental methods for the evaluation of reactive chemical hazards, 141-149, Copyright (2002) and Process Safety Progress, 21 (4), M. S. Mannan, A. A. Aldeeb, and W. J. Rogers, Understanding the role of process chemistry in fires and explosions, 323-328, Copyright (2002).

To prevent peroxides thermal decomposition reactions during storage, transport, and handling, extensive safety precautions, primarily with respect to temperature control, are necessary. Traditionally, safe temperature margins of 10 – 20 °C for handling the peroxides are used. In the past, these safe temperature margins were determined by empirical methods based on experiments that were conducted to determine the self-accelerating decomposition temperature of the peroxides [92].

The above methodology of determining safe handling temperature of peroxide is certainly reliable, but impractical. For large-scale container scenarios, it was found that serious deviation from predicted temperatures are possible due to scale-up errors. Also this approach is unable to provide enough information about the amount and rate of energy that may be generated, or pressure behavior in case peroxide thermal decomposition reaction is initiated. To develop a more general approach for thermal stability evaluation of peroxides, a more through study is needed.

In this research, the systematic approach for evaluating reactive systems as presented in Chapter III is used to evaluate the thermal decomposition reaction of *di-tert*-butyl peroxide (DTBP) in toluene. DTBP is one of the most preferred dialkyl peroxides (R-OO-R') for generating free radicals for commercial applications. Molecular structure and physical properties of DTBP are presented in Figure 5.1. The main aim of this evaluation is to identify thermal decomposition reaction stoichiometries in toluene and estimate thermodynamic and kinetic parameters of potentially hazardous reactions. Computational quantum chemistry methods and thermodynamic-energy correlations are used to investigate the reaction stoichiometry and heat of reaction to predict the most

dominant and hazardous reaction pathways. Screening thermal analysis testing using the RSST™, heat flow thermal analysis using the C80D, and adiabatic thermal analysis using the APTAC™ calorimeters were performed to evaluate thermodynamic and kinetic parameters of this system.

$\begin{array}{c} \text{CH}_3 \\ \\ \text{H}_3\text{C} - \text{C} - \text{O} - \text{O} - \text{C} - \text{CH}_3 \\ \qquad \qquad \\ \text{CH}_3 \qquad \qquad \text{CH}_3 \end{array}$	
Molecular formula	C ₈ H ₁₈ O ₂
CAS number	110-05-4
Molecular mass	146.2
Boiling point	111 °C
Melting point	-40°C
Specific gravity	0.8
Solubility in water	None
Vapor pressure at 20°C	2.6 kPa
Flash point	12°C
Relative vapor density (air = 1)	5

Figure 5.1. *Di-tert*-butyl peroxide molecular structure and physical properties

2. Application of the Systematic Approach

Thermal decomposition of DTBP is one of the most extensively studied kinetic systems. It can be characterized by its simple first-order kinetic behavior and wide range of applications in process chemistry. However, DTBP has been involved in a number of incidents due to its vigorous decomposition behavior [93,94]. Because of its simplicity, applications, and involvement in reactive chemicals incidents, DTBP solution in toluene was selected as the first reactive system to be investigated by applying the systematic approach for chemical reactivity evaluation.

The evaluation of chemical reactivity hazards of DTBP decomposition must be based on essential information, which includes possible operating scenarios, storage and handling conditions, process chemistry mechanisms, and parameters for quantifying reactive chemical hazards.

Defining these conditions and parameters will help to simulate a chemical process for optimum safe and economical operating, storage, and handling conditions. Laboratory testing has been the traditional approach to evaluate chemical reactivity of peroxides in general, and DTBP in particular. As discussed earlier, the experimental approach is practical for simple systems, but may not be applicable for more complex systems. Because of the large number of chemical compounds and different reaction scenarios, evaluation can be very expensive and time consuming. Moreover, for complex reactive system with more than one reaction pathway, experimental procedures will provide an overall evaluation of system thermokinetic data, but will not explain

reaction stoichiometry. In fact, system analysis is required beyond laboratory measurements.

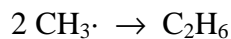
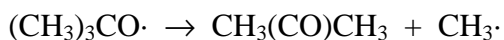
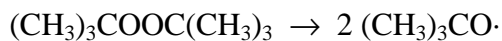
In this research, the suggested systematic approach for chemical reactivity evaluation is applied to understand the reaction chemistry, identify exothermic activity, and pressure behavior of the thermal decomposition of DTBP in toluene at different concentrations. This understanding is based on predicting dominant reaction pathways and then applying various experimental techniques to justify the thermodynamic, kinetic, and pressure behavior of the decomposition reaction of DTBP in toluene.

3. Pre-screening Evaluation

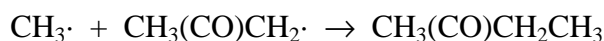
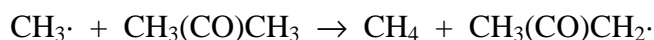
Literature and database search for relevant data of the various substances in the chemical system is the first step in the systematic approach. Relevant data include physical and chemical properties, thermodynamics, kinetics, incidents, and case studies as discussed in Chapter III.

The major goal of reviewing some of the previous studies on DTBP thermal decomposition was to suggest the decomposition reaction pathways. Although the possible reaction pathways are many, literature information can be used to help select the most probable scenarios.

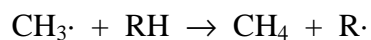
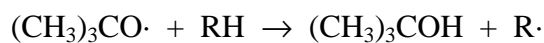
Milas and Surgenor [95] have studied the nature of the thermal decomposition of DTBP in the gas phase. The pyrolysis of DTBP at temperatures between 200 and 300 °C suggests that the only products formed under these conditions are acetone and ethane. On the basis of these results the following reaction mechanism was adopted:



The above mechanism gained further support from the extensive studies of Raley et al. [96,97], Rust et al. [98], and Murwaski et al. [99]. This mechanism clearly indicates that the decomposition of DTBP in the vapor phase is a clean-cut, homogeneous, first-order process, and the rate-determining step is the scission of the peroxy-oxygen linkage to form the *t*-butoxy radicals. The resultant radicals can react with co-present molecules according to the steps: chain initiation, propagation, and termination. Raley and coworkers [96] suggested that the interaction between the alkyl radical and the ketone might become important. Thus, methyl, ethyl, and higher ketones and methane can also be formed

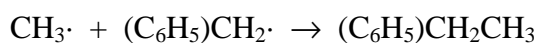
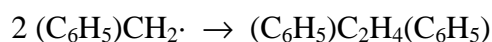
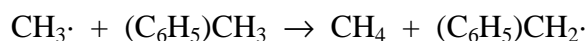


The decomposition of DTBP in the condensed phase and in various organic solvents was also extensively evaluated. Raley et al. [97] indicated that the reaction mechanism of the condensed-phase decomposition would be the same as that in the vapor phase. Likewise the energies of activation in solution and vapor are approximately equivalent. In the presence of an organic solvent, they indicated that the formed *t*-butoxy and alkyl radicals will react with solvent molecules as follows



In this mechanism, RH denotes a molecule of the solvent. The validity of all these assumed mechanisms was confirmed by isolating respective molecules and dimers experimentally.

Murawski and coworkers [99] studied the decomposition of DTBP in the presence of excess toluene using static and flow system with temperatures ranging from 120 to 280 °C. They indicated that in the presence of excess toluene both methane and ethane are produced, and that the relative amounts depend on the toluene to peroxide ratio. In that study it was suggested that the formed methyl radical will react with toluene as follows



These results and several other studies [100–104] were used to establish an overall possible DTBP in toluene decomposition pathways as shown in Figure 5.2.

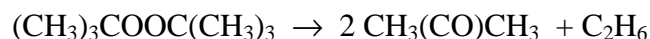
4. Computational Models

Applying computational quantum chemistry methods for each molecule of the different pathways in Figure 5.2 permits estimation of the enthalpy of formation and the ideal absolute entropy. Applying these results, the Gibbs free energy (ΔG_r) and the

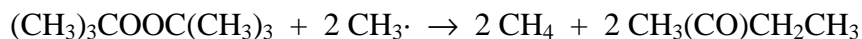
enthalpy (ΔH_r) of each proposed reaction were calculated in the ideal gas phase. From these calculations, we focus on the thermodynamically feasible pathways ($\Delta G_r < 0$) and the most exothermic stoichiometries. At the same time, possible reaction pathways that may lead to high-pressure increases should be considered. In this study, various levels of computational quantum chemistry calculations were performed including semi-empirical (AM1), Hartree-Fock (HF), Density Functional Theory (DFT) B3LYP level, Complete Basis Set (CBS-4M) and Gaussian-2 (G2).

From the suggested reaction pathways in Figure 5.2, six major reaction pathways can be identified as follows

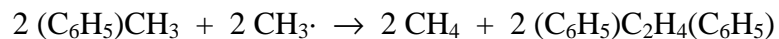
Pathway I:



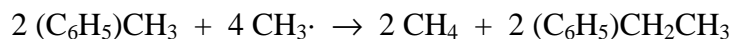
Pathway II:



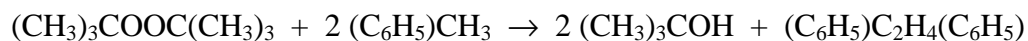
Pathway III:



Pathway IV:



Pathway V:



Pathway VI:



The Gibbs free energy of system components calculated using the four levels of theory are presented in Table 5.1. A summary of the reaction Gibbs free energy, ΔG_r , for the nine elementary reactions in the system is presented in Table 5.2. These Gibbs free energies of reaction, ΔG_r , represent the ideal gas phase. The solvent and mixture interaction contributions are usually small when compared to the ideal gas contribution and are significant only when the solvent has particularly strong affinities with the solutes [38]. Therefore, these effects were neglected.

Table 5.1

Gibbs free energy of DTBP decomposition components calculated using four levels of theory

Component	Gibbs free energy of component (Hartree/particle)*			
	AM1	HF/6-31G(d)	B3LYP/6-31G(d)	CBS-4M
$(\text{CH}_3)_3\text{COOC}(\text{CH}_3)_3$	0.134250	-462.824674	-465.855835	-465.354488
$(\text{CH}_3)_3\text{CO}\cdot$	0.059371	-231.435506	-232.912551	-232.651984
$\text{CH}_3\cdot$	0.059778	-39.546259	-39.826612	-39.7787390
$\text{CH}_3(\text{CO})\text{CH}_3$	-0.021236	-191.900542	-193.100242	-192.889734
C_2H_6	0.023135	-79.172062	-79.778294	-79.686102
CH_4	0.012973	-40.164692	-40.490499	-40.446502
$\text{CH}_3(\text{CO})\text{CH}_2\cdot$	0.019072	-191.296472	-192.452807	-192.230806
$\text{CH}_3(\text{CO})\text{CH}_2\text{CH}_3$	-0.006152	-230.907802	-232.388196	-232.130923
$(\text{C}_6\text{H}_5)\text{CH}_3$	0.123886	-269.633338	-271.468858	-271.118746
$(\text{CH}_3)_3\text{COH}$	-0.008269	-232.036556	-233.563790	-233.326697
$(\text{C}_6\text{H}_5)\text{CH}_2\cdot$	0.147693	-269.017050	-270.809062	-270.452198
$(\text{C}_6\text{H}_5)_2\text{C}_2\text{H}_4(\text{C}_6\text{H}_5)$	0.257020	-538.105400	-541.731711	-541.036828
$(\text{C}_6\text{H}_5)\text{CH}_2\text{CH}_3$	0.140106	-308.638699	-310.754830	-310.360826

* Hartree/particle = 627.51 kcal/mol

Table 5.2

Gibbs free energy of elementary reactions of DTBP decomposition calculated using four levels of theory

Reaction	Gibbs free energy of reaction, ΔG_r , (kcal/mol)			
	AM1	HF/6-31G(d)	B3LYP/6-31G(d)	CBS-4M
i	-9.7	-29.1	19.3	31.7
ii	-13.1	-7.1	-9.0	-10.3
iii	-60.5	-49.9	-78.5	-80.7
iv	-4.1	-9.0	-10.3	-5.5
v	-53.3	-40.8	-68.3	-76.2
vi	-27.5	9.6	5.4	-5.1
vii	-24.1	-44.7	-71.3	-83.1
viii	-42.3	-47.3	-74.8	-81.5
ix	-14.4	-1.3	-2.6	-0.8

Table 5.3

Gibbs free energy of DTBP decomposition pathways calculated using four levels of theory

Reaction Pathway	Gibbs free energy of reaction pathway, ΔG_r , (kcal/mol)			
	AM1	HF/6-31G(d)	B3LYP/6-31G(d)	CBS-4M
I	-96.4	-93.2	-77.2	-69.7
II	-150.7	-142.9	-155.8	-152.4
III	-52.9	-47.4	-76.4	-84.6
IV	-113.4	-97.3	-154.7	-164.5
V	-88.8	-54.7	-41.3	-61.7
VI	-149.3	-104.6	-119.5	-141.6

Based on these results, we found that all the proposed reactions pathways are thermodynamically feasible ($\Delta G_r < 0$) as presented in Table 5.3. The enthalpies of system components were also calculated and are presented in Table 5.4. Reaction enthalpies, ΔH_r , for the nine elementary reactions in the system are presented in Table 5.5. Also enthalpies of reaction pathways were calculated and summarized in Table 5.6.

Table 5.4

Enthalpy of DTBP decomposition components calculated using four levels of theory

Component	Enthalpy of component (Hartree/particle)*			
	AM1	HF/6-31G(d)	B3LYP/6-31G(d)	CBS-4M
$(\text{CH}_3)_3\text{COOC}(\text{CH}_3)_3$	0.187724	-462.775896	-465.855835	-465.298458
$(\text{CH}_3)_3\text{CO}\cdot$	0.099034	-231.399154	-232.875561	-232.614763
$\text{CH}_3\cdot$	0.081713	-39.523837	-39.804432	-39.756479
$\text{CH}_3(\text{CO})\text{CH}_3$	0.011484	-191.866167	-193.065253	-192.855528
C_2H_6	0.050992	-79.144651	-79.750773	-79.658502
CH_4	0.034161	-40.143599	-40.469367	-40.425399
$\text{CH}_3(\text{CO})\text{CH}_2\cdot$	0.053406	-191.262649	-192.418298	-192.196313
$\text{CH}_3(\text{CO})\text{CH}_2\text{CH}_3$	0.032923	-230.870016	-232.349982	-232.093169
$(\text{C}_6\text{H}_5)\text{CH}_3$	0.159095	-269.596429	-271.431177	-271.083658
$(\text{CH}_3)_3\text{COH}$	0.029647	-232.000646	-233.527113	-233.289878
$(\text{C}_6\text{H}_5)\text{CH}_2\cdot$	0.184265	-268.981001	-270.772826	-270.415888
$(\text{C}_6\text{H}_5)\text{C}_2\text{H}_4(\text{C}_6\text{H}_5)$	0.310848	-538.053692	-541.678705	-540.984272
$(\text{C}_6\text{H}_5)\text{CH}_2\text{CH}_3$	0.180957	-308.599049	-310.714551	-310.320711

* Hartree/particle = 627.51 kcal/mol

Table 5.5

Enthalpy of elementary reaction of DTBP decomposition calculated using four levels of theory

Reaction	Enthalpy of reaction, ΔH_r , (kcal/mol)			
	AM1	HF/6-31G(d)	B3LYP/6-31G(d)	CBS-4M
i	6.5	-14.6	31.8	43.3
ii	-3.7	5.7	3.7	1.7
iii	-70.6	-60.9	-89.0	-91.3
iv	-3.5	-10.2	-11.3	-6.1
v	-64.1	-52.4	-79.8	-88.1
vi	-27.7	8.7	4.3	-4.6
vii	-36.2	-57.5	-83.5	-95.7
viii	-53.4	-59.1	-86.2	-93.1
ix	-14.0	-2.7	-4.1	-0.7

Table 5.6

Enthalpies of DTBP decomposition pathways calculated using four levels of theory

Reaction Pathway	Enthalpies of reaction pathway, ΔH_r , (kcal/mol)			
	AM1	HF/6-31G(d)	B3LYP/6-31G(d)	CBS-4M
I	-71.4	-63.4	-49.8	-44.6
II	-136.2	-127.8	-143.1	-141.6
III	-64.3	-63.0	-91.8	-97.1
IV	-134.8	-123.7	-180.6	-187.6
V	-85.2	-54.1	-43.1	-61.7
VI	-155.7	-114.8	-131.9	-152.1

To predict the dominant reaction pathway, Polanyi and Marcus equations as presented in Chapter III, were applied to calculate the elementary reaction activation energies. The intrinsic barriers of the reactions, E_A° , and the transfer coefficients, γ_P , were obtained from literature [72] for the simple bond scission, recombination, and atom transfer reactions. Enthalpies of reactions calculated using high levels of theory, B3LYP/6-31G(d) and CBS-4M, were used in calculating the activation energies of the elementary reactions. Summary of calculation results are presented in Tables 5.7 and 5.8.

Table 5.7

Activation energy of DTBP decomposition elementary reactions calculated using the Polanyi and Marcus equations and the B3LYP/6-31G(d) enthalpy of reaction

Reaction	Transfer coefficient, γ_P	Intrinsic activation energy, E_A° (kcal/mol)	Activation energy of reaction, E_A (kcal/mol)	
			Polanyi Equation	Marcus Equation
i	1	1	32.8	80.3
ii	1	1	4.7	3.7
iii	0	1	1	---
iv	0.3	12	8.6	7.0
v	0	1	1	---
vi	0.3	12	13.3	14.2
vii	0	1	1	---
viii	0	1	1	---
ix	0.3	12	10.8	10.0

Table 5.8

Activation energy of DTBP decomposition elementary reactions calculated using the Polanyi and Marcus equations and the CBS-4M enthalpy of reaction

Reaction	Transfer coefficient, γ_P	Intrinsic activation energy, E_A° (kcal/mol)	Activation energy of reaction, E_A (kcal/mol)	
			Polanyi Equation	Marcus Equation
i	1	1	44.3	139.6
ii	1	1	2.7	2.1
iii	0	1	1	---
iv	0.3	12	10.2	9.2
v	0	1	1	---
vi	0.3	12	10.6	9.8
vii	0	1	1	---
viii	0	1	1	---
ix	0.3	12	11.78	11.64

It should be noted that applying the Marcus equation with recombination elementary steps as in Reactions iii, v, vii, and viii (with $\gamma_P = 0$), the predicted activation energy had led to unrealistic values, hence, the Polanyi equation was found to be more reliable in this comparison.

According to the results in Tables 5.7 and 5.8, we can predict that Pathway I products will probably be the main products of DTBP decomposition in toluene. In other words, Pathway I is the dominant reaction pathway. This very important conclusion is based on the following discussion:

The formation of free radicals $(\text{CH}_3)_3\text{CO}\cdot$ in the elementary reaction (i) will be the rate-determining step of DTBP decomposition, and then free radicals $(\text{CH}_3)_3\text{CO}\cdot$ will proceed through elementary reactions (ii) and (vi). However, elementary reaction (ii)

has lower activation energy compared to elementary reaction (vi) based on both Polanyi and Marcus equations. Assuming similar reaction rates, the ratio of free radicals $(\text{CH}_3)_3\text{CO}\cdot$ that will react to form methyl free radical $[\text{CH}_3\cdot]$ and acetone $[\text{CH}_3(\text{CO})\text{CH}_3]$ through elementary reaction (ii) is expected to be higher than the ratio that will react with a toluene molecule $[(\text{C}_6\text{H}_5)\text{CH}_3]$ according to elementary reaction (vi) to form isobutanol $[(\text{CH}_3)_3\text{COH}]$ and free radical $(\text{C}_6\text{H}_5)\text{CH}_2\cdot$. Proceeding through elementary reaction (ii), formed methyl radical $[\text{CH}_3\cdot]$ may react through elementary reactions (iii), (iv), (viii) and (ix). Comparing the calculated activation energies of these reactions we find that elementary reactions (iii) and (viii) are more dominant as compared to elementary reactions (iv) and (ix). However methyl radical reaction via elementary reaction (viii) may be excluded because its occurrence will depend directly on elementary reactions (vi) and (ix) and those two elementary steps were assumed to have a negligible share of the reacting free radical $(\text{CH}_3)_3\text{CO}\cdot$.

Based on these expectations, Pathway II products methane $[\text{CH}_4]$ and butanone $[\text{CH}_3(\text{CO})\text{CH}_2\text{CH}_3]$ will form in a very small amount because their formation directly depends on the occurrence of reaction (iv). The same conclusions are valid for Pathways III, IV, V, and VI. The formation of methane $[\text{CH}_4]$, bibenzyl $[(\text{C}_6\text{H}_5)_2\text{C}_2\text{H}_4]$, ethylbenzene $[(\text{C}_6\text{H}_5)\text{CH}_2\text{CH}_3]$, and isobutanol $[(\text{CH}_3)_3\text{COH}]$ will be limited.

According to this analysis Pathway I may be considered as the primary (dominant) reaction pathway in the decomposition of DTBP in the presence of toluene as a solvent.

These expectations agree with the findings of Milas and Surgenor [95], that acetone and ethane are the only products of DTBP decomposition in the gas phase at 250°C and

it confirms that the DTBP primary decomposition mechanisms in the gas and condensed phases are the same. In different studies [96,98], it was concluded that Pathway I is the main pathway of the decomposition reaction of DTBP, although some of the methyl free radicals may react with the acetone. Rust et al. [96] found that no more than 5 to 10 % of the methyl free radicals will react with acetone, and the majority will follow elementary reaction (ii) stoichiometry. In fact, the conclusion that Pathway I is the main pathway of DTBP decomposition is consistent with experimental findings of pressure increase. It was found [96] that the final pressure relationship is

$$\text{Final pressure} = 2.88 \times \text{initial pressure} \quad (5.1)$$

According to the theoretical analysis based on Pathway I, it is expected to have a final pressure that is approximately three times the initial pressure due to formation of two moles of acetone and one mole of ethane. The slight deviation from this experimental value would be expected due to other possible but minor reaction pathways.

According to this analysis, an estimation of enthalpy of reaction based on the Pathway I scenario was also calculated using the G2 level of theory and the Benson group contribution method from the ASTM CHETAHTM program. A summary of the results is presented in Table 5.9.

In our calculations of enthalpy of reaction, the heats of vaporization of DTBP and toluene were not included. The heats of vaporization of DTBP and toluene at 25°C are 9.49 and 9.16 kJ/mol, respectively [105]. These values do not represent the actual values because temperature, pressure, and composition change throughout the reaction.

Not including these values in our calculation will yield an estimated heat of reaction for DTBP alone that is higher than that measured for DTBP with toluene. Therefore, each measured (ΔH_r) reported here is for DTBP with toluene and includes the heats of vaporization. In the following experimental evaluation sections, overall heat of reaction will be corrected for the heat of vaporization effects.

Table 5.9

Enthalpy of DTBP decomposition calculated with six levels of theory for the Pathway I

Level of theory	Enthalpy of reaction, ΔH_r , (kcal/mol)
AM1	-71.4
HF/6-31G(d)	-63.4
B3LYP/6-31G(d)	-49.8
CBS-4M	-44.6
G2	-47.0
Benson group contribution method (CHETAH™)	-42.2

As the previous results show, the calculation method selection is a major factor in determining the quality of the calculated values. AM1 and HF/6-31G(d) are known to be of lower quality and less expensive methods, whereas B3LYP/6-31G(d), CBS-4M and G2 are known as higher quality and more expensive methods.

As shown in Table 5.9, the Benson group contribution method provides a value of ΔH_r , which differs by about 7.6, 2.4, and 4.8 kcal/mol from the values, calculated using

B3LYP/6-31G(d), CBS-4M, and G2, respectively, which are assumed to be more accurate for this evaluation. However, AM1 and HF/6-31G(d) results deviated by about 29.2 and 21.2 kcal/mol, respectively. These observations indicate the importance of selecting the computational model for predicting accurate thermodynamic parameters. More information on deviations of predicted values from experimentally measured values is available in the literature [81]. However for relative properties and thermodynamic predictions, the level of computational method will not be that critical. For example, when comparing elementary reactions based on their thermodynamic feasibility and activation energies we would find that no matter what was the level of theory applied, the same trend of relative properties would be achieved and this will give the advantage to the low cost computational methods (AM1, HF/6-31G(d)) over the more expensive ones (B3LYP/6-31G(d), CBS-4M, G2). Sometimes the computational modeling can be highly expensive compared to experimental analysis. However, the expense of computation depends on the molecular size, property to be predicted, and the accuracy level required.

Based on this systematic approach of reactivity evaluation, the stoichiometry of DTBP decomposition as estimated using the computational level should be verified using experimental analysis, which was performed on the screening and advanced levels and in parallel with the computational analysis of this system.

5. Experimental Analysis

Most safety and reactive chemical hazard estimations are based on the exact characterization of a reactive system. Experimental analysis is performed when the

theoretical approach indicates a potential for exothermal activity or high-pressure generation and for more exact parameter determinations. Up to this point, theoretical computational methods can help to exclude non-hazardous reaction pathways, indicate exothermic reactions, and predict reliable stoichiometric, thermodynamic, and sometimes kinetic parameters. Such knowledge helps guide the experimental investigations.

Following a review of the literature, the screening experimental analysis of the thermal decomposition of DTBP in toluene using the RSST™ was performed and in parallel to the previous theoretical computational evaluation. Following that, a detailed thermal analysis using the C80D and the APTAC™ calorimeters were conducted. In this section the results of both screening and detailed thermal analyses of the decomposition of DTBP in toluene system will be presented and discussed.

5.1. Materials

Aldrich 98% DTBP and Merck 99.5% toluene were used to prepare 30, 50, and 60 wt.% DTBP in toluene solution samples for testing. In another stage of thermal analysis, Matheson Coleman and Bell 99.5% benzene was used as an alternative solvent to confirm the results of the DTBP-toluene analysis. DTBP, toluene, and benzene were used with no additional purification or treatment processes. Samples were prepared at the same day of testing. High purity compressed nitrogen was used in the RSST™ and APTAC™ experiments to reduce liquid boil-off and to backup the cell, respectively.

5.2. Apparatus

Thermal analysis of these samples was performed using three calorimeters: RSST™, C80D, and APTAC™. A detailed description of each of these calorimeters, operating procedures, and data quality presented in detailed in Chapter IV.

5.3. Data Analysis

Experimental data analysis was performed on the time-temperature-pressure data that were collected. Thermodynamic and kinetic parameters of the suggested reaction pathways were calculated according to the methods and procedures presented in Chapter IV and later in this chapter.

5.4. RSST™ Thermal Analysis

Initially testing a solution of DTBP in toluene using the RSST™ showed a highly exothermic reactivity. A stoichiometric explanation could not be achieved based on this testing alone. To further understand this behavior, reaction stoichiometry analysis was performed.

Experimental screening analysis using the RSST™ was performed for 30, 50, and 60 wt.% DTBP in toluene. Initially DTBP and toluene were mixed, and then sample masses of 8.0 to 9.6 g were placed in the RSST™ glass cell for testing. Sample solutions were tested under a nitrogen backup pressure of about 250 psig to reduce liquid boil-off before decomposition, except for Sample 30a that was tested under nitrogen pressure of about 300 psig. The sample and glass cell mass produce a thermal inertia factor, ϕ , of

about 1.03. Several temperature ramping rates of 0.8 to 2.1 °C/min were applied. Stirring was present during the experiments and it was kept at a constant speed for all the experimental runs. Table 5.10 presents a summary of the tested samples parameters.

Temperature and pressure profiles during the DTBP in toluene decomposition are shown in Figures 5.3 and 5.4, respectively. Clearly these profiles indicate an exothermic reactivity and a rapid pressure increase. Temperature and pressure profiles also show similar behavior of reaction onset temperature irrespective of the sample DTBP concentration and heating rate. A summary of the experimental data for the tested samples is presented in Table 5.11.

Table 5.10
Summary of the RSST™ DTBP in toluene samples

Sample	DTBP wt. %	Sample weight (g)	Cell weight (g)	Temperature ramping rate (°C/min)
30a	30	8.45	1.38	2.14
30b	30	8.87	1.25	0.76
30c	30	8.57	1.51	1.28
30d	30	8.03	1.54	1.44
30e	30	9.39	1.43	1.57
50a	50	8.84	1.26	1.51
50b	50	9.22	1.36	1.09
50c	50	9.19	1.43	1.44
60a	60	9.11	1.34	0.76
60b	60	9.08	1.46	1.58
60d	60	9.27	1.25	1.10

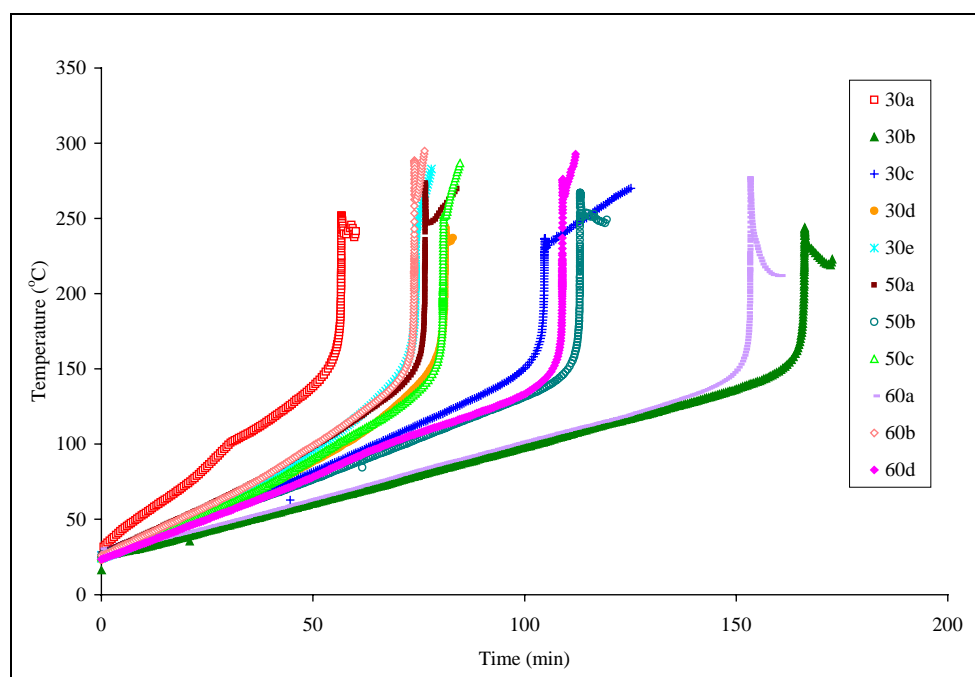


Figure 5.3. DTBP decomposition in toluene temperature profiles using the RSST™

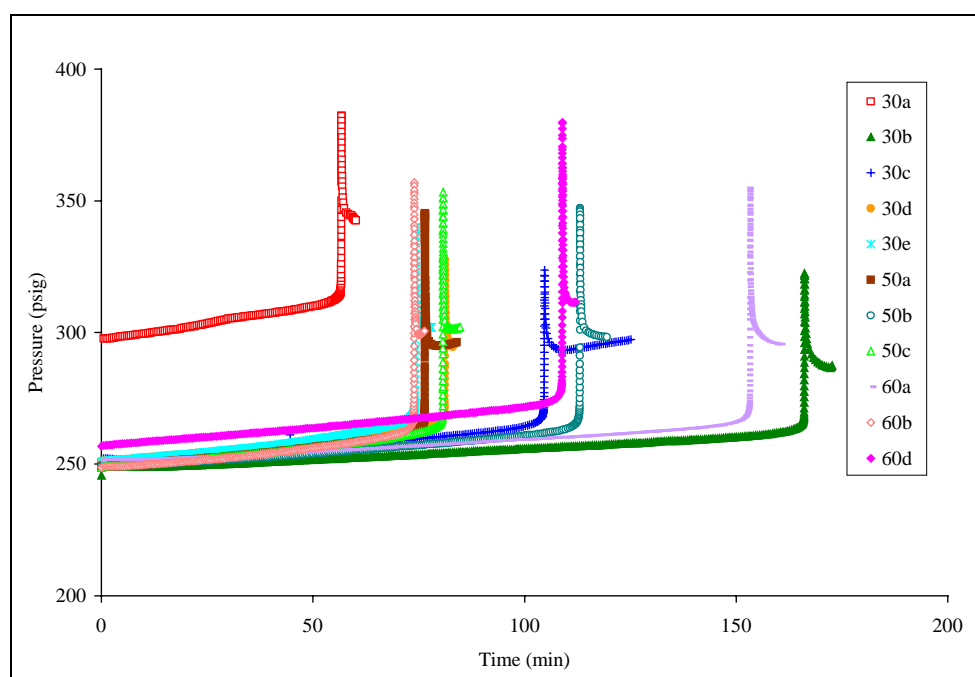


Figure 5.4. DTBP decomposition in toluene pressure profiles using the RSST™

Table 5.11

Experimental results of DTBP decomposition in toluene with the RSST™

Sample	T_o (°C)	T_{max} (°C)	ΔT_{ad} (°C)	ϕ -Factor	C_s (cal/(g · K))	C_c (cal/(g · K))
30a	133	252	119	1.03	0.573	0.105
30b	134	244	110	1.03	0.564	0.104
30c	125	237	112	1.03	0.554	0.104
30d	120	244	124	1.04	0.558	0.105
30e	120	250	130	1.03	0.564	0.106
50a	118	273	155	1.02	0.613	0.105
50b	135	267	132	1.03	0.613	0.104
50c	119	258	139	1.03	0.597	0.104
60a	128	277	149	1.03	0.636	0.105
60b	125	288	163	1.03	0.648	0.104
60d	135	276	141	1.02	0.638	0.104

The heat capacities of the sample solution, C_s , as in Table 5.11 were estimated at an average temperature of reaction onset temperature, T_o , and the maximum reaction temperature achieved, T_{max} . This estimate also considered the proportion of DTBP and toluene in each sample and was based on the correlations available in literature [105]. The heat capacities of the glass test cell, C_c , were provided by the manufacturer and estimated at the same average temperatures. Implicitly we assumed that the change in average heat capacity during the decomposition reaction is negligible. In fact, heat capacity estimation is one of the main sources of uncertainty in the estimated heat of reaction because of continuous temperature and composition changes during the experiment.

The heat of the decomposition reaction of DTBP in toluene is calculated using the following equation

$$\Delta H_r = \frac{\phi C_s (T_{\max} - T_o)}{x} \quad (5.2)$$

where, ϕ is thermal inertia factor as described in Equation 4.18 and x is the DTBP mass fraction the sample solution.

Equation 5.2 gives the overall heat of reaction adjusted to pure DTBP sample. This adjustment allows comparison of the overall heat of reaction of different solution concentrations on the same basis. In addition, this adjustment allows comparison of the findings of this study with the results of other researchers.

Experimental data analysis, as presented in Chapter IV, was conducted on the RSST™ data. A first-order kinetic model was assumed to fit the DTBP decomposition in toluene. The reaction rate constant, k , can be calculated using

$$k = \frac{\left(\frac{dT}{dt}\right) - (\text{RSST}^{\text{TM}} \text{ temperature ramping rate})}{(T_{\max} - T)} \quad (5.3)$$

Substituting the experimental value of k from Equation 5.3 into the Arrhenius expression as in Equation 4.10 yields the following equation

$$\log(k) = \log(A) - \frac{E_A}{2.303 R T} \quad (5.4)$$

which is used to estimate the Arrhenius parameters of activation energy and frequency factor. Experimental rate constant, reaction order, activation energy, and frequency

factor are the required information to evaluate the reaction kinetics. The plot of $(-\log k)$ vs. $(1/T)$ for the thermal decomposition of all tested DTBP in toluene samples is presented in Figure 5.5. This plot validates the assumed first-order reaction kinetic model with an average linear fitting regression coefficient of 0.996. Table 5.12 summarizes the onset temperatures, heats of reaction, reaction order, and Arrhenius parameters determined from the RSST™ data.

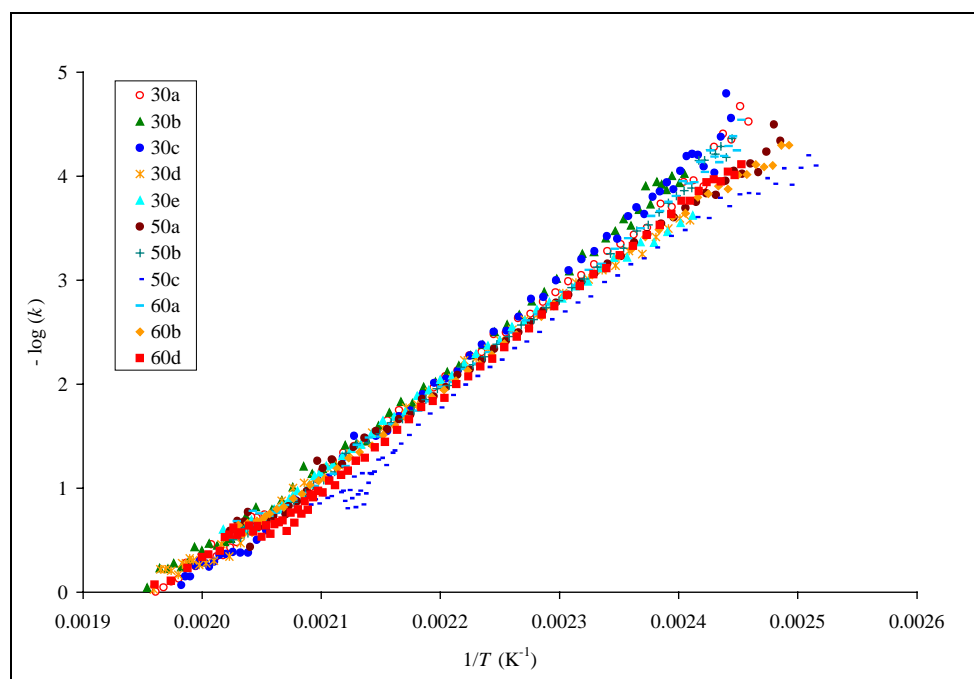


Figure 5.5. First-order kinetics of DTBP decomposition in toluene with the RSST™

Table 5.12

Summary of the RSST™ thermodynamic and kinetic parameters of DTBP decomposition in toluene

DTBP Conc. (wt.%)	T_o (°C)	ΔH_r (kcal/mol)	Reaction order, n	E_A (kcal/mol)	$\log(A)$ (s ⁻¹)
30	126 ± 7	-33.6 ± 2.5	1	40.2 ± 2.8	17.3 ± 1.3
50	124 ± 10	-25.9 ± 2.3	1	39.6 ± 2.0	17.2 ± 0.9
60	129 ± 5	-24.2 ± 2.0	1	39.6 ± 2.0	17.1 ± 0.9

Reaction kinetics of the exothermic decomposition reaction is also presented in the self-heating rate plot shown in Figure 5.6. Self-heating rates of the RSST™ samples were calculated using the following equation

$$\text{Self-heating rate} = (\text{measured heating rate}) - (\text{temperature ramping rate}) \quad (5.5)$$

In Figure 5.6, the three samples have the same sample size and ϕ factor, but have different DTBP concentrations. Clearly, as the DTBP concentration increases, the maximum self-heating rate also increases. Also a slight increase in the self-heating rate is measured with increasing DTBP concentration. A deviation in the 50% and 60% sample self-heating rate curves peak is not noticed with the 30% samples.

The differences in behavior could be due to the vaporization of the solvent (toluene) that occurs due to the rapid increase in the sample temperature. Because the RSST™ test is an open cell experiment, large quantities of the solvent are vaporized into the larger RSST™ container causing the self-heating rate to be reduced. This phenomenon is evident with higher DTBP concentration samples (50% and 60% samples) because the released energy of reaction is larger causing a rapid vaporization rate that could be

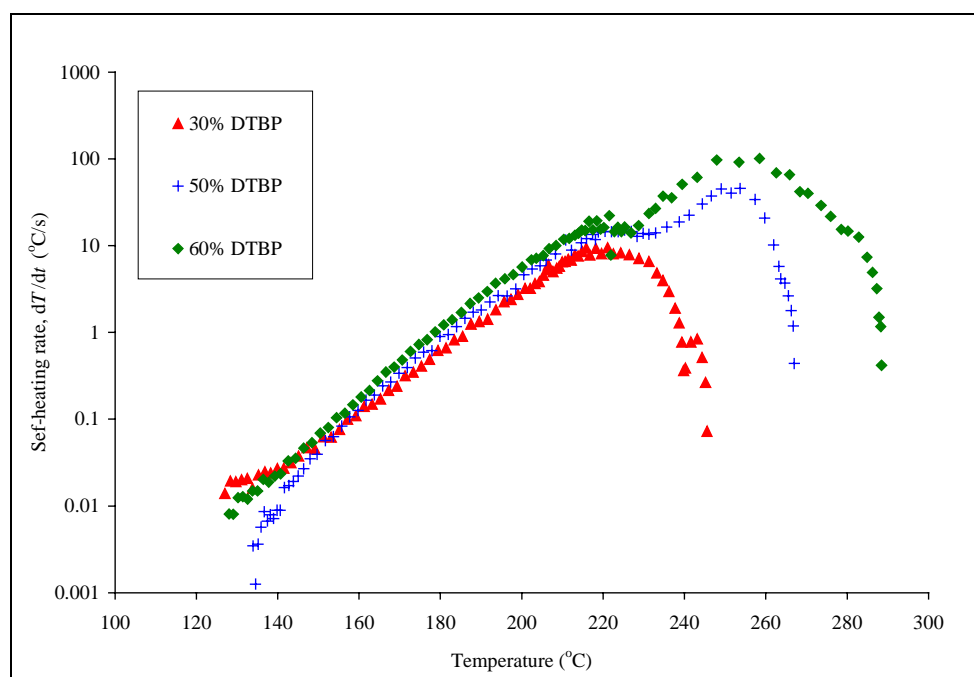


Figure 5.6. Self-heating rate of DTBP decomposition in toluene using the RSST™

measured easily with the RSST™. This possible elucidation of this phenomenon is justified in the APTAC™ thermal analysis results in this chapter. Pressurization rate is also measured with the RSST™ and presented in Figure 5.7. The pressurization rate behavior was similar to the self-heating rate. However, no reduction in the pressurization rate was detected in any of the samples or concentrations because solvent vaporization keeps adding to the overall pressurization rate. Values of maximum self-heating and pressurization rates are presented in Table 5.13. Several parameters affect these rates such as thermal inertia factor, sample size, and concentration.

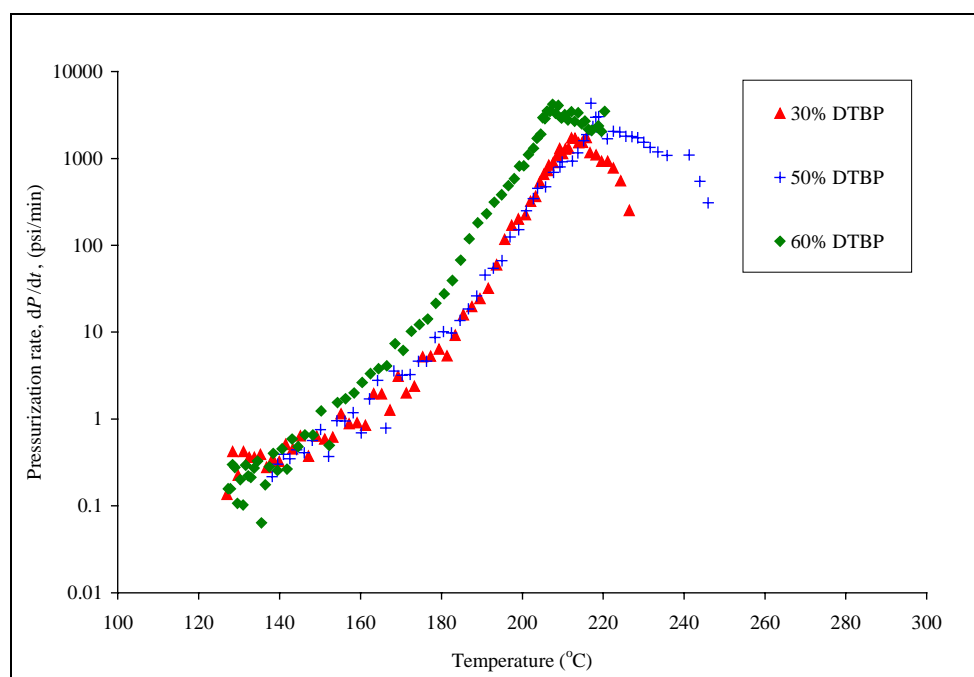


Figure 5.7. Pressurization rate of DTBP decomposition in toluene using the RSST™

Table 5.13

Maximum self-heating and pressurization rates of DTBP decomposition in toluene using the RSST™

Sample	Sample weight (g)	ϕ -Factor	$(dT/dt)_{\max}$ (°C/s)	$(dP/dt)_{\max}$ (psi/min)
30a	8.45	1.03	16	2015
30b	8.87	1.03	8	1185
30c	8.57	1.03	8	957
30d	8.03	1.04	10	1693
30e	9.39	1.03	9	1732
50a	8.84	1.02	53	4290
50b	9.22	1.03	46	2265
50c	9.19	1.03	11	3455
60a	9.11	1.03	61	2855
60b	9.08	1.03	101	3484
60d	9.27	1.02	43	4203

5.5. C80D Thermal Analysis

Overall heat of reaction can be measured more accurately by using a heat flux calorimeter. Applying heat flux thermal analysis technique reduces the heat losses associated with the exothermic reaction. Also it reduces the dependency on temperature measurement and sample heat capacity variations.

Reaction heat flux analysis using the C80D calorimeter was performed for 30, 50, and 60 wt.% DTBP in toluene to measure a more accurate heat of reaction to be compared with those values determined by the RSST™ and APTAC™ calorimeters. Similar to the RSST™ sample preparation, initially DTBP and toluene were mixed, and then sample masses of 500 mg were placed in the C80D 1-mL glass cell for testing. For thermal analysis, application of lower scanning rates usually detects earlier reaction onset temperatures. In this reaction heat flux analysis, a scanning rate of 0.1°C/min was applied for 1800 min. Heat flux, pressure, and pressurization rate data were collected for each experiment. Figure 5.8 shows the heat flow rate of each of the tested concentrations. As the DTBP concentration increases, the heat flux also increases. Also from Figure 5.8, reaction onset temperature is measured at the point the heat flux curve deviates from the temperature-scanning baseline. Integrating the area under each of the heat flow curves yields the overall heat of reaction. Figure 5.9 presents the pressurization rate of samples throughout the decomposition reaction. The increase in pressurization rate with increasing DTBP concentration is expected since larger DTBP concentration is associated with larger reaction energy release. Table 5.14 summarizes the onset temperatures and heats of reaction measured using the C80D calorimeter.

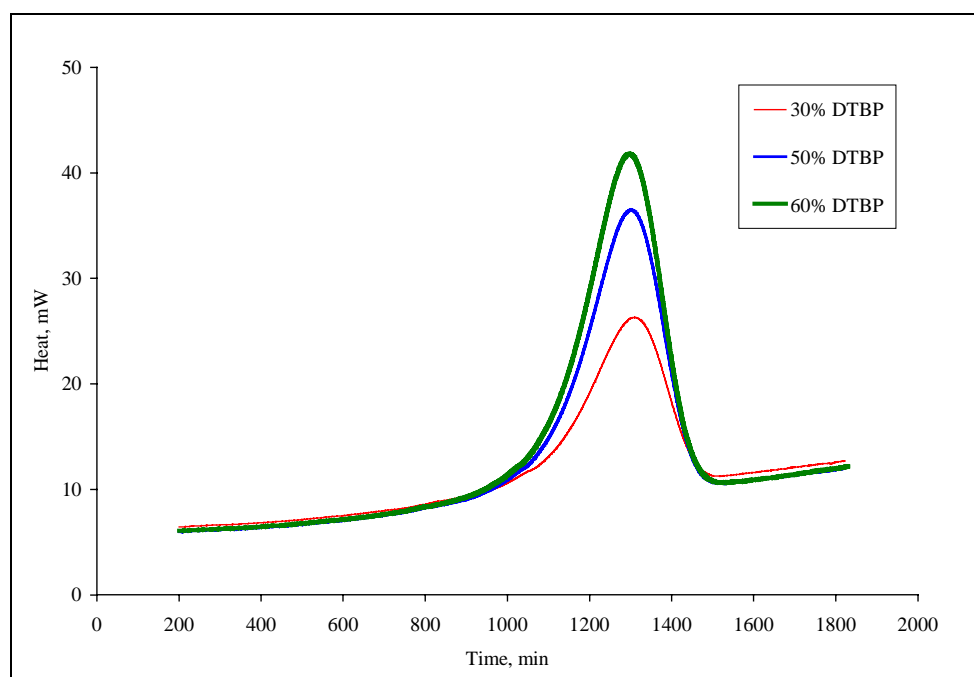


Figure 5.8. Heat flow profiles of DTBP decomposition in toluene using the C80D

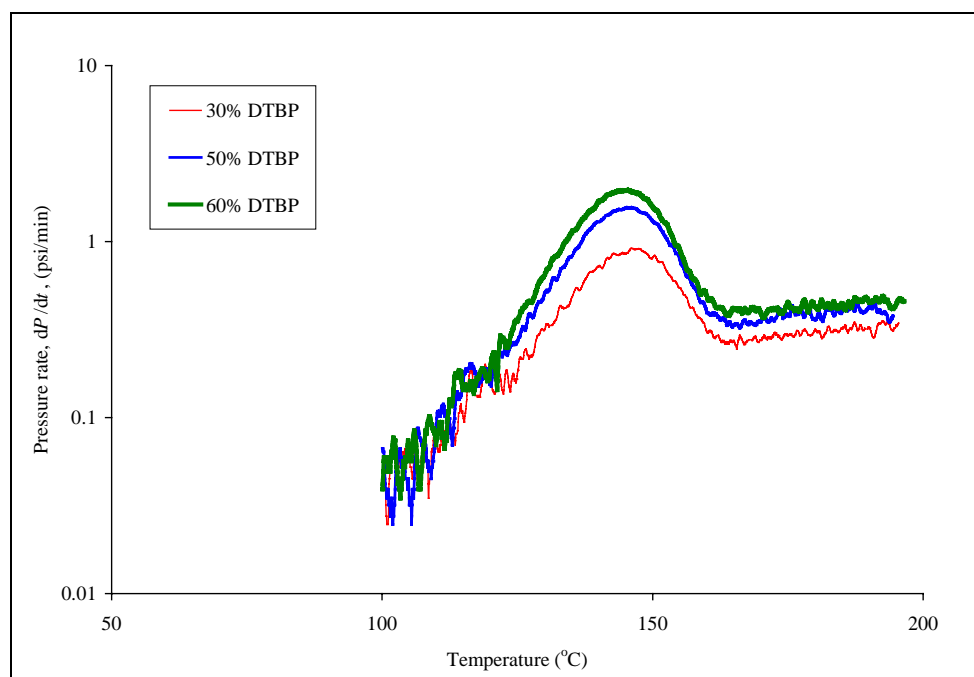


Figure 5.9. C80D pressurization rate profiles of DTBP decomposition in toluene

Table 5.14

The C80D onset temperature and heat of reaction of DTBP decomposition in toluene

DTBP Conc. (wt.%)	T_o (°C)	ΔH_r (kcal/mol)
30	124.0 ± 1.0	-52.5 ± 2.1
50	123.8 ± 0.8	-52.5 ± 1.8
60	123.5 ± 1.1	-52.4 ± 2.5

5.6. APTAC™ Thermal Analysis

More accurate overall reaction thermodynamic and kinetic parameters are obtained from adiabatic thermal analysis. Adiabatic calorimetry will simulate, to a great extent, the real plant reaction runaway environment. To test the findings of our approach up to this point of evaluation, the same set of DTBP in toluene samples were tested with the APTAC™. Adiabatic calorimetry analysis is classified as advanced chemical reactivity evaluation. We believe that this level of evaluation is not necessary all the times; however, in this research we are investigating the significance of this systematic approach with all the different levels of evaluation.

The heat-wait-search mode of operation was applied in these experiments. This APTAC™ mode of operation, as discussed in Chapter IV, is useful to measure and calculate various reactivity parameters such as, onset temperature, T_o , adiabatic time to maximum rate, TMR_{ad} , maximum self-heating rate $(dT/dt)_{max}$, and maximum pressurization rate $(dP/dt)_{max}$. A total of 19 samples were tested with various sample weights varying from 4 to 40 g. 130-mL APTAC™ cells of glass and titanium were used

in these tests. The combinations of the cell material and sample sizes resulted in thermal inertia factors, ϕ , ranging from 1.24 – 3.20. These variations are useful in evaluating the effects of thermal inertia on reactivity parameters for scale-up procedures, as it will be discussed later in this chapter. A heating rate of 2°C/min in the heat-wait-search mode was applied to all the samples. Table 5.15 presents a summary of tested samples experimental conditions. Figures 5.10 and 5.11 presents typical temperature and

Table 5.15
Summary of the APTAC™ DTBP in toluene samples

Sample	DTBP wt.%	Cell material	Sample weight (g)	Cell weight (g)	Heating rate (°C/min)
30a	30	Glass	40.23	47.45	2.0
30b	30	Glass	40.04	47.45	2.0
30c	30	Titanium	40.30	42.04	2.0
30d	30	Titanium	39.73	42.02	2.0
30e	30	Titanium	40.07	42.01	2.0
30f	30	Titanium	20.02	42.00	2.0
30g	30	Titanium	40.08	42.07	2.0
30h	30	Titanium	20.02	42.04	2.0
30i	30	Titanium	20.12	42.19	2.0
30j	30	Titanium	20.03	42.08	2.0
50a	50	Glass	24.25	62.63	2.0
50b	50	Titanium	18.55	42.02	2.0
50c	50	Titanium	14.34	42.01	2.0
50d	50	Titanium	10.11	42.03	2.0
50e	50	Titanium	7.11	42.03	2.0
50f	50	Titanium	5.07	42.06	2.0
60a	60	Titanium	7.20	42.02	2.0
60b	60	Titanium	7.28	42.02	2.0
60c	60	Titanium	4.22	42.03	2.0

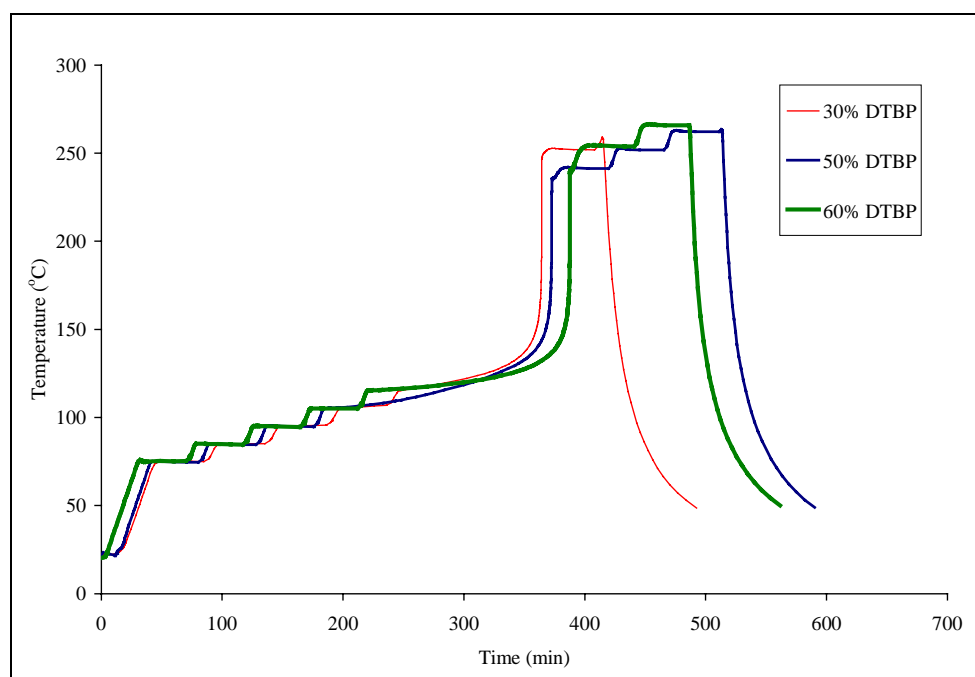


Figure 5.10. DTBP decomposition in toluene temperature profiles using the APTAC™

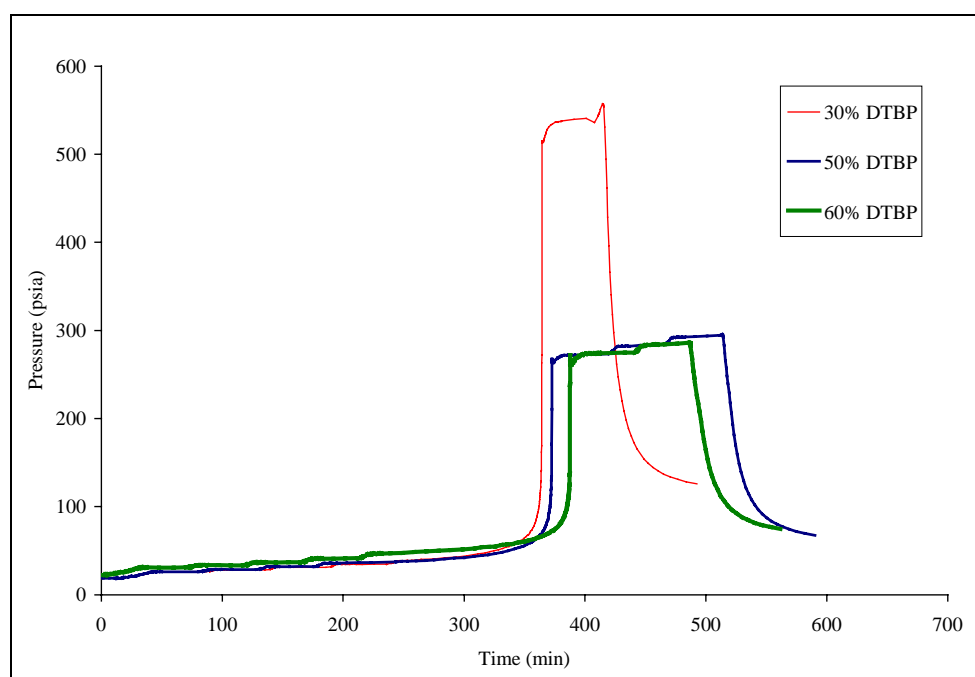


Figure 5.11. DTBP decomposition in toluene pressure profiles using the APTAC™

pressure profiles of the three tested DTBP concentrations, respectively. In Figure 5.11 the pressure profile of the 30% sample represents a 20 g sample while the pressure profiles of the 50 and 60% samples are of 5 and 4 g samples, respectively. This explains the large differences in maximum pressure achieved for these samples. The larger maximum pressure achieved for the 30% DTBP sample is due to the large quantity of solvent (toluene) available for vaporization. Figure 5.10 illustrates the temperature profiles of different concentrations, but it is clear that these curves are comparable.

Table 5.16 summarizes the onset temperatures, maximum temperatures, and heat capacities for the tested samples. The onset temperatures were determined at a self-heating rate of $0.05^{\circ}\text{C}/\text{min}$. The heat capacities of the sample solution, C_s , and testing cells, C_c , as in Table 5.16, were estimated at an average temperature of reaction onset temperature, T_o , and the maximum reaction temperature achieved, T_{max} , considering the proportion of DTBP and toluene in each sample. Correlations available in the literature were used for DTBP-toluene mixture [24] and titanium cell [25]. Glass cell heat capacity values were obtained from DSC experimental study provided by the manufacturer. As the case with the RSST™ analysis, implicitly we assumed that the change in average heat capacity during the decomposition reaction is negligible. As discussed earlier, heat capacity estimation is one of the main sources of uncertainty in the estimated heat of reaction because of continuous temperature and composition changes during the experiment.

Table 5.16

Experimental results of DTBP decomposition in toluene with the APTAC™

Sample	T_o (°C)	T_{max} (°C)	ΔT_{ad} (°C)	ϕ -Factor	C_s (cal/(g · K))	C_c (cal/(g · K))
30a	115	235	120	1.30	0.549	0.105
30b	120	229	109	1.29	0.546	0.105
30c	121	244	123	1.25	0.559	0.131
30d	115	248	133	1.25	0.560	0.131
30e	116	249	133	1.25	0.561	0.131
30f	116	252	136	1.49	0.564	0.131
30g	121	264	143	1.24	0.577	0.131
30h	121	248	127	1.49	0.562	0.131
30i	116	250	134	1.49	0.562	0.131
30j	121	250	129	1.49	0.564	0.131
50a	115	230	115	1.48	0.569	0.105
50b	118	278	160	1.48	0.618	0.131
50c	118	270	152	1.63	0.608	0.131
50d	108	263	155	1.91	0.598	0.131
50e	120	252	132	2.32	0.591	0.131
50f	109	238	129	2.90	0.574	0.131
60a	109	257	148	2.26	0.605	0.131
60b	118	258	140	2.24	0.610	0.131
60c	119	241	119	3.20	0.594	0.131

The adjusted to pure DTBP overall heat of decomposition of DTBP in toluene is calculated using Equation 5.2. A first-order kinetic model was used to fit the DTBP decomposition in toluene. The reaction rate constant, k , can be calculated using

$$k = \frac{\left(\frac{dT}{dt}\right)}{(T_{max} - T)} \quad (5.6)$$

Arrhenius parameters (activation energy and frequency factor) were obtained by plotting Equation 5.4 as presented in Figure 5.12. This plot validates our assumption of first-order reaction kinetics with an average linear fitting regression coefficient of 0.998. Time to maximum rate under adiabatic conditions was also calculated using Equation 4.13. Table 5.17 summarizes the onset temperatures, heats of reaction, time to maximum rate, reaction order, and Arrhenius parameters obtained from the APTACTM data. Arrhenius parameters are almost identical for the various DTBP concentrations. However, slight variation in the onset temperature and overall heat of reaction is measured but still within the experimental error margins.

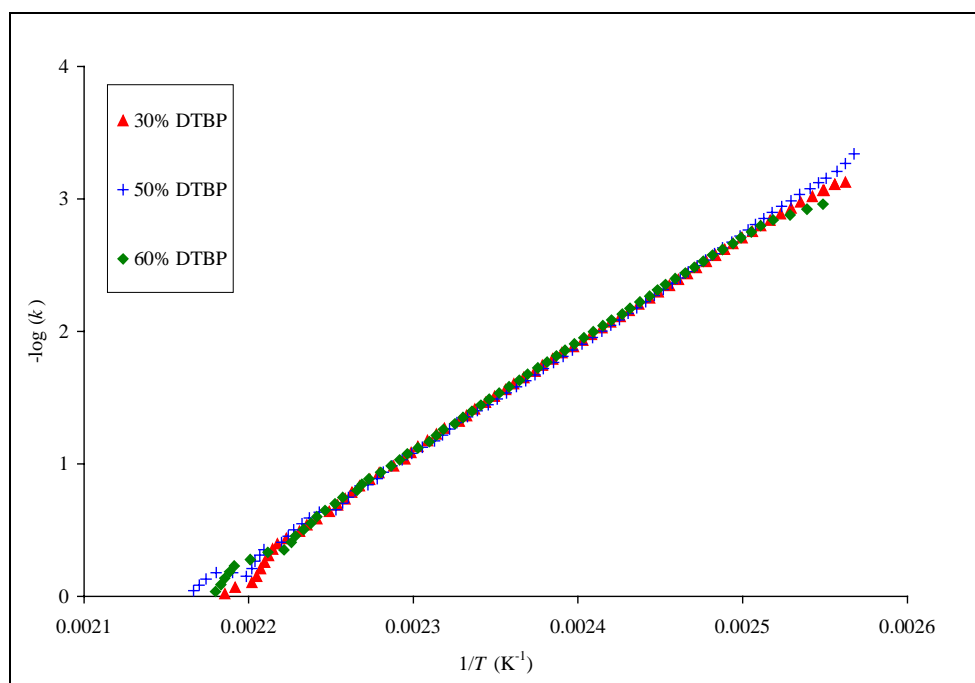


Figure 5.12. First-order kinetics of DTBP decomposition in toluene with the APTACTM

Table 5.17

Summary of the APTAC™ thermodynamic and kinetic parameters of DTBP decomposition in toluene

DTBP Conc. (wt.%)	T_o (°C)	ΔH_r (kcal/mol)	TMR_{ad} (min)	Reaction order, n	E_A (kcal/mol)	$\log(A)$ (s ⁻¹)
30	118 ± 3	-49.6 ± 5.0	161 ± 2	1	37.8 ± 1.0	17.9 ± 0.5
50	115 ± 5	-49.6 ± 4.7	158 ± 4	1	37.7 ± 1.0	17.9 ± 0.5
60	116 ± 7	-50.4 ± 4.4	159 ± 4	1	37.2 ± 0.9	17.6 ± 0.5

Self-heating and pressurization rates of reaction are also measured with the APTAC™ with the advantage of maintaining almost adiabatic conditions. Direct measurement of these two rates was applicable with no further mathematical treatment.

Figure 5.13 demonstrates measured self-heating rate of five 50% DTBP samples. These samples were tested in the same titanium cell but with different sample sizes. The effect of ϕ factor on the self-heating rate is demonstrated. Clearly as the sample ϕ factor increases, the maximum self-heating rate decreases. Also, it can be concluded that an increase in the self-heating rate is measured with decreasing ϕ factor. Comparing these self-heating rate curves with that of the 50% DTBP sample tested in the RSST™ and illustrated in Figure 5.6, we can conclude that the two-hump behavior measured with RSST™ open-cell does not exist with the APTAC™ closed-cell. In fact the APTAC™ results justify the explanation provided earlier. The APTAC™ closed cell experiment prevents sample losses and hence reduces the effects of solvent vaporization on the self-heating rate significantly.

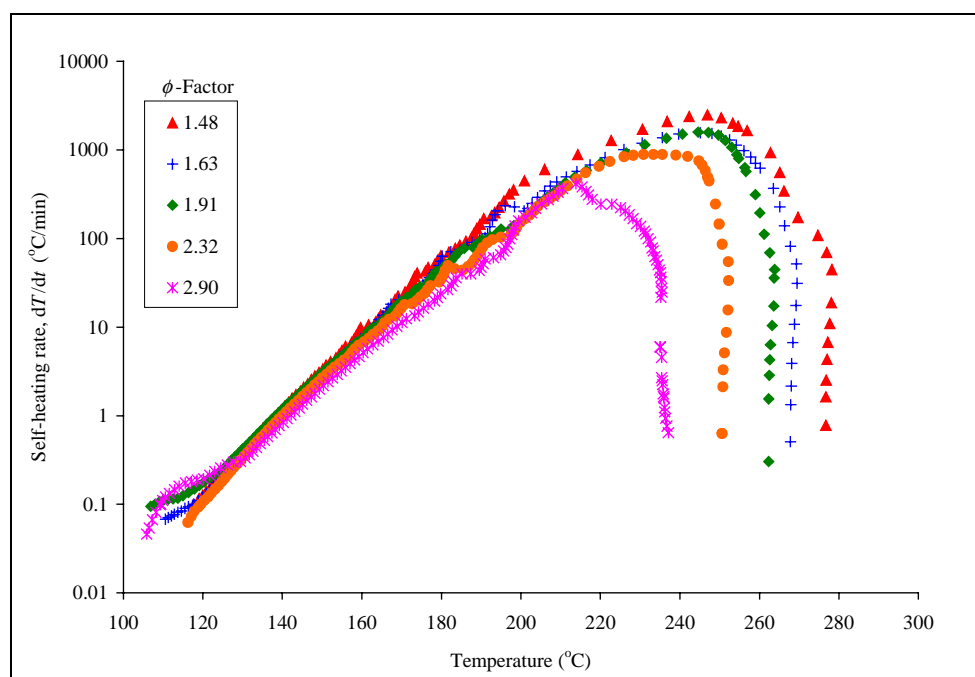


Figure 5.13. Self-heating rate of DTBP decomposition in toluene using the APTAC™

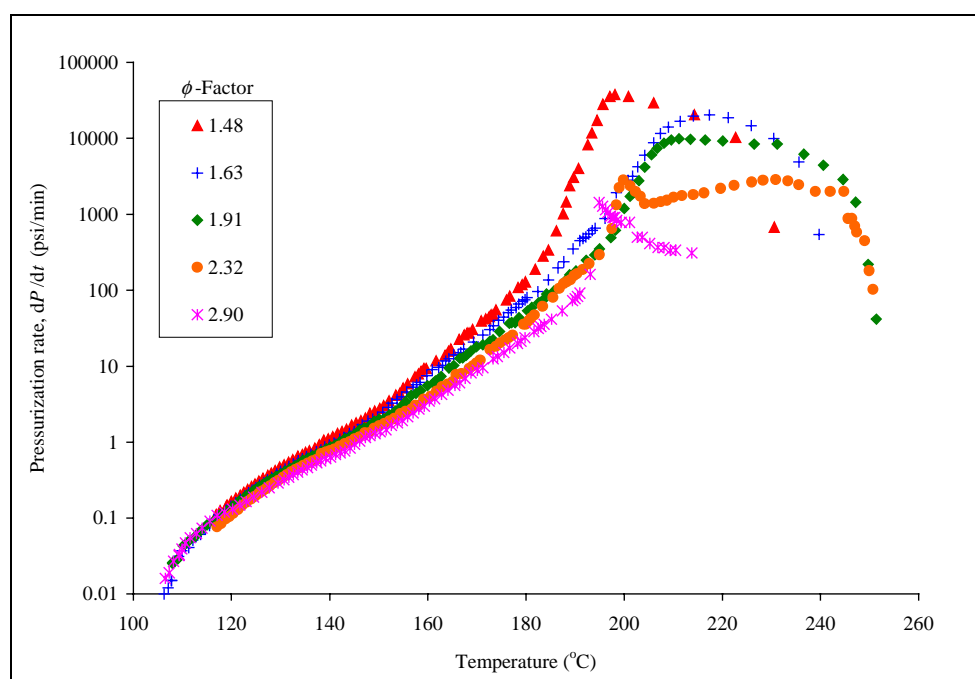


Figure 5.14. Pressurization rate of DTBP decomposition in toluene using the APTAC™

Pressurization rate is also measured with the APTAC™ and presented in Figure 5.14. Similar behavior of pressurization rate was found compared to that of self-heating rate in Figure 5.13. Values of maximum self-heating and pressurization rates are presented in Table 5.18. It is clear that these rates are strong functions of several parameters including thermal inertia factors, sample size, and sample concentrations. Parameter effect on maximum self-heating and pressurization rates is discussed later in this chapter.

Table 5.18

Maximum self-heating and pressurization rates of DTBP decomposition in toluene using the APTAC™

Sample	Sample weight (g)	ϕ -Factor	$(dT/dt)_{\max}$ ($^{\circ}\text{C}/\text{min}$)	$(dP/dt)_{\max}$ (psi/min)
30a	40.23	1.30	172	7727
30b	40.04	1.29	123	10086
30c	40.30	1.25	396	18397
30d	39.73	1.25	1021	15066
30e	40.07	1.25	1548	18958
30f	20.02	1.49	661	4170
30g	40.08	1.24	1011	15953
30h	20.02	1.49	646	3737
30i	20.12	1.49	922	3956
30j	20.03	1.49	625	4403
50a	24.25	1.48	1001	20411
50b	18.55	1.48	2484	37772
50c	14.34	1.63	1565	20303
50d	10.11	1.91	1588	9923
50e	7.11	2.32	889	2824
50f	5.07	2.90	416	1431
60a	7.20	2.26	1004	8048
60b	7.28	2.24	N/A	N/A
60c	4.22	3.20	404	1833

5.7. DTBP in Benzene Analysis

Theoretical reaction pathway analysis presented earlier in this chapter suggests that the solvent does not affect the primary reaction pathway of DTBP decomposition in toluene. To evaluate this conclusion, the toluene was replaced with benzene as the solvent. The same set of DTBP concentrations were tested using RSST™ and APTAC™ calorimeters. Comparing the results of this analysis with the previous one provides a definite answer to the effect of toluene on the decomposition reaction. Selection of benzene as an alternative solvent was based on the absence of highly accessible hydrogen atom for abstraction by free radicals compared to that in toluene. Accordingly, we expect the decomposition reaction of DTBP in benzene to be more independent from the solvent than that of DTBP in toluene.

Experimental screening analysis using the RSST™ was performed for 30, 50, and 60 wt.% DTBP in benzene. Initially DTBP and benzene were mixed, and then sample masses of 8.0 to 10.0 g were placed in the RSST™ glass cell for testing. Similar to DTBP-toluene RSST™ testing, sample solutions were tested under a nitrogen backup pressure of about 250 psig to reduce liquid boil-off before decomposition. The sample and glass cell masses produced a thermal inertia factor, ϕ , of about 1.03. Several temperature ramping rates of 1.0 to 1.9 °C/min were applied. Stirring was present during the experiments and it was kept at a constant speed for all the experimental runs. Table 5.19 presents a summary of the experimental conditions and parameters of the tested samples.

Temperature and pressure profiles during the DTBP in benzene decomposition are shown in Figures 5.15 and 5.16, respectively. Clearly these profiles indicate an exothermic reactivity and a rapid pressure increase. Temperature and pressure profiles also show similar behavior of reaction onset temperature irrespective of the sample DTBP concentration and heating rate. A summary of the experimental data for the tested samples is presented in Table 5.20. Onset temperatures of the 30% DTBP in benzene samples are lower than that of toluene sample (presented in Table 5.11), however no significant differences were found between the 50 and 60 % samples.

Table 5.19
Summary of the RSST™ DTBP in benzene samples

Sample	DTBP wt. %	Sample weight (g)	Cell weight (g)	Temperature ramping rate (°C/min)
30a	30	8.57	1.49	1.62
30b	30	8.10	1.49	1.10
30c	30	7.62	1.32	1.10
50a	50	9.15	1.47	1.72
50b	50	9.97	1.43	1.02
60a	60	8.06	1.40	1.85
60b	60	9.82	1.43	0.96

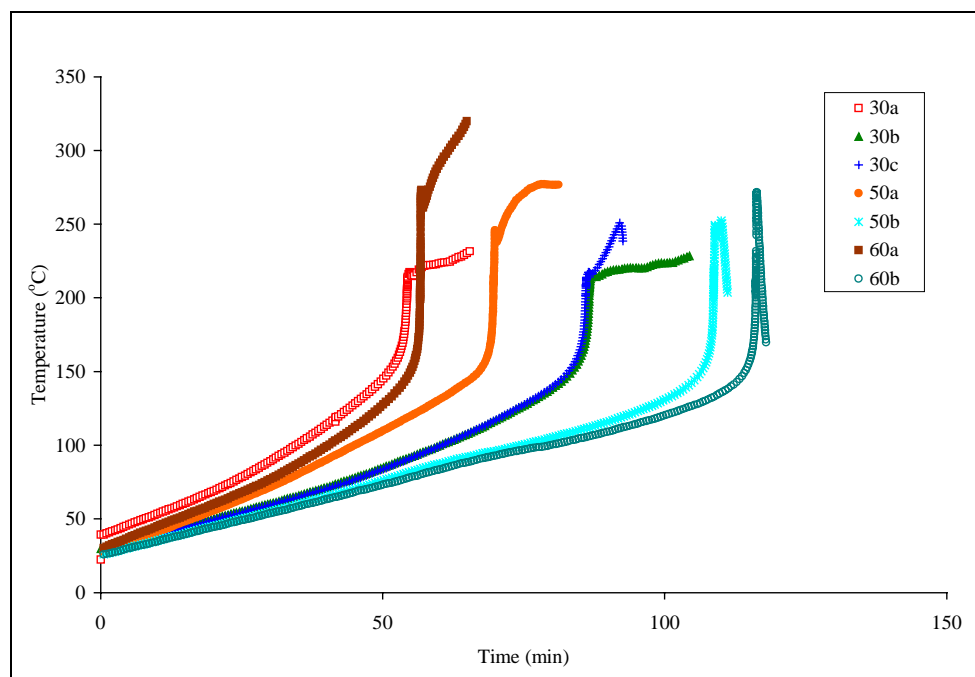


Figure 5.15. DTBP decomposition in benzene temperature profiles using the RSST™

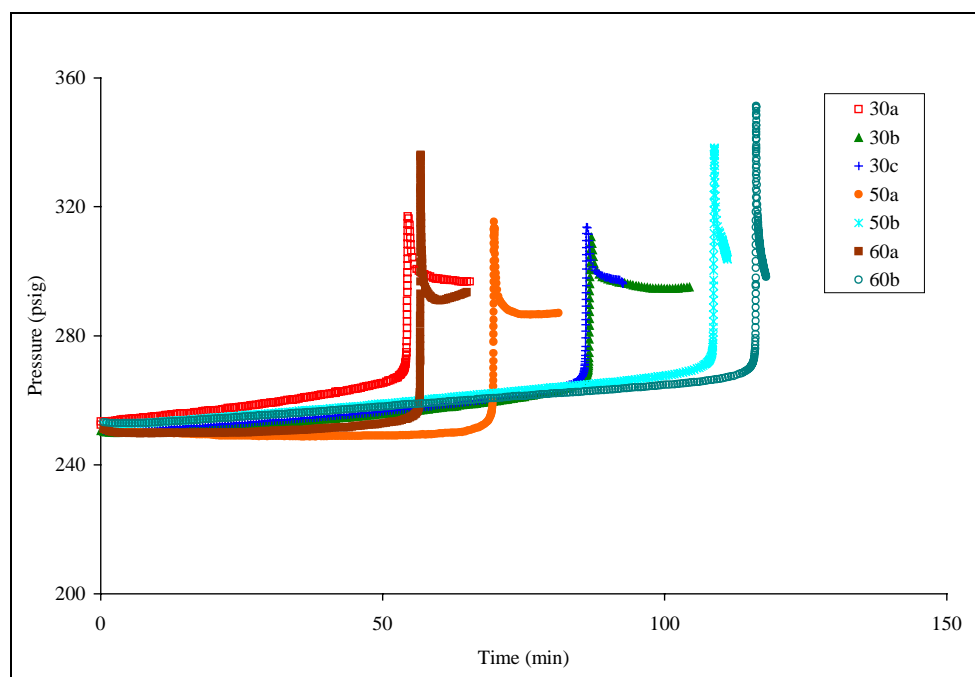


Figure 5.16. DTBP decomposition in benzene pressure profiles using the RSST™

Table 5.20

Experimental results of DTBP decomposition in benzene with the RSST™

Sample	T_o (°C)	T_{max} (°C)	ΔT_{ad} (°C)	ϕ -Factor	C_s (cal/(g · K))	C_c (cal/(g · K))
30a	85	217	132	1.04	0.489	0.105
30b	93	215	122	1.04	0.490	0.104
30c	93	219	126	1.04	0.493	0.104
50a	117	246	129	1.03	0.559	0.105
50b	121	252	131	1.03	0.567	0.104
60a	118	273	155	1.03	0.608	0.105
60b	124	272	148	1.02	0.610	0.104

Overall heat of decomposition reaction of DTBP in benzene is calculated by applying the same procedure used with toluene samples. Also, first-order kinetic model of the DTBP decomposition in benzene is presented in Figure 5.17 with an average linear fitting regression coefficient of 0.991. A summary of onset temperature, overall heat of reaction, and Arrhenius parameters are shown in Table 5.21.

Self-heating and pressurization rates of the DTBP-benzene samples are presented in Figures 5.18 and 5.19, respectively. The same behavior of DTBP concentration effect measured with DTBP-toluene samples earlier is presented here. The same deviation in the 50 and 60 % DTBP samples self-heating rate curves is also noticed here, which again proves the findings and conclusions discussed earlier in this chapter. Values of maximum self-heating and pressurization rates are presented in Table 5.22.

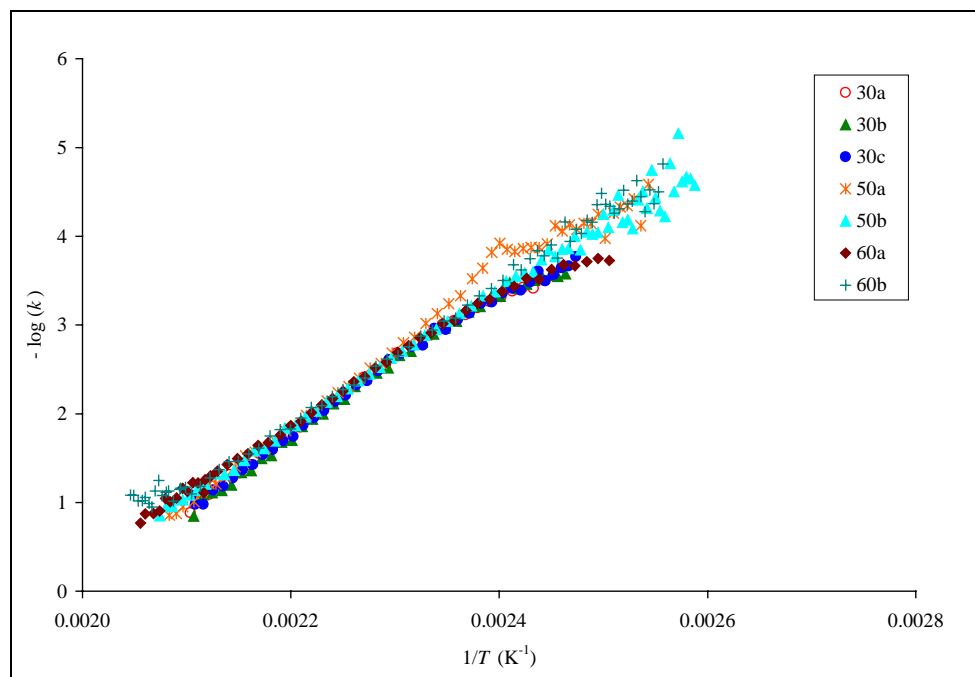


Figure 5.17. First-order kinetics of DTBP decomposition in benzene with the RSST™

Table 5.21

Summary of the RSST™ thermodynamic and kinetic parameters of DTBP decomposition in benzene

DTBP Conc. (wt.%)	T_o (°C)	ΔH_r (kcal/mol)	Reaction order, n	E_A , (kcal/mol)	$\log(A)$ (s^{-1})
30	90 ± 5	-31.4 ± 1.2	1	35.4 ± 0.4	15.2 ± 0.2
50	119 ± 3	-22.0 ± 0.4	1	36.1 ± 2.1	15.5 ± 1.0
60	121 ± 4	-23.1 ± 0.8	1	33.4 ± 1.4	14.1 ± 0.6

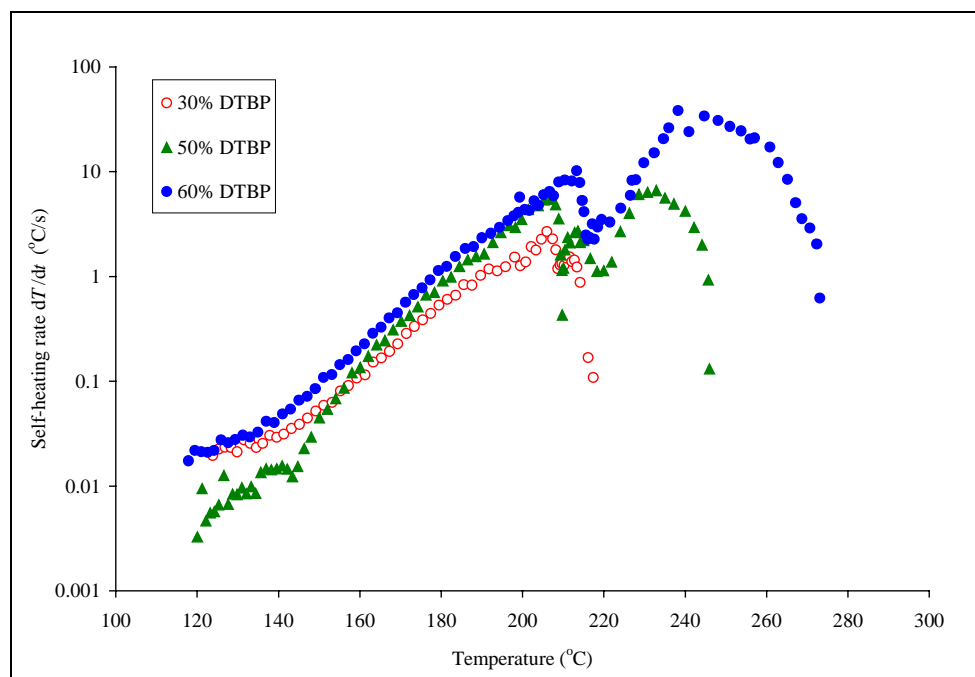


Figure 5.18. Self-heating rate of DTBP decomposition in benzene using the RSST™

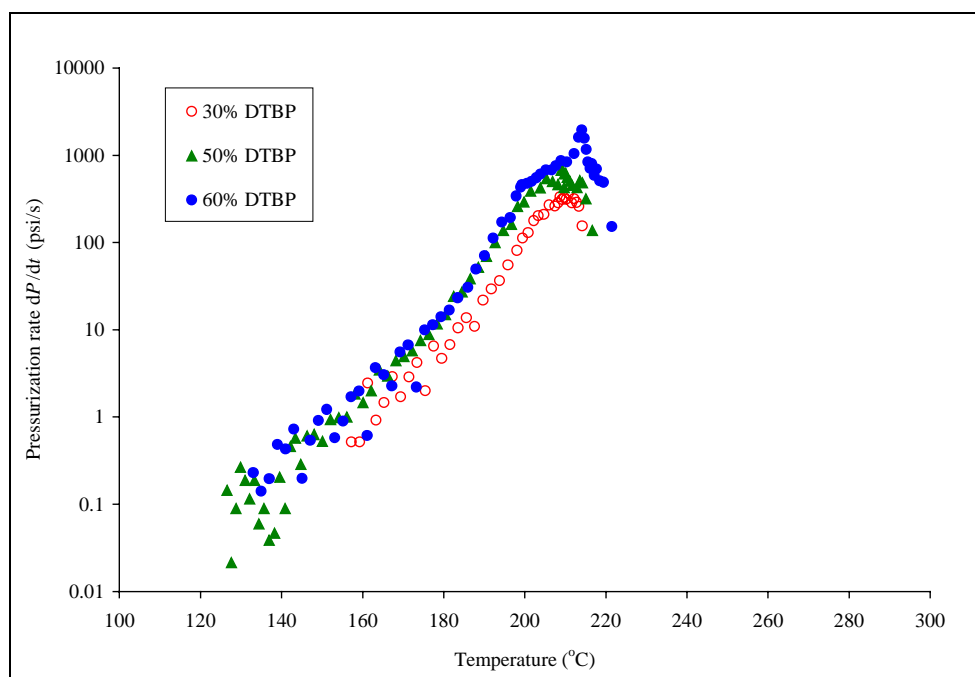


Figure 5.19. Pressurization rate of DTBP decomposition in benzene using the RSST™

Table 5.22

Maximum self-heating and pressurization rates of DTBP decomposition in benzene using the RSST™

Sample	Sample weight (g)	ϕ -Factor	$(dT/dt)_{\max}$ (°C/s)	$(dP/dt)_{\max}$ (psi/min)
30a	8.57	1.04	3	367
30b	8.10	1.04	2	263
30c	7.62	1.04	3	374
50a	9.15	1.03	7	679
50b	9.97	1.03	7	851
60a	8.06	1.03	38	2549
60b	9.82	1.02	40	2575

DTBP-benzene samples were also tested using the APTAC™ heat-wait-search mode with heating rate of 2°C/min. A total of eight samples were tested with various sample weights ranging from 5 to 20 g. A 130-mL titanium APTAC™ cell was used in these tests. The thermal inertia factor, ϕ , ranged from 1.5 – 3.8. Table 5.23 presents a summary of the experimental conditions of the tested samples. Figures 5.20 and 5.21 present typical temperature and pressure profiles of the three tested DTBP concentrations, respectively. In Figure 5.21 the pressure profile of the 30, 50, and 60 % sample are 20, 10, and 5 g sample, respectively. The larger the sample size, the larger the maximum pressure achieved and that is due to the large quantity of solvent (benzene) available for vaporization in larger samples. Although Figure 5.20 presents the temperature profiles of different concentrations, but it is clear that these curves are comparable and no significant difference are realized. A summary of reaction onset and maximum temperatures is presented in Table 5.24.

Table 5.23

Summary of the APTAC™ DTBP in benzene samples

Sample	DTBP wt.%	Cell material	Sample weight (g)	Cell weight (g)	Heating rate (°C/min)
30a	30	Titanium	20.05	42.03	2.0
30b	30	Titanium	20.20	42.03	2.0
30c	30	Titanium	20.39	42.04	2.0
50a	50	Titanium	14.05	42.02	2.0
50b	50	Titanium	10.10	42.03	2.0
60a	60	Titanium	7.18	42.01	2.0
60b	60	Titanium	5.09	42.03	2.0
60c	60	Titanium	7.03	42.16	2.0

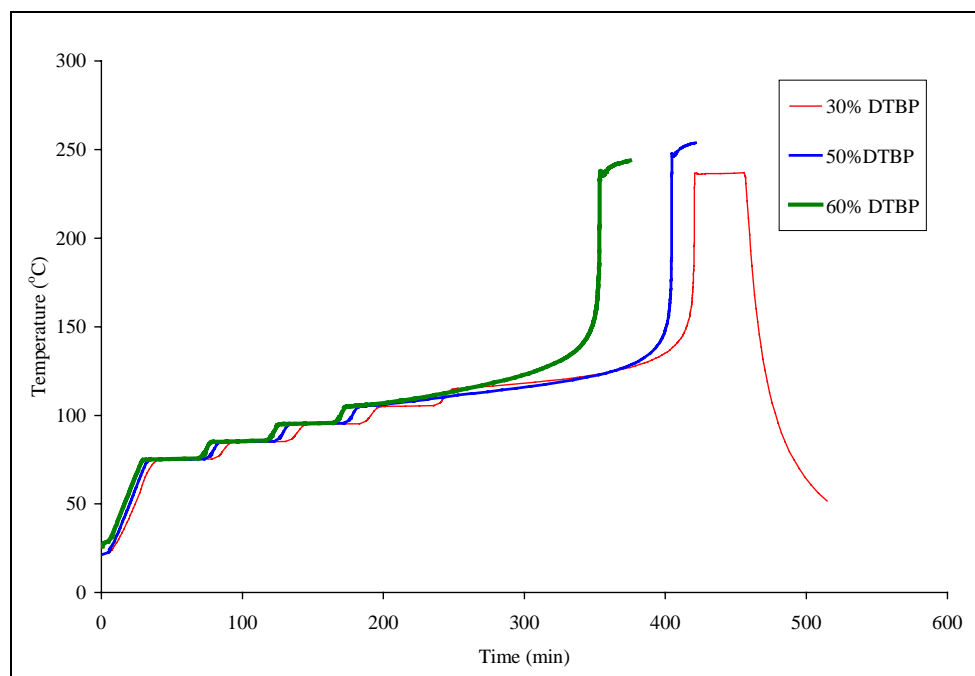


Figure 5.20. DTBP decomposition in benzene temperature profiles using the APTAC™

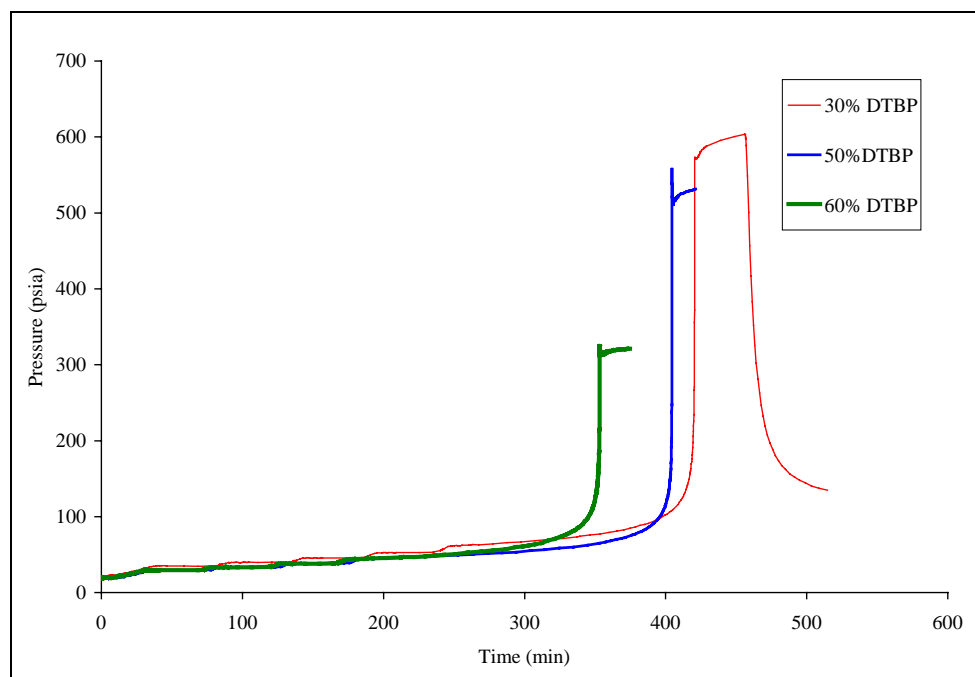


Figure 5.21. DTBP decomposition in benzene pressure profiles using the APTAC™

Table 5.24

Experimental results of DTBP decomposition in benzene with the APTAC™

Sample	T_o (°C)	T_{max} (°C)	ΔT_{ad} (°C)	ϕ -Factor	C_s (cal/(g · K))	C_c (cal/(g · K))
30a	118	235	117	1.48	0.573	0.131
30b	122	236	114	1.47	0.575	0.131
30c	119	237	118	1.47	0.575	0.131
50a	116	266	150	1.66	0.591	0.131
50b	116	248	132	1.92	0.593	0.131
60a	109	247	138	2.28	0.600	0.131
60b	108	238	130	2.80	0.602	0.131
60c	118	242	124	2.31	0.602	0.131

The adjusted to pure DTBP overall heat of decomposition in benzene is calculated and a first-order kinetic model was used to fit the data. The Arrhenius parameters were obtained by plotting Equation 5.4. Figure 5.22 shows first-order kinetic linear fitting. This plot validates the assumed kinetic model with an average linear fitting regression coefficient of 0.998. Summarized reaction parameters in Table 5.25 are comparable and within experimental margin errors; however, some deviation is measured for the Arrhenius parameters of the 60% sample.

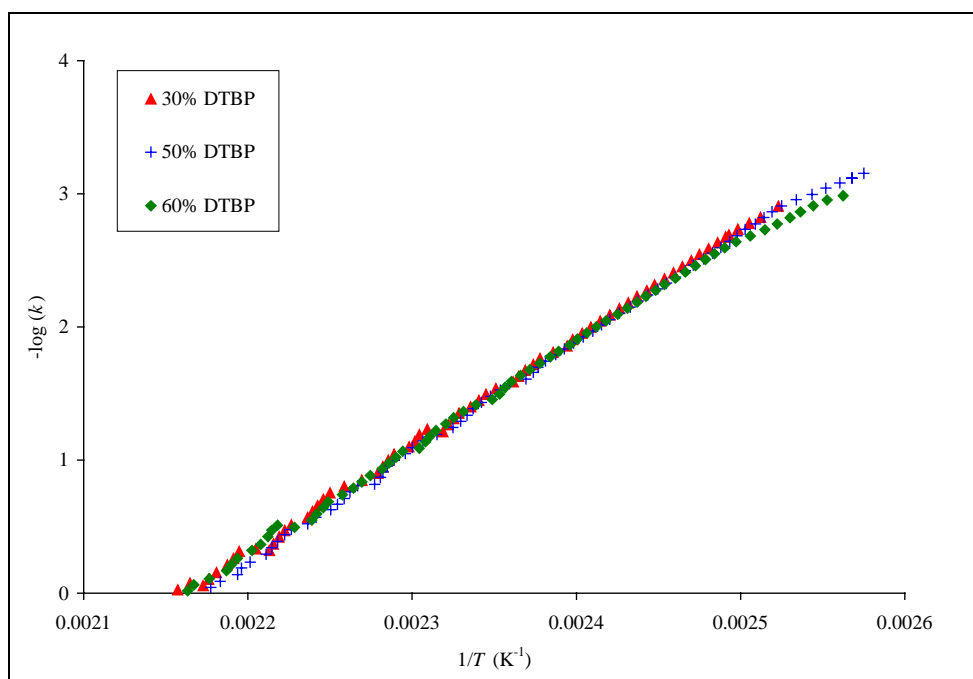


Figure 5.22. First-order kinetics of DTBP decomposition in benzene with the APTAC™

Table 5.25

Summary of the APTAC™ thermodynamic and kinetic parameters of DTBP decomposition in benzene

DTBP Conc. (wt.%)	T_o (°C)	ΔH_r (kcal/mol)	Reaction order, n	E_A (kcal/mol)	$\log(A)$ (s ⁻¹)
30	120 ± 2	-48.0 ± 0.8	1	37.3 ± 0.2	17.6 ± 0.1
50	116 ± 0	-43.5 ± 0.6	1	37.0 ± 0.1	17.5 ± 0.0
60	112 ± 6	-47.1 ± 5.8	1	34.8 ± 0.9	16.4 ± 0.5

Self-heating and pressurization rates of the 30% DTBP in benzene samples are presented in Figures 5.23 and 5.24, respectively. Identical self-heating and pressurization rates of these samples provide an indication of high reproducibility of the APTAC™ experiments. Values of maximum self-heating and pressurization rates are presented in Table 5.26.

5.8. Experimental Analysis Discussion

The experimental analysis results of DTBP decomposition in toluene using the RSST™ C80D, and APTAC™ calorimeters are not of the same quality. Comparing the first-order activation energy and frequency factor measured by RSST™ and APTAC™ show an acceptable agreement for the three tested DTBP concentrations. Although the activation energies measured by the RSST™ are slightly higher than those by the APTAC™, they are still within the calculated experimental error margins. Reaction onset temperatures detected by the RSST™ and C80D are generally higher than those detected by the APTAC™ by about 10 and 7 °C, respectively. These differences in the

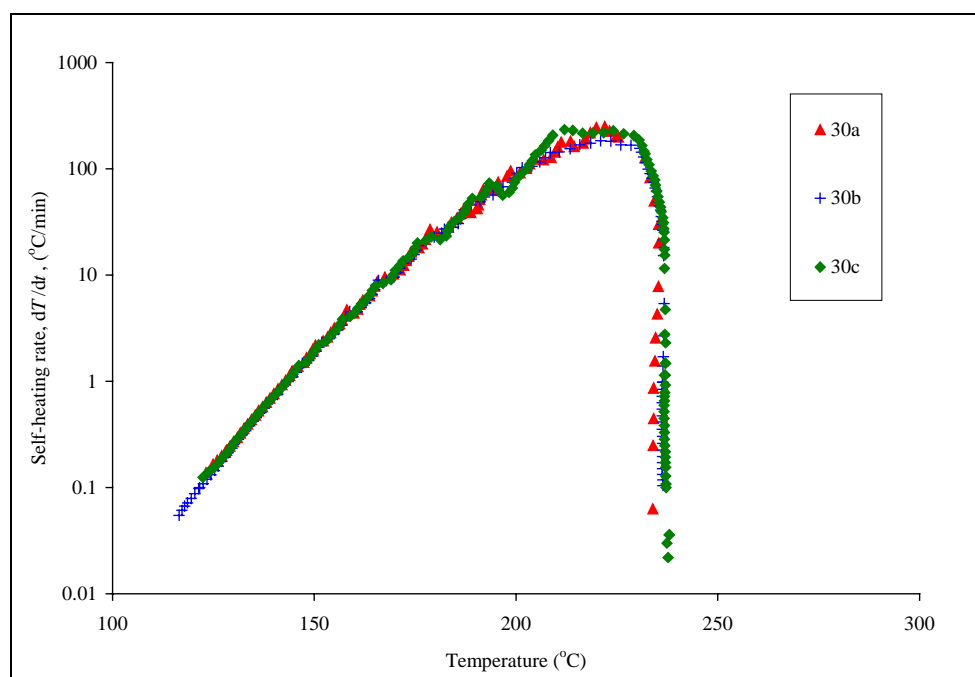


Figure 5.23. Self-heating rate of DTBP decomposition in benzene using the APTAC™

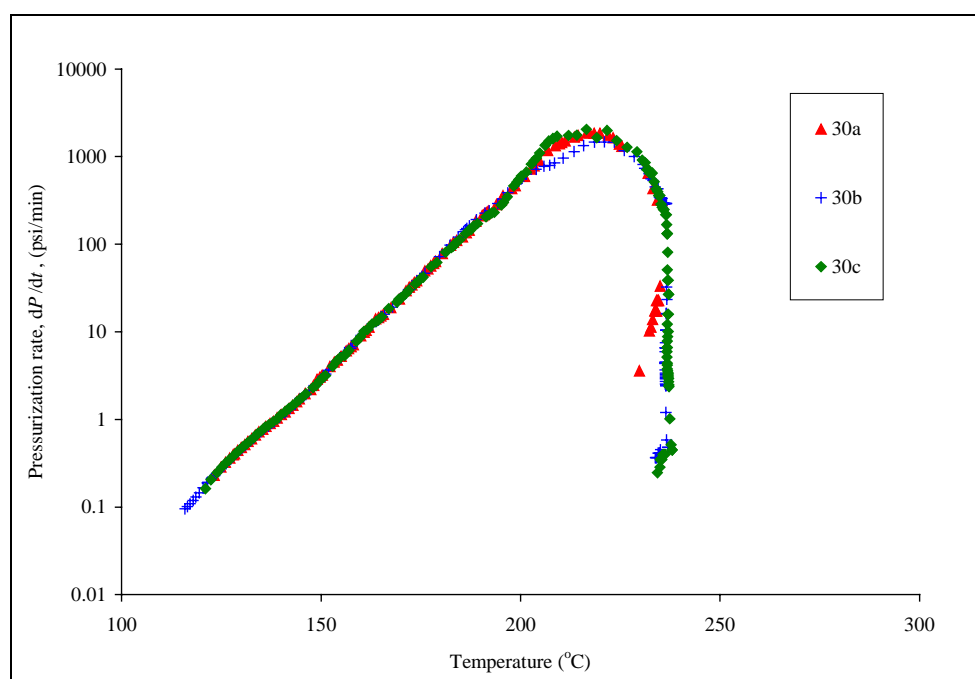


Figure 5.24. Pressurization rate of DTBP decomposition in benzene using the APTAC™

Table 5.26

Maximum self-heating and pressurization rates of DTBP decomposition in benzene using the APTAC™

Sample	Sample weight (g)	ϕ -Factor	$(dT/dt)_{\max}$ ($^{\circ}\text{C}/\text{min}$)	$(dP/dt)_{\max}$ (psi/min)
30a	20.05	1.48	250	1871
30b	20.20	1.47	184	1472
30c	20.39	1.47	234	2040
50a	14.05	1.66	1214	13336
50b	10.10	1.92	477	5410
60a	7.18	2.28	402	4455
60b	5.09	2.80	238	2585
60c	7.03	2.31	365	4200

reaction onset temperatures are due to the temperature-rate measurement sensitivity of the apparatus. The open-cell system, i.e., the RSST™, requires higher temperatures to initiate the same reaction than that required for the closed-cell system such as the APTAC™. The heat and material losses associated with the open system reduce the reactivity detection sensitivity of the system. For the heat flow calorimeter, C80D, the heat flux rate measurement sensitivity directly affects the reaction onset temperature detection. For the C80D calorimeter, the detection limit is 10 μW , which is not low enough to match the APTAC detection sensitivity of $0.05^{\circ}\text{C}/\text{min}$.

Similarly, heat and material losses in the open-cell calorimeter have a significant effect on the measured overall heats of reaction. Measured overall heats of reaction by the RSST™, APTAC™, and C80D calorimeters are presented in Figure 5.25. The heats

of reaction measured by the closed-cell calorimeters (APTAC™ and C80D) are comparable

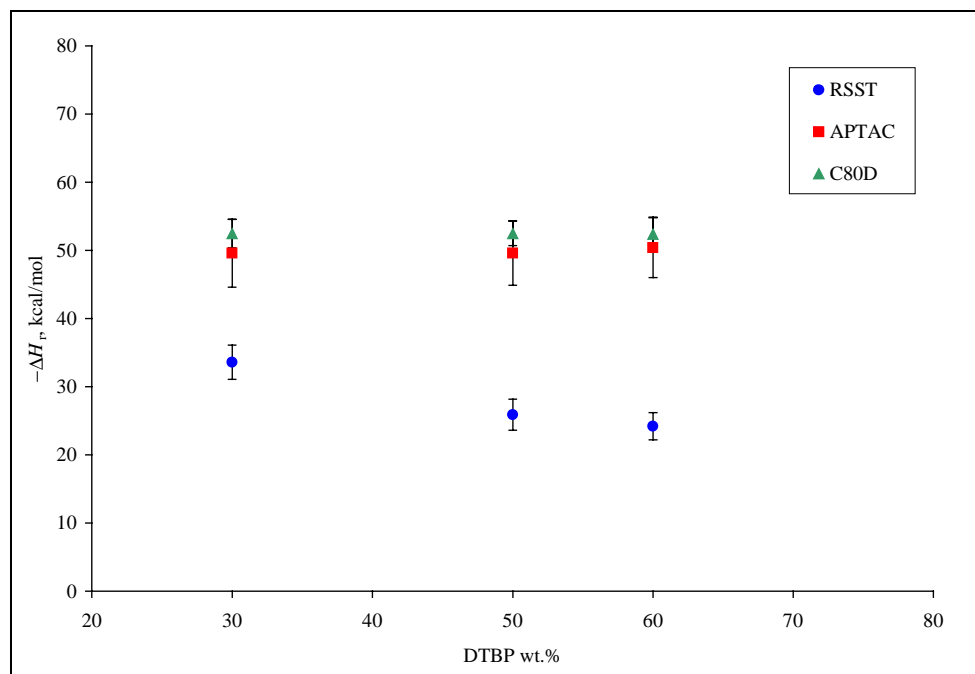


Figure 5.25. Measured overall heats of reaction of DTBP decomposition in toluene

with differences in the range of 2.6 kcal/mol. However, significant differences (up to 28 kcal/mol) are found when comparing the RSST™ to the APTAC™ and C80D results. Also, in the RSST™, as the DTBP concentrations increase the measured overall heat of reaction decreases. High DTBP concentration samples are expected to have larger amount of energy released due to the DTBP decomposition. However, this large release of energy is associated with higher solvent endothermic evaporation rates causing the

overall measured heat of reaction to be reduced, especially when the test cell is open to a larger space volume, as in the RSST™, causing extensive loss of materials. Also, the DTBP evaporation and losses before being decompose reduces the overall measured heat of reaction significantly. In the APTAC™, the effects of heat and material losses are reduced through conducting closed-cell analysis under adiabatic conditions, whereas for the C80D, applying closed-cell heat flux measurement instead of temperature measurement minimizes these effects. These techniques cause the measured overall heat of reaction to be more reliable.

Earlier in this chapter, theoretical predictions of the heat of reaction for the DTBP decomposition in toluene were presented using various levels of theory. To evaluate the accuracy of these calculations, a comparison with the experimental APTAC™ and C80D calorimeters is performed. However, the experimental overall heat of reaction should initially be corrected for the DTBP, reaction products, and solvent heat of vaporization. Prior to conducting the heat of vaporization effect corrections, it was found that with the APTAC™ and C80D the overall heats of reaction (Tables 5.14 and 5.17) remain the same irrespective of the DTBP concentration. This observation suggests that the effects of DTBP and toluene during the decomposition reactions are negligible. For DTBP, it is expected that the decomposing rate is higher than its vaporization rate at the experimental conditions. The experimental maximum achieved pressure indicates that toluene vapors are not the major cause of this high pressure. It is expected that the reaction products (mainly acetone and ethane) are responsible for that sharp pressure increase. Table 5.27 presents a comparison among the overall APTAC™ and C80D, and

the predicted B3LYP/6-31G(d), CBS-4M, and G2 heats of reaction. Comparable values of heats of reactions are obtained, which validates Pathway I as the primary reaction pathway.

Table 5.27

Heat of reaction comparison of experimental measurements and theoretical calculations

DTBP wt. %	APTAC™ heat of reaction (kcal/mol)	C80D heat of reaction (kcal/mol)	B3LYP heat of reaction (kcal/mol)	CBS-4M heat of reaction (kcal/mol)	G2 heat of reaction (kcal/mol)
30	-49.6 ± 5.0	-52.5 ± 2.1			
50	-49.6 ± 4.7	-52.5 ± 1.8	-49.8	-44.6	-47.0
60	-50.4 ± 4.4	-52.4 ± 2.5			

The overall proposed reaction mechanism significantly agrees with more comprehensive kinetic model [107]. The measured heat of reaction and Arrhenius parameters acceptably agree with published data found through isothermal time-concentration studies [103,104], thermal analysis using the Accelerating Rate Calorimeter (ARC) [108], or other low-thermal-inertia apparatus [109]. Table 5.28 presents selected literature results on DTBP decomposition in toluene.

The effect of the thermal losses associated with test cell (thermal inertia) is of a great importance for chemical reactivity evaluation as discussed earlier. Experimental analysis results should be corrected for near adiabatic conditions ($\phi \approx 1$) to simulate the real process conditions. The thermal inertia factor, ϕ , correction was presented in

Chapter IV. In this analysis, the adiabatic calorimeter (APTAC™) results were corrected for near-adiabatic conditions ($\phi \approx 1$). Table 5.29 presents the onset temperatures, maximum temperature, time to maximum rate, and maximum self-heating rates at adiabatic conditions.

Table 5.28

Literature heat of reaction and Arrhenius parameters for DTBP decomposition in toluene

DTBP (%)	ΔH_r (kcal/mol)	E_A (kcal/mol)	$\log(A)$ (s^{-1})	Experiment	Ref.
25	-42.4	37.71	15.95	Low ϕ -factor	[109]
30	-41	37.94	16.21	ARC™	[108]
60	-45 to -49	37.8 ± 1.1	16.15 ± 0.61	ARC™	[108]
100	----	37.83 ± 0.32	15.82 ± 0.11	Isothermal static system	[104]
100	----	37.20	15.62	Average of 11 studies	[103]

Table 5.29

Summary of the APTAC™ corrected parameters of DTBP in toluene at $\phi \approx 1$

DTBP Conc. (wt.%)	T_o (°C)	T_{max} (°C)	TMR_{ad} (min)	$(dT/dt)_{max}$ (°C/min)
30	116 ± 3	290 ± 21	120 ± 10	19,615
50	110 ± 6	383 ± 32	86 ± 22	93,423
60	$108 \pm$	431 ± 9	63 ± 11	354,086

In the computational quantum chemistry analysis, we assumed that the solvent effects are negligible. To justify this assumption, toluene was replaced with benzene as a solvent, and another set of samples was tested using the RSST™ and APTAC™.

Comparing the results obtained by the RSST™ (Tables 5.12 and 5.21), it was noticed that there are slight differences among the onset temperatures and Arrhenius parameters for the DTBP decomposition in toluene and benzene. Heats of reaction agree better. However, these slight differences do not necessarily indicate a reaction mechanism change. The differences in the physical behavior of benzene may have an effect on the measured parameters. When comparing the APTAC™ results (Tables 5.17 and 5.25), a much better agreement is found among onset temperatures, heats of reaction, and Arrhenius parameters of the two solvents. A statistical analysis on the means of a two normal distribution with unknown variances was performed on the two sets of toluene and benzene samples. This analysis validates the hypothesis of the same means for all various measured parameters. A confidence interval for differences in mean ($1-\alpha$) of 95% was used. Table 5.30 presents the calculated P -values of the various tested parameters. Because the P -value exceeds $\alpha = 0.05$, the hypothesis of equal means cannot be rejected. The DTBP decomposition in toluene analysis is a strong indication of the suitability of the assumption made in the theoretical evaluation that minimizes the effect of toluene as a solvent on the decomposition of the DTBP.

6. Conclusions

The applied approach of chemical reactivity evaluation has provided the required comprehensive information to understand the thermodynamics, kinetics, and reaction stoichiometry of the DTBP decomposition of toluene.

Table 5.30

P-value statistical analysis of the APTAC™ DTBP in toluene and benzene

DTBP Conc. (wt.%)	T_o (°C)	ΔH_r (kcal/mol)	E_A , (kcal/mol)	$\log(A)$ (s ⁻¹)
30	0.380	0.407	0.161	0.136
50	0.546	0.158	0.115	0.125
60	0.403	0.475	0.215	0.082

Computational quantum chemistry and thermodynamic-energy correlations were applied at different levels of theory to predict the most probable reaction stoichiometry, and the heat of reaction of the dominant pathway was calculated. The predicted reaction stoichiometry was able to provide significant information about the system pressure behavior and DTBP-toluene interaction under reaction runaway scenarios. Thermal analysis using the RSST™, C80D, and APTAC™ calorimeters was performed. The heat of reaction was measured showing an acceptable agreement with the theoretical calculation and hence corroborating the proposed reaction stoichiometry. Also, Arrhenius parameters were estimated using the results from this thermal analysis study and showed a good agreement with literature values calculated from using other experimental techniques. Other reactivity evaluation parameters, such as reaction onset temperature, adiabatic temperature increase, time to maximum rate, maximum self-heating rate, and maximum pressurization rate were measured and adjusted to adiabatic conditions.

CHAPTER VI

THERMAL COPOLYMERIZATION OF STYRENE- ACRYLONITRILE*

1. Précis

Copolymerization is a very useful process for synthesizing polymers with the required combination of properties and may be compared to alloying in metallurgy. Free-radical chain polymerization is the most common reaction mechanism, but other polymerization mechanisms also are possible, such as anionic and cationic polymerization. Free-radical chain polymerization can be obtained from mixtures of two or more monomers to form polymeric products that obtain two or more structures in the polymer chain, which is termed as copolymerization reaction to form a copolymer.

Polystyrene is a good example to demonstrate the features and importance of the copolymerization process. Polystyrene is a brittle plastic with a low impact strength and low solvent resistance, but copolymerization greatly enhances these properties and the applications of polystyrene. Also, styrene copolymers are useful not only as plastics but elastomers. Thus free-radical copolymerization of the styrene monomer with 15 – 35 %

* This chapter contains material reprinted from the Oil and Gas Journal, 101 (24), A. A. Aldeeb, W. J. Rogers, and M. S. Mannan, New method estimates the parameters of evaluating process reactivity hazards, 66-70, Copyright (2003) and Journal of Hazardous Materials, A. A. Aldeeb, W. J. Rogers, and M. S. Mannan, Evaluation of styrene-acrylonitrile copolymerization thermal stability and runaway behavior, in press with permission from Elsevier Science.

by weight of the acrylonitrile monomer produces an enhanced impact and solvent resistant copolymer. Copolymers with over 30% acrylonitrile are available and have good barrier properties. If the acrylonitrile content of the copolymer is increased to more than 40%, the copolymer becomes ductile [91,110].

The process of two monomers to form a copolymer in random arrangement is



The concentrations of the two monomers in the copolymer are determined by their relative initial concentrations and reactivities. The arrangement of monomer units in a copolymer can be random, alternative, block, or graft. For styrene-acrylonitrile copolymers, a random arrangement is the most common. The composition of the produced copolymer by simultaneous polymerization of two monomers is usually different from the composition of the monomer feed, which shows that different monomers have different tendencies to undergo copolymerization. These tendencies often have little or no resemblance to their behavior in homopolymerization. A typical free-radical copolymerization reaction of two monomers, A and B, will follow the scheme of initiation, propagation, and termination, as presented in Figure 6.1.

It is well established today that initiation, growth, and termination are the principal, although not necessarily the only steps that determine the kinetics of free radical chain polymerization/copolymerization reactions. The rates of these individual steps vary widely, but the propagation reactions are the most rapid. The initiation reaction, which produces an activated radical from a stable monomer, is by far the slowest step whenever long chains are formed [111].

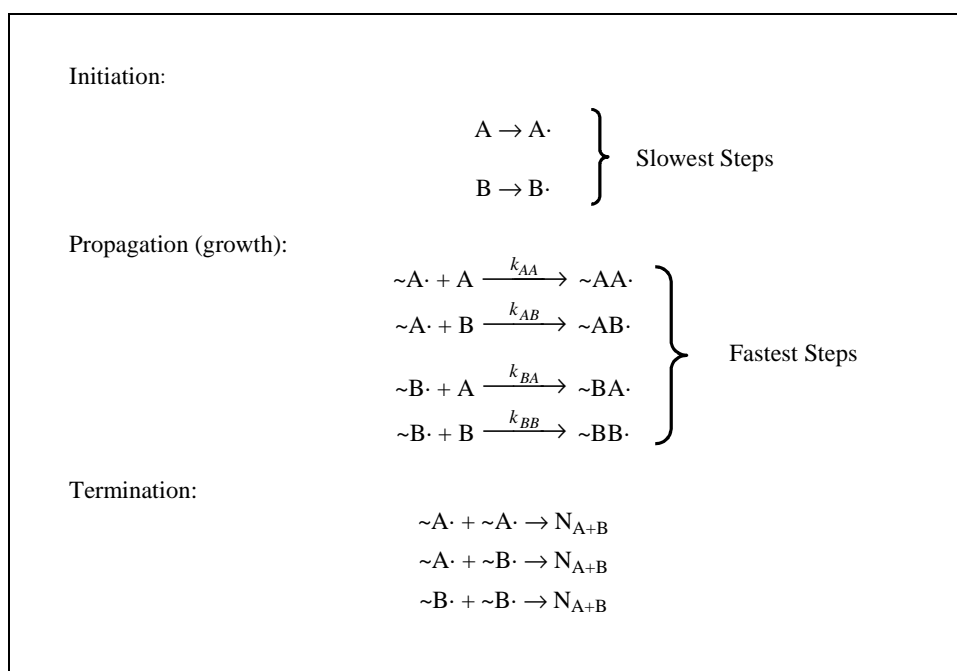


Figure 6.1. Typical free radical copolymerization reaction of two monomers, A and B

From the four growth reactions in Figure 6.1, the parameters r_A and r_B can each be defined as a monomer reactivity ratio and are defined as

$$r_A = k_{AA}/k_{AB} \quad \text{and} \quad r_B = k_{BB}/k_{BA} \quad (6.1)$$

The monomer reactivity ratio is the ratio of rate constants for a reactive propagating species addition to its own type of monomer to the rate constant for its addition to the other monomer. The monomer reactivity ratio can be considered to be the relative tendency for homopolymerization and cross-propagation copolymerization [110].

In spite of the commercial interest in the styrene (S) and acrylonitrile (AN) copolymer (SAN), limited information is available on its thermal stability and runaway

behavior under different monomer feeding ratios. Traditionally, modeling and simulation of copolymerization reactions have been centered on predicting composition and conversion, but understanding chemical reactivity and runaway reaction behavior is necessary for safe and economic processes.

In this research, copolymerization of styrene-acrylonitrile in bulk was evaluated for its thermal reactivity and runaway behavior using theoretical computational models and thermal analysis techniques. The Reactive System Screening Tool (RSST™) was used for preliminary analysis and the Automatic Pressure Tracking Adiabatic Calorimeter (APTAC™) was used for a more detailed characterization of the temperature and pressure profiles of the copolymerization reaction. Several styrene-acrylonitrile monomer feed ratios were tested to analyze the effect of composition on the temperature and pressure behavior during a runaway scenario. At the same time, theoretical evaluation was conducted to predict reaction pathways to explain the experimental results and also to compare with literature values.

2. Thermal Hazards Evaluation

The thermal runaway in polymerization reactors is characterized by a rapid increase in reaction rate and an accelerating temperature rise. The consequence of thermal runaway may not be only the large temperature rise and possible instability. Runaway could cause also a sharp reduction in polymer/copolymer molecular weight and an increased spread in molecular weight distribution [112-115].

As discussed in Chapter III, the evaluation of thermal hazards due to chemical reactivity should be based on a thorough understanding of reaction chemistry, which includes reaction thermodynamic, kinetic, and stoichiometric parameters. Calorimetric analysis is a very fundamental procedure for reactivity thermal hazards evaluation, but this procedure is expensive for the study of copolymerization reactions. Also, calorimetric analysis provides an overall thermal hazard evaluation, with poor reaction stoichiometric information especially for this kind of reaction mechanisms. Combining theoretical analysis with the experimental evaluation helps to reduce the cost of experimental analysis and helps to improve the understanding of the reaction mechanisms and pathways.

Theoretical analysis may be based on thermodynamic and kinetic parameters available in the literature or they can be calculated using computational quantum chemistry methods and empirical, thermodynamic-energy correlations. In this work literature information and thermodynamic-energy correlations were combined to provide an explanation of the styrene-acrylonitrile runaway behavior.

3. Computational Models

Providing a comprehensive level of theoretical reactivity analysis depends on the ability to provide possible and acceptable reaction pathways. As discussed earlier, the propagation steps in the copolymerization reactions are by far the fastest reaction steps and are responsible for most of the released energy and hence, pressure build-up.

In the propagation steps of copolymerization reaction that contain styrene and acrylonitrile monomers, the two major reaction pathways are the homopolymerization of

each monomer and the copolymerization (cross-polymerization) of the two monomers. Even for each of these two major reaction pathways, there is still large number of reaction pathway possibilities due to the orientation of the monomers and the alternating formed hydrocarbon chain. Styrene readily copolymerizes with many other monomers spontaneously. The styrene double bond is electronegative on account of the donating effect of the phenyl ring. Monomers that have electron-withdrawing substituents, e.g., acrylonitrile, tend to copolymerize most readily with styrene because their electropositive double bonds are attached to the electronegative styrene double bond [91,116]. Figure 6.2 demonstrates a summary of the possible homopolymerization and copolymerization pathways for the styrene and acrylonitrile monomers.

Styrene and acrylonitrile are non-symmetric molecules, therefore, there are two reactive ends for each monomer and hence the orientation of the reactive sites should be considered when analyzing the possible reaction pathways. In this research and for the purpose of simplicity, the styrene monomer is defined as A–B monomer and the acrylonitrile monomer is defined as C–D monomer. A–B and C–D defines the two reactive ends of each monomer. Based on these A–B and C–D monomer definitions, the monomer orientation during the reaction is considered. Figure 6.3 illustrates the two reactive ends that were used for each molecule.

To predict the relative tendency for homopolymerization and cross-propagation copolymerization, Gibbs free energy and enthalpy of reactions were calculated using the computational semi-empirical method, AM1 [68]. These calculations were performed for the styrene and acrylonitrile homopolymerization and for the styrene-acrylonitrile

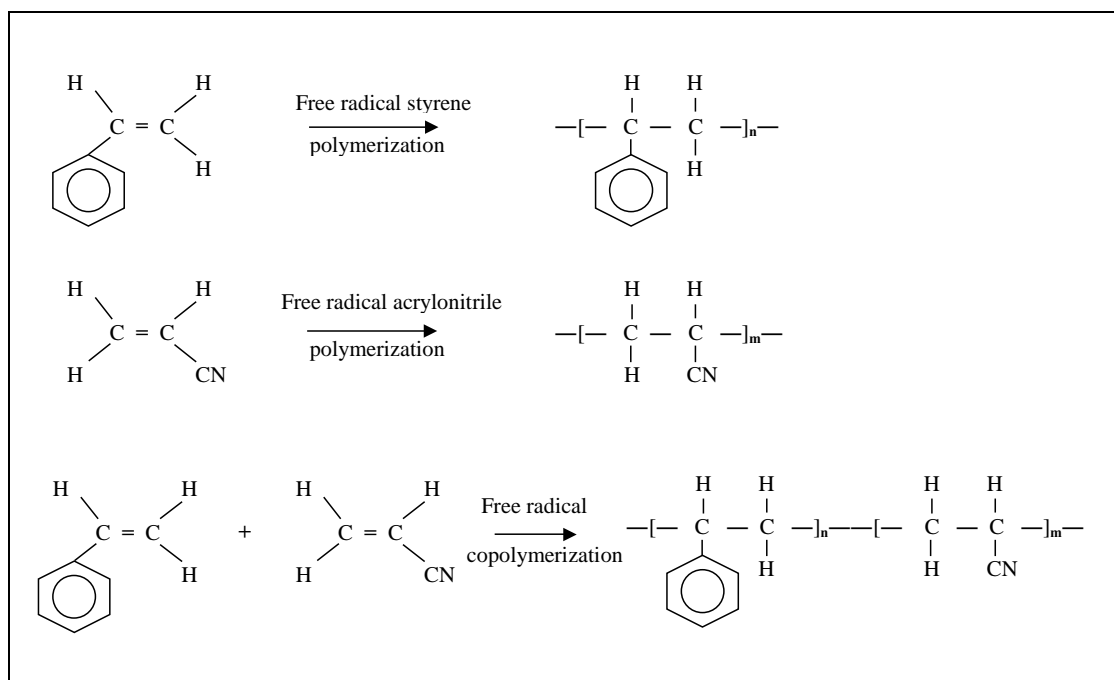


Figure 6.2. Possible free radical homopolymerization and copolymerization pathways for the styrene and acrylonitrile monomers

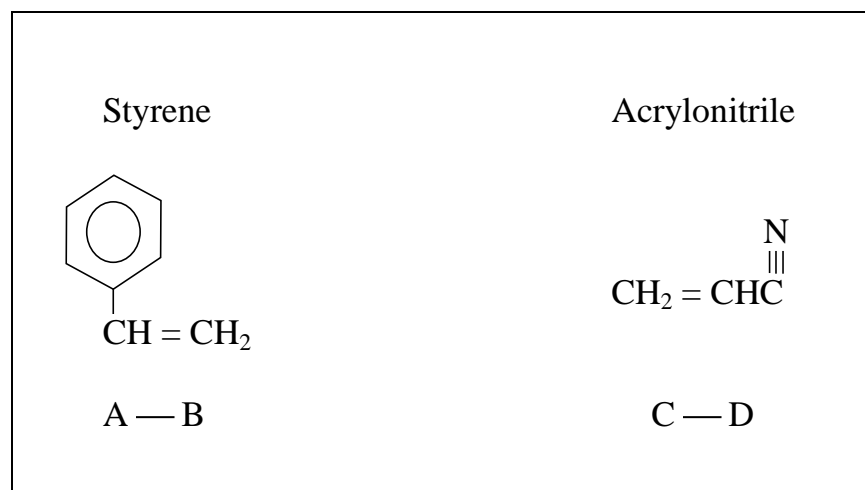


Figure 6.3. Styrene and acrylonitrile reactive ends as identified in this research

cross-propagation copolymerization. A three-monomer chain formation was considered with various combinations of monomer alternating and orientation. Examples of these considerations are illustrated in Figure 6.4 for the copolymerization of two styrene monomers with one acrylonitrile monomer. The enthalpies of reaction calculated using AM1 for these different monomer orientation possibilities are presented in Table 6.1.

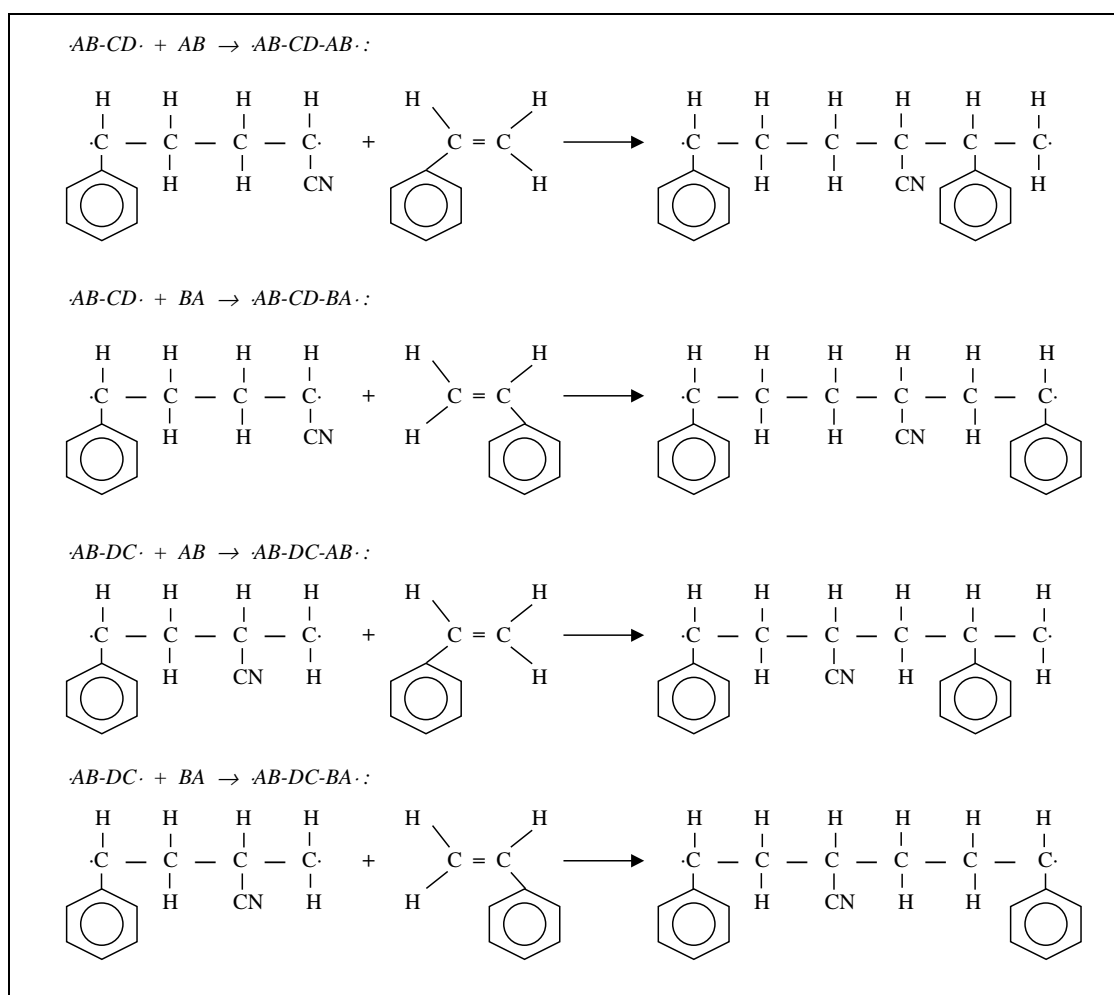


Figure 6.4. Examples of styrene and acrylonitrile monomers copolymerization reactions

Table 6.1

Heats of reaction for styrene and acrylonitrile homopolymerization and styrene-acrylonitrile cross-polymerization using the semi-empirical level of theory AM1

Reaction	Propagation reactions	AM1 heat of reaction, (kcal/mol)
1	$\cdot\text{AB-AB}\cdot + \text{AB} \rightarrow \cdot\text{AB-AB-AB}\cdot$	-40.0
2	$\cdot\text{AB-BA}\cdot + \text{BA} \rightarrow \cdot\text{AB-BA-BA}\cdot$	-41.2
3	$\cdot\text{BA-AB}\cdot + \text{AB} \rightarrow \cdot\text{BA-AB-AB}\cdot$	-39.7
4	$\cdot\text{AB-AB}\cdot + \text{BA} \rightarrow \cdot\text{AB-AB-BA}\cdot$	-57.0
5	$\cdot\text{BA-AB}\cdot + \text{BA} \rightarrow \cdot\text{BA-AB-BA}\cdot$	-55.6
6	$\cdot\text{AB-BA}\cdot + \text{AB} \rightarrow \cdot\text{AB-BA-AB}\cdot$	-21.8
7	$\cdot\text{BA-BA}\cdot + \text{AB} \rightarrow \cdot\text{BA-BA-AB}\cdot$	-21.5
8	$\cdot\text{AB-AB-AB}\cdot + \text{AB} \rightarrow \cdot\text{AB-AB-AB-AB}\cdot$	-37.3
9	$\cdot\text{CD-CD}\cdot + \text{CD} \rightarrow \cdot\text{CD-CD-CD}\cdot$	-48.5
10	$\cdot\text{CD-DC}\cdot + \text{DC} \rightarrow \cdot\text{CD-DC-DC}\cdot$	-47.4
11	$\cdot\text{DC-CD}\cdot + \text{CD} \rightarrow \cdot\text{DC-CD-CD}\cdot$	-49.0
12	$\cdot\text{CD-DC}\cdot + \text{CD} \rightarrow \cdot\text{CD-DC-CD}\cdot$	-58.3
13	$\cdot\text{DC-DC}\cdot + \text{CD} \rightarrow \cdot\text{DC-DC-CD}\cdot$	-59.6
14	$\cdot\text{CD-CD}\cdot + \text{DC} \rightarrow \cdot\text{CD-CD-DC}\cdot$	-38.5
15	$\cdot\text{DC-CD}\cdot + \text{DC} \rightarrow \cdot\text{DC-CD-DC}\cdot$	-38.9
16	$\cdot\text{CD-CD-CD}\cdot + \text{CD} \rightarrow \cdot\text{CD-CD-CD-CD}\cdot$	-44.6
17	$\cdot\text{AB-CD}\cdot + \text{AB} \rightarrow \cdot\text{AB-CD-AB}\cdot$	-31.1
18	$\cdot\text{BA-CD}\cdot + \text{AB} \rightarrow \cdot\text{BA-CD-AB}\cdot$	-24.2
19	$\cdot\text{AB-CD}\cdot + \text{BA} \rightarrow \cdot\text{AB-CD-BA}\cdot$	-48.4
20	$\cdot\text{BA-CD}\cdot + \text{BA} \rightarrow \cdot\text{BA-CD-BA}\cdot$	-49.2
21	$\cdot\text{AB-DC}\cdot + \text{AB} \rightarrow \cdot\text{AB-DC-AB}\cdot$	-41.4
22	$\cdot\text{BA-DC}\cdot + \text{AB} \rightarrow \cdot\text{BA-DC-AB}\cdot$	-33.9
23	$\cdot\text{AB-DC}\cdot + \text{BA} \rightarrow \cdot\text{AB-DC-BA}\cdot$	-57.6
24	$\cdot\text{BA-DC}\cdot + \text{BA} \rightarrow \cdot\text{BA-DC-BA}\cdot$	-57.8
25	$\cdot\text{CD-AB}\cdot + \text{AB} \rightarrow \cdot\text{CD-AB-AB}\cdot$	-40.1
26	$\cdot\text{CD-BA}\cdot + \text{BA} \rightarrow \cdot\text{CD-BA-BA}\cdot$	-40.5
27	$\cdot\text{DC-AB}\cdot + \text{AB} \rightarrow \cdot\text{DC-AB-AB}\cdot$	-40.5
28	$\cdot\text{DC-BA}\cdot + \text{BA} \rightarrow \cdot\text{DC-BA-BA}\cdot$	-35.0
29	$\cdot\text{CD-AB}\cdot + \text{BA} \rightarrow \cdot\text{CD-AB-BA}\cdot$	-57.1
30	$\cdot\text{DC-AB}\cdot + \text{BA} \rightarrow \cdot\text{DC-AB-BA}\cdot$	-57.4
31	$\cdot\text{CD-BA}\cdot + \text{AB} \rightarrow \cdot\text{CD-BA-AB}\cdot$	-22.7
32	$\cdot\text{DC-BA}\cdot + \text{AB} \rightarrow \cdot\text{DC-BA-AB}\cdot$	-21.7
33	$\cdot\text{BA-BA}\cdot + \text{DC} \rightarrow \cdot\text{BA-BA-DC}\cdot$	-31.0
34	$\cdot\text{AB-BA}\cdot + \text{DC} \rightarrow \cdot\text{AB-BA-DC}\cdot$	-32.4
35	$\cdot\text{BA-AB}\cdot + \text{DC} \rightarrow \cdot\text{BA-AB-DC}\cdot$	-49.3
36	$\cdot\text{AB-AB}\cdot + \text{DC} \rightarrow \cdot\text{AB-AB-DC}\cdot$	-49.0
37	$\cdot\text{BA-BA}\cdot + \text{CD} \rightarrow \cdot\text{BA-BA-CD}\cdot$	-41.1
38	$\cdot\text{AB-BA}\cdot + \text{CD} \rightarrow \cdot\text{AB-BA-CD}\cdot$	-42.3
39	$\cdot\text{BA-AB}\cdot + \text{CD} \rightarrow \cdot\text{BA-AB-CD}\cdot$	-57.5
40	$\cdot\text{AB-AB}\cdot + \text{CD} \rightarrow \cdot\text{AB-AB-CD}\cdot$	-52.7

Table 6.1
Continued

Reaction	Propagation reactions	AM1 heat of reaction, (kcal/mol)
41	$\cdot\text{CD-AB}\cdot + \text{CD} \rightarrow \cdot\text{CD-AB-CD}\cdot$	-57.2
42	$\cdot\text{DC-AB}\cdot + \text{CD} \rightarrow \cdot\text{DC-AB-CD}\cdot$	-58.2
43	$\cdot\text{CD-AB}\cdot + \text{DC} \rightarrow \cdot\text{CD-AB-DC}\cdot$	-48.0
44	$\cdot\text{DC-AB}\cdot + \text{DC} \rightarrow \cdot\text{DC-AB-DC}\cdot$	-48.6
45	$\cdot\text{CD-BA}\cdot + \text{CD} \rightarrow \cdot\text{CD-BA-CD}\cdot$	-40.8
46	$\cdot\text{DC-BA}\cdot + \text{CD} \rightarrow \cdot\text{DC-BA-CD}\cdot$	-41.2
47	$\cdot\text{CD-BA}\cdot + \text{DC} \rightarrow \cdot\text{CD-BA-DC}\cdot$	-30.5
48	$\cdot\text{DC-BA}\cdot + \text{DC} \rightarrow \cdot\text{DC-BA-DC}\cdot$	-30.5
49	$\cdot\text{AB-CD}\cdot + \text{CD} \rightarrow \cdot\text{AB-CD-CD}\cdot$	-48.6
50	$\cdot\text{BA-DC}\cdot + \text{DC} \rightarrow \cdot\text{BA-DC-DC}\cdot$	-45.2
51	$\cdot\text{BA-CD}\cdot + \text{CD} \rightarrow \cdot\text{BA-CD-CD}\cdot$	-49.4
52	$\cdot\text{AB-DC}\cdot + \text{DC} \rightarrow \cdot\text{AB-DC-DC}\cdot$	-47.5
53	$\cdot\text{AB-CD}\cdot + \text{DC} \rightarrow \cdot\text{AB-CD-DC}\cdot$	-38.9
54	$\cdot\text{BA-CD}\cdot + \text{DC} \rightarrow \cdot\text{BA-CD-DC}\cdot$	-39.1
55	$\cdot\text{AB-DC}\cdot + \text{CD} \rightarrow \cdot\text{AB-DC-CD}\cdot$	-58.6
56	$\cdot\text{BA-DC}\cdot + \text{CD} \rightarrow \cdot\text{BA-DC-CD}\cdot$	-57.7
57	$\cdot\text{DC-DC}\cdot + \text{BA} \rightarrow \cdot\text{DC-DC-BA}\cdot$	-58.8
58	$\cdot\text{CD-DC}\cdot + \text{BA} \rightarrow \cdot\text{CD-DC-BA}\cdot$	-57.9
59	$\cdot\text{DC-CD}\cdot + \text{BA} \rightarrow \cdot\text{DC-CD-BA}\cdot$	-49.0
60	$\cdot\text{CD-CD}\cdot + \text{BA} \rightarrow \cdot\text{CD-CD-BA}\cdot$	-48.5
61	$\cdot\text{DC-DC}\cdot + \text{AB} \rightarrow \cdot\text{DC-DC-AB}\cdot$	-42.6
62	$\cdot\text{CD-DC}\cdot + \text{AB} \rightarrow \cdot\text{CD-DC-AB}\cdot$	-41.2
63	$\cdot\text{DC-CD}\cdot + \text{AB} \rightarrow \cdot\text{DC-CD-AB}\cdot$	-30.6
64	$\cdot\text{CD-CD}\cdot + \text{AB} \rightarrow \cdot\text{CD-CD-AB}\cdot$	-28.7

In this theoretical evaluation, the semi-empirical AM1 method was employed for its simplicity and low calculation cost. These calculations are used for relative comparisons and are not intended for exact prediction of reaction enthalpies. For more accurate thermochemical predictions, more advanced computational models should be employed.

The Polanyi equation, as discussed earlier in Chapters IV and V, was used to quantify the behavior of some elementary reactions to be less probable than other

reactions based on the activation energies. In addition, activation barriers to reaction allow favorable reaction pathways [75]. This principle was used here to predict the most favored propagation reaction pathways. All the propagation steps, as presented in Table 6.1, share the same reaction mechanism, and based on the Polanyi equation; these steps have approximately the same intrinsic barrier of reaction and transfer coefficient. Therefore, it is expected that the highest exothermic reactions will have the lowest activation energies. Therefore, they will be considered the most probable reactions.

From the results presented in Table 6.1 it is clear that Reactions 23, 24, 29, 30, 39, 40, 41, 42, 55, 56, 57, and 58 are the most exothermic reactions among the cross-propagation reactions. When compared to the homopolymerization reactions, the cross-propagation reactions are dominant. This indicates that in the presence of the two monomers in the mixtures, they, most probably, will go through a cross-propagation mechanism. Another important finding from the AM1 calculations is the negligible effect of the adjacent monomer units to the chain reactive end. It is clear from these calculations that the two reacting sites determine the enthalpy of reaction. In addition, it can be noticed that when the copolymerization reactive sites are B and C, the resultant enthalpy of reaction is the maximum.

Generally, these findings were found to be in agreement with conclusions in literature. Hill et al. [117,118] reported that the styrene-acrylonitrile copolymerization follows the penultimate model. In this model, the rate constants of the monomer addition onto the macro-radical depend on the nature of the monomer and the last two monomer

units of the macro-radical. The reactivity ratios of styrene (S) - acrylonitrile (A) copolymerization are defined as:

$$r_{SS} = k_{SSS}/k_{SSA} \quad r_{AA} = k_{AAA}/k_{AAS} \quad r_{AS} = k_{ASS}/k_{ASA} \quad r_{SA} = k_{SAA}/k_{SAS}$$

In their study, researchers reported the experimental reactivity ratios of the copolymerization reactions as $r_{SS} = 0.22$, $r_{AA} = 0.03$, $r_{AS} = 0.63$, and $r_{SA} = 0.09$.

Other researchers [105,111,119] indicated that r_S has values ~ 0.41 and r_A has values ~ 0.04 . Both r_S and r_A were defined in Equation 6.1. These findings suggest that most of the monomers will go through a copolymerization mechanism. Acrylonitrile will have a very weak tendency to go through a homopolymerization path, but styrene exhibits a better tendency to do so.

As mentioned earlier, the AM1 level of theory was not used for absolute property estimation but as a relative prediction approach to determine the most critical or dominant reactions. In addition to AM1, the density functional level of theory B3LYP/6-31G(d) was employed to calculate the heat of reaction for Reactions 23, 24, 41, and 42 as presented in Table 6.2. These calculated heats of reaction are assumed to be representative of the most dominant reaction pathways of the SAN copolymerization. According to these values, AM1 systematically overestimated the heats of reaction.

4. Experimental Analysis

The complexity of polymerization/copolymerization reactions will not allow the low-cost theoretical evaluation methods to provide an exact description of the reactivity hazardous pathways. Up to this point, theoretical computational methods helped us to

predict a trend of possible reaction pathways of styrene-acrylonitrile copolymerization and a relative tendency of homopolymerization and cross-linking pathways. Moreover, theoretical heat of reaction calculations using a higher level of theory provided a sense of possible energy liberation. Such knowledge helps to guide the experimental investigations.

Table 6.2

Heats of reaction of selected propagation steps for styrene-acrylonitrile cross-polymerization using the density functional level of theory B3LYP/6-31G(d)

Reaction no.	Propagation reactions	B3LYP/6-31G(d) heat of reaction, (kcal/mol)
23	$\cdot\text{AB-DC}\cdot + \text{BA} \rightarrow \cdot\text{AB-DC-BA}\cdot$	-30.8
24	$\cdot\text{BA-DC}\cdot + \text{BA} \rightarrow \cdot\text{BA-DC-BA}\cdot$	-38.7
41	$\cdot\text{CD-AB}\cdot + \text{CD} \rightarrow \cdot\text{CD-AB-CD}\cdot$	-32.5
42	$\cdot\text{DC-AB}\cdot + \text{CD} \rightarrow \cdot\text{DC-AB-CD}\cdot$	-35.7

The thermal copolymerization of SAN in bulk using the RSST™ was performed and in parallel to the previous theoretical computational evaluation. Following that, a detailed thermal analysis using the APTAC™ was conducted. In this section the results of both screening and detailed thermal analyses of the thermal copolymerization of SAN in bulk system will be presented and discussed.

4.1. Materials

Aldrich 99+% styrene and Aldrich 99+% acrylonitrile monomers were used to prepare several feeding ratios, as presented in Table 6.3. Styrene and acrylonitrile monomers were used with no additional purification or treatment processes. The styrene monomer is inhibited with 10-15 ppm of 4-tert-butylcatechol, while the acrylonitrile monomers is inhibited with 35-45 ppm of monomethyl ether hydroquinone. Samples were prepared on the same day of testing. All experiments were conducted under nitrogen environment following evacuation of air from the test cells. High purity compressed nitrogen was used in the RSST™ and APTAC™ experiments to provide the no-air environment, reduce liquid boil-off, and backup the cell.

Table 6.3

Styrene-acrylonitrile monomers feed ratios

Feed sample	S:AN weight ratio	S:AN mole ratio
1	80 : 20	1.0 : 0.49
2	70 : 30	1.0 : 0.84
3	60 : 40	1.0 : 1.31
4	50 : 50	1.0 : 1.96
5	40 : 60	1.0 : 2.94
6	30 : 70	1.0 : 4.58
7	20 : 80	1.0 : 7.85

4.2. Apparatus

Thermal analysis of these samples was performed using the RSST™ and APTAC™ calorimeters. A detailed description of each of these calorimeters, operating procedures, and data quality was discussed in Chapter IV.

4.3. Data Analysis

Experimental data analysis was performed on the time-temperature-pressure data that was collected. Thermodynamic and kinetic parameters of the suggested reaction pathways were calculated according to the methods and procedures described in Chapter IV and later in this chapter.

4.4. RSST™ Thermal Analysis

Experimental screening analysis using the RSST™ was performed for each of the seven monomer feed ratios presented in Table 6.3. Styrene-acrylonitrile monomers were mixed at room temperature. RSST™ cell was evacuated from air using a vacuum pump and then purged with nitrogen and evacuated again. This process was repeated for several times to ensure the absence of air from the test cell. The mixed styrene-acrylonitrile samples were injected with a special injection syringe into the evacuated RSST™ glass cell, and then pressurized with nitrogen. RSST™ testing was performed with a nitrogen backup pressure of about 300 psig to reduce liquid boil-off before copolymerization. Temperature ramping rates of 0.7 to 3.3 °C/min were applied for sample masses of 7.6 to 8.2 g in a glass cell with a thermal inertia factor, ϕ , of about

1.03. Stirring was present during the experiments and it was kept at a constant speed for all the experimental runs. Table 6.4 presents a summary of the experimental conditions of the tested samples.

Temperature and pressure profiles during the SAN copolymerization are shown in Figures 6.5 and 6.6, respectively. Clearly, these profiles indicate an exothermic reactivity and a rapid pressure increase. Temperature and pressure profiles also show similar reaction onset temperatures despite of the samples styrene-acrylonitrile feed ratio or RSST™ temperature ramping rate. However, temperature profiles demonstrate that the maximum reached temperature decreases as the styrene content decreases. On the other hand, pressure profiles show higher maximum pressure increase for samples with lower styrene content. A summary of the measured temperatures for the tested samples is presented in Table 6.5.

Table 6.4

Summary of the experimental parameters of SAN copolymerization samples with the RSST™

S:AN wt. ratio	Replicate	Sample wt. (g)	Cell wt. (g)	Temperature ramping rate range, (°C/min)
80 : 20	10	8.0 ± 0.1	1.5 ± 0.1	1.0 – 3.3
70 : 30	3	8.2 ± 0.0	1.4 ± 0.1	1.3 – 1.7
60 : 40	4	8.1 ± 0.1	1.4 ± 0.1	1.1 – 1.7
50 : 50	4	8.2 ± 0.1	1.4 ± 0.1	1.1 – 1.4
40 : 60	4	8.0 ± 0.3	1.4 ± 0.1	0.7 – 1.8
30 : 70	2	8.2 ± 0.0	1.5 ± 0.0	1.1
20 : 80	2	8.0 ± 0.1	1.5 ± 0.1	1.0 – 1.1

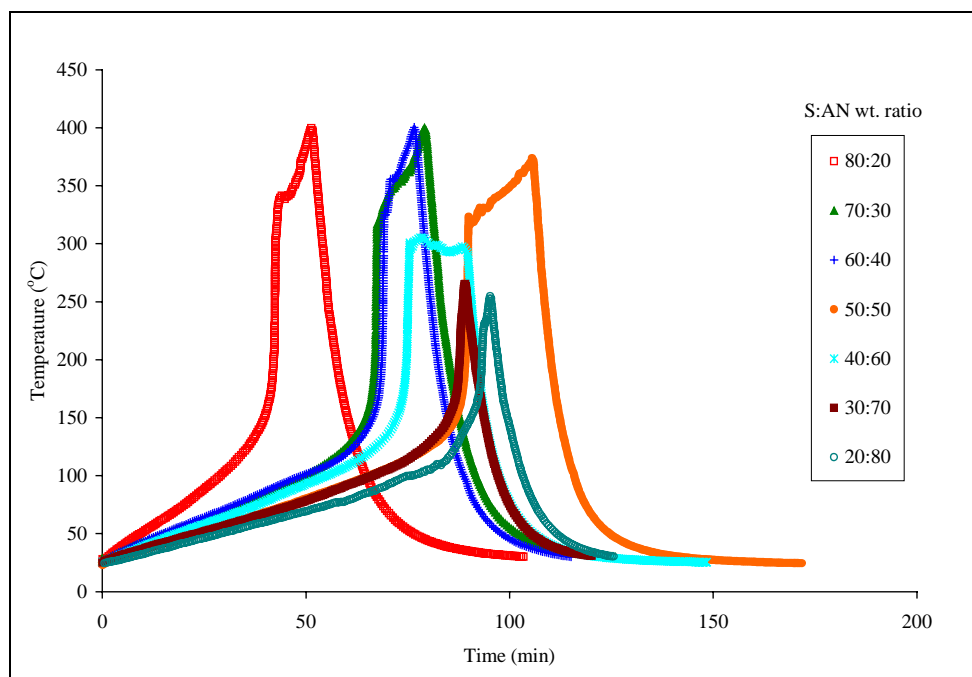


Figure 6.5. SAN copolymerization temperature profiles with the RSST™

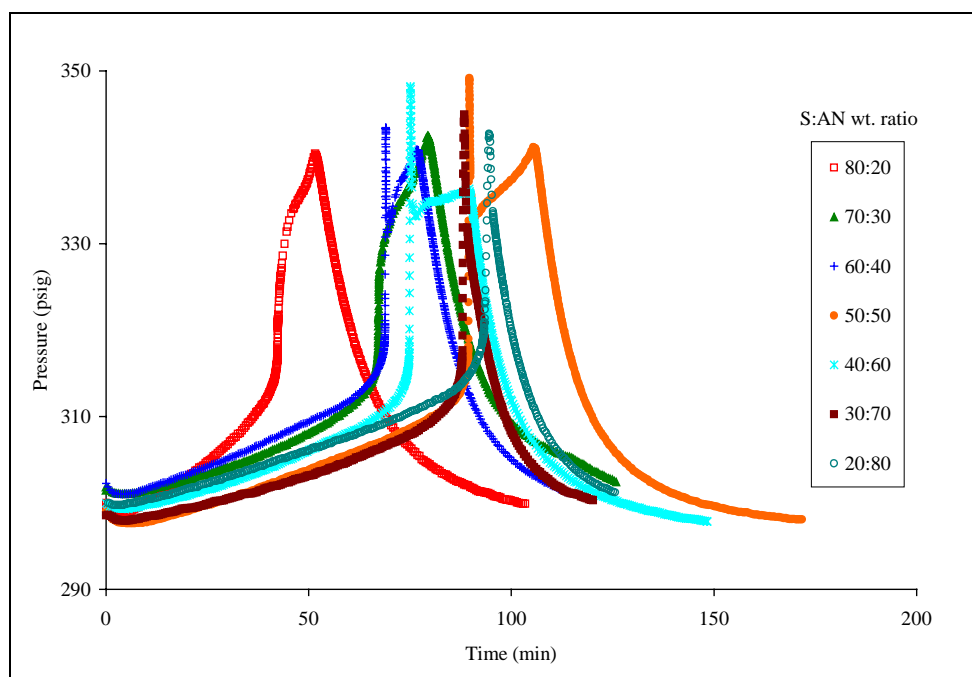


Figure 6.6. SAN copolymerization pressure profiles with the RSST™

Table 6.5

Summary of the measured temperatures of SAN copolymerization samples with the RSST™

S:AN wt. ratio	T_o (°C)	T_{max} (°C)	ΔT_{ad} (°C)	ϕ -Factor	C_s (cal/(g · K))	C_c (cal/(g · K))
80 : 20	108 ± 3	335 ± 22	219 ± 25	1.03	0.635	0.098
70 : 30	103 ± 1	355 ± 6	252 ± 7	1.02	0.695	0.096
60 : 40	107 ± 5	320 ± 9	214 ± 9	1.02	0.675	0.099
50 : 50	103 ± 5	318 ± 5	216 ± 4	1.03	0.697	0.099
40 : 60	114 ± 7	303 ± 9	189 ± 3	1.03	0.703	0.100
30 : 70	102 ± 4	268 ± 4	167 ± 8	1.03	0.668	0.105
20 : 80	103 ± 4	251 ± 6	148 ± 10	1.03	0.664	0.106

The heat capacities of the sample solution, C_s , as in Table 6.5 were estimated at an average temperature of reaction onset temperature, T_o , and the maximum reaction temperature achieved, T_{max} , considering the proportion of styrene and acrylonitrile in each sample and based on the correlations available in the literature [105]. The heat capacities of the glass cells, C_c , were estimated at the same average temperatures. Implicitly we assumed that the change in average heat capacity during the decomposition reaction is negligible. In fact, heat capacity estimation is one of the main sources of uncertainty in the measured heat of reaction, because of the continuous temperature and composition changes during the experiment.

Experimental data analysis, as presented in Chapter IV, was conducted on the RSST™ data. The heat of the copolymerization reaction of SAN is calculated using Equation 4.7. A first-order kinetic model was assumed to fit the SAN copolymerization.

Figure 6.7 shows $(-\log k)$ vs. $(1/T)$ plot for the thermal copolymerization of all tested SAN samples. The plotted first-order reaction kinetics has an average linear fitting regression coefficient of 0.975. Table 6.6 summarizes the onset temperatures, heats of reaction, and Arrhenius parameters determined from the RSST™ data. Generally, the measured heat of reaction is a function of the styrene-acrylonitrile feed ratio. The Arrhenius parameters show comparable values for styrene wt. ratio as low as 50%; however, below this ratio, Arrhenius parameters start to change. These observations will be discussed later in this chapter.

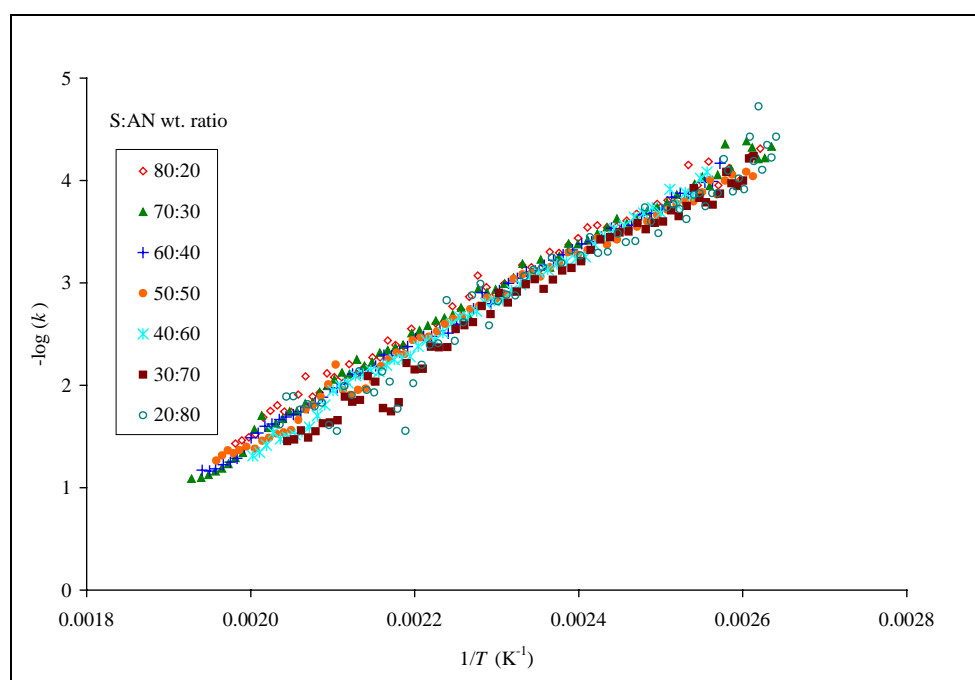


Figure 6.7. First-order kinetics of SAN copolymerization with the RSST™

Table 6.6

Summary of the experimental thermodynamic and kinetic parameters of SAN copolymerization with the RSST™

S:AN wt. ratio	ΔH_r (cal/g)	Reaction order, n	E_A , (kcal/mol)	$\log(A)$ (s ⁻¹)
80:20	-155 ± 11	1	21.3 ± 1.7	7.8 ± 0.7
70:30	-179 ± 7	1	20.6 ± 0.6	7.5 ± 0.3
60:40	-148 ± 9	1	20.9 ± 0.1	7.8 ± 0.0
50:50	-154 ± 4	1	21.1 ± 1.1	7.9 ± 0.5
40:60	-136 ± 5	1	23.7 ± 4.1	9.4 ± 2.2
30:70	-114 ± 6	1	21.2 ± 0.8	8.0 ± 0.5
20:80	-101 ± 8	1	19.8 ± 1.5	7.4 ± 0.6

Reaction kinetics of the exothermic copolymerization reaction is also presented in the self-heating rate plot shown in Figure 6.8. Self-heating rates of the RSST™ samples were corrected for the ramping temperature rate of each experiment, as discussed in Chapter IV.

In studying self-heating rate plotting as in Figure 6.8, the sample size, concentration, and ϕ factor should be considered. All of these samples have the same sample size and ϕ factor, however, they are different in the styrene-acrylonitrile ratios. Clearly as the styrene monomer concentration decreases, the maximum self-heating rate is also decreases. In addition, it can be noticed that the measured self-heating rate is almost the same for the various styrene-acrylonitrile ratios.

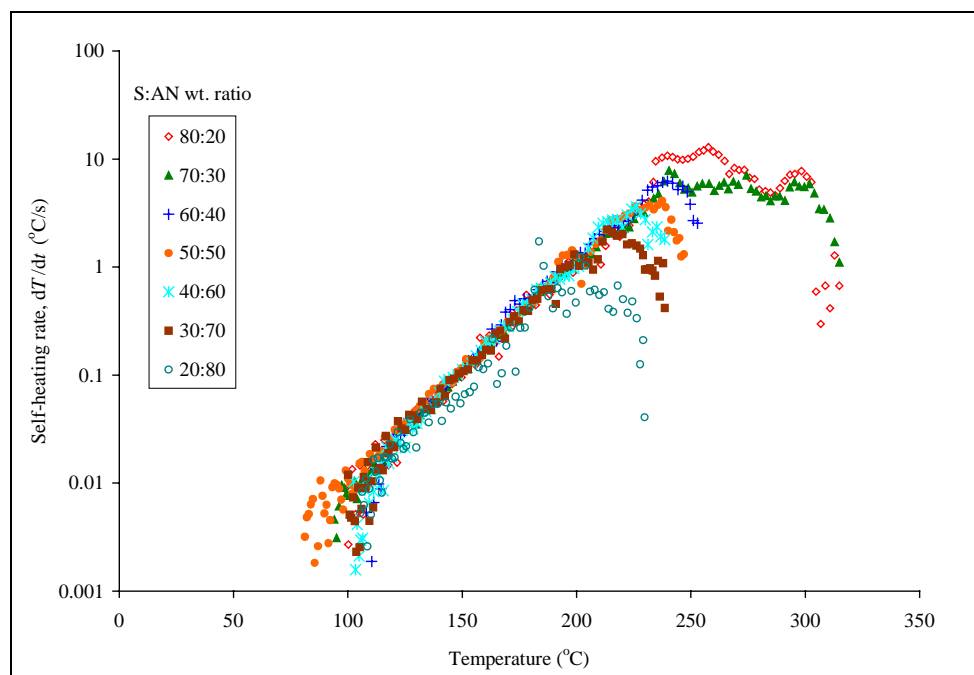


Figure 6.8. Self-heating rates of SAN copolymerization with the RSST™

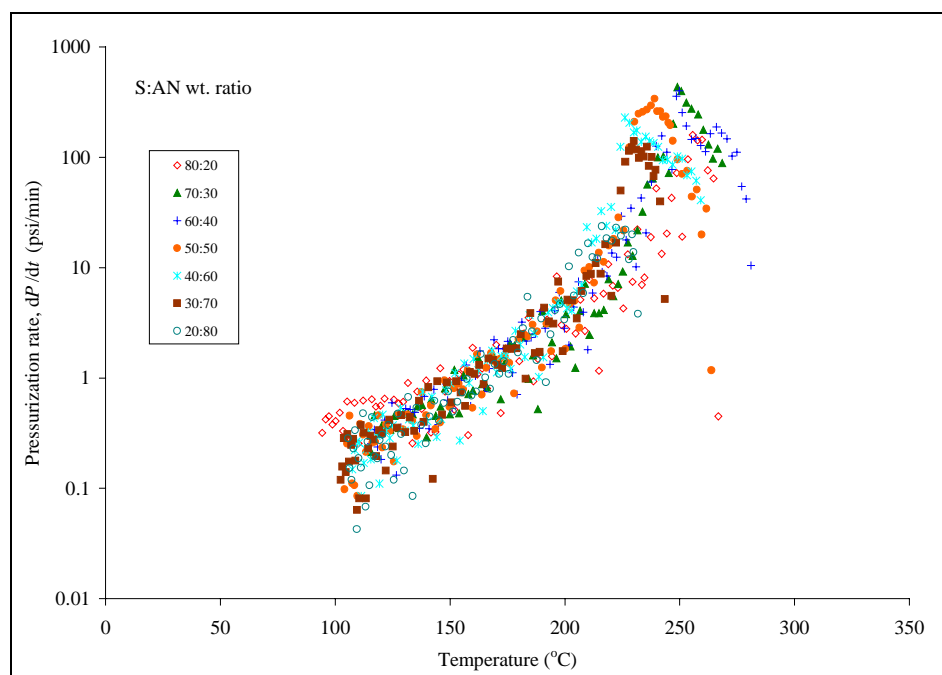


Figure 6.9. Pressurization rates of SAN copolymerization with the RSST™

Pressurization rate is presented in Figure 6.9. Similar behavior of pressurization rate was found compared to that of self-heating rate. Values of maximum self-heating and pressurization rates are presented in Table 6.7. Obviously, these rates are strong functions of styrene-acrylonitrile ratios.

Table 6.7

Maximum self-heating and pressurization rates of SAN copolymerization in the RSST™

S:AN wt. ratio	$(dT/dt)_{\max}$ (°C/s)	$(dP/dt)_{\max}$ (psi/min)
80:20	10.3 ± 4.0	N/A
70:30	7.9 ± 0.5	433 ± 13
60:40	6.8 ± 1.2	453 ± 74
50:50	4.1 ± 0.4	302 ± 28
40:60	3.0 ± 0.8	242 ± 17
30:70	2.0 ± 0.3	127 ± 21
20:80	2.1 ± 0.5	30 ± 8

4.5. APTAC™ Thermal Analysis

Adiabatic experimental analysis using the APTAC™ was performed for the same set of samples. Styrene-acrylonitrile monomers were each mixed at room temperature, frozen with liquid nitrogen at -102°C in an evacuated APTAC™ cell, and then pressurized with nitrogen. Both glass and titanium APTAC™ cells were used in this

analysis to allow various ϕ factor testing. APTAC™ adiabatic thermal analysis was performed under nitrogen environment for all the reported experiments.

The heat-wait-search mode of operation with heating rate of 2°C/min was applied in these experiments to test a total of 19 samples. Sample weights were ranging from 4 to 10 g. 130-ml APTAC™ cells of glass and titanium were used in these tests. The combinations of these cell material and samples sizes resulted in thermal inertia factors, ϕ factor, ranging from 1.53 – 3.57. These variations in the ϕ factor are useful in evaluating the effects of thermal inertia on reactivity parameters for scale-up procedures, as will be discussed later in this chapter.

Temperature and pressure profiles for the copolymerization reaction in the APTAC™ are shown in Figures 6.10 and 6.11, respectively. Table 6.8 summarizes the experimental measured temperatures for the tested samples. The reported onset temperature for each APTAC™ test was determined at a self-heating rate of 0.1°C/min.

Studying Figures 6.10 and 6.11 reveals quite different observations from those obtained by the RSST™ calorimeter. In these two sets of profiles, secondary temperature and pressure peaks start to form as the acrylonitrile concentration increases. At the same time, the copolymerization reaction peaks start to decrease, which is in agreement with the RSST™ results. The secondary peak causes larger temperature increase and larger pressure build-up until it exceeds those maximum temperature and pressure values of the copolymerization reaction at styrene-acrylonitrile weight ratio of 50:50. This is a clear indication of a secondary exothermic reaction resulting in either gaseous products or pressure increase due to temperature rise. RSST™ calorimeter

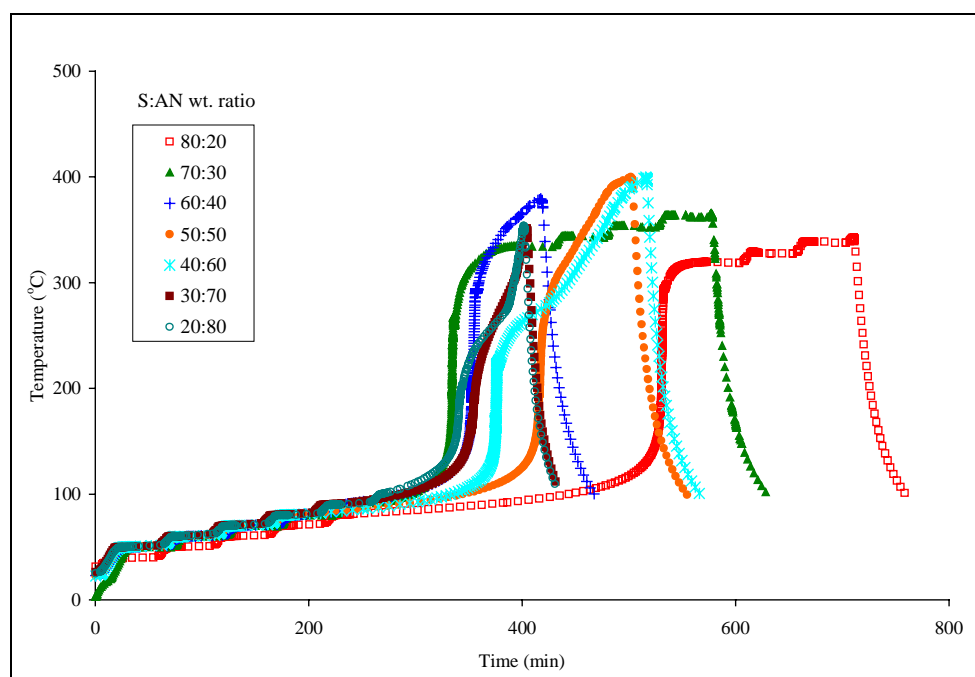


Figure 6.10. SAN copolymerization temperature profiles with the APTAC™

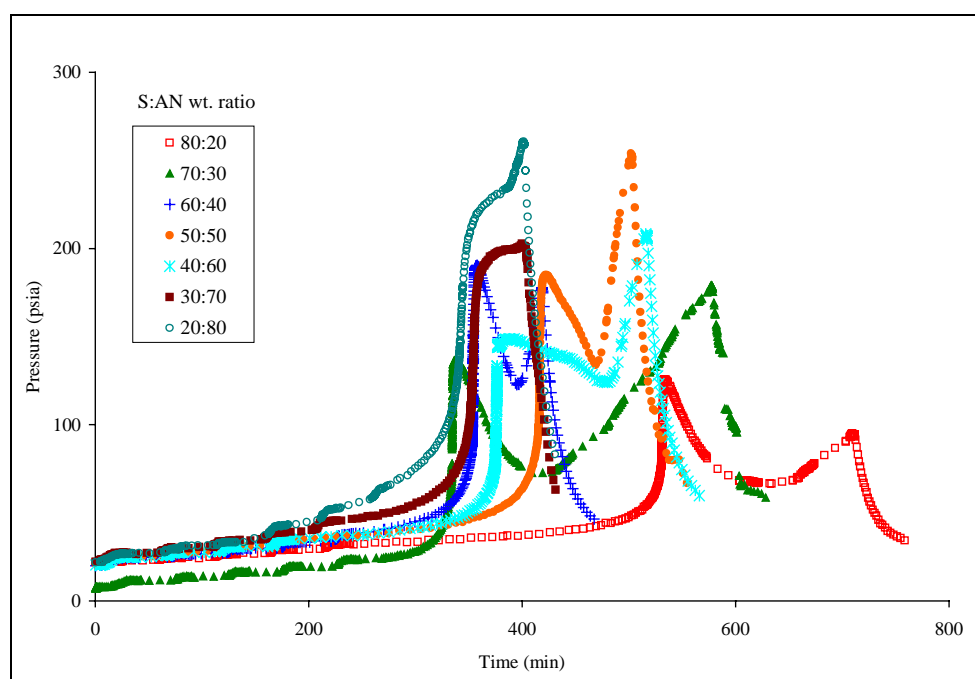


Figure 6.11. SAN copolymerization pressure profiles with the APTAC™

Table 6.8

Summary of the experimental results of SAN copolymerization samples with the APTAC™

S:AN wt. Ratio	Sample wt. (g)	Cell material	ϕ -Factor	T_o (°C)	T_{max} (°C)	ΔT_{ad} (°C)	C_s (cal/(g · K))
80 : 20	9.9	Titanium	1.65	89	338	249	0.636
	10.1	Titanium	1.65	87	336	249	0.633
	10.1	Titanium	1.64	92	339	247	0.638
	10.2	Glass	2.29	94	286	192	0.588
	10.1	Glass	1.87	92	320	228	0.616
70 : 30	10.6		2.23	90	284	194	0.600
	10.1	Glass	1.94	94	276	182	0.593
	10.1		1.96	93	270	177	0.587
	10.0		1.93	88	306	218	0.624
60 : 40	10.1		Glass	1.91	90	297	207
9.5	2.00	90		282	192	0.617	
50 : 50	10.1	Glass	1.85	90	304	214	0.670
	7.4		2.28	87	276	189	0.632
40 : 60	5.0	Glass	3.07	87	227	140	0.596
	4.0		3.65	95	209	114	0.582
30 : 70	4.1	Glass	2.80	102	231	129	0.622
	4.0		3.01	93	220	127	0.606
20 : 80	8.0	Titanium	1.93	90	227	187	0.620
	4.0	Glass	3.57	96	203	107	0.605

failed to show this behavior because of its open-cell setup that caused large material and heat losses that will not allow the developed secondary reaction to be presented. The temperatures reported in Table 6.8 are for primary copolymerization reaction. The maximum temperature was determined at the start temperature of the secondary reactions as presented in Figure 6.12. In this figure, a comparison between 80:20 and

40:60 SAN wt. ratio sample temperature and pressure profiles is presented. These temperatures will be used for total liberated energy calculation due to the copolymerization reaction and will be compared with the RSST™ results.

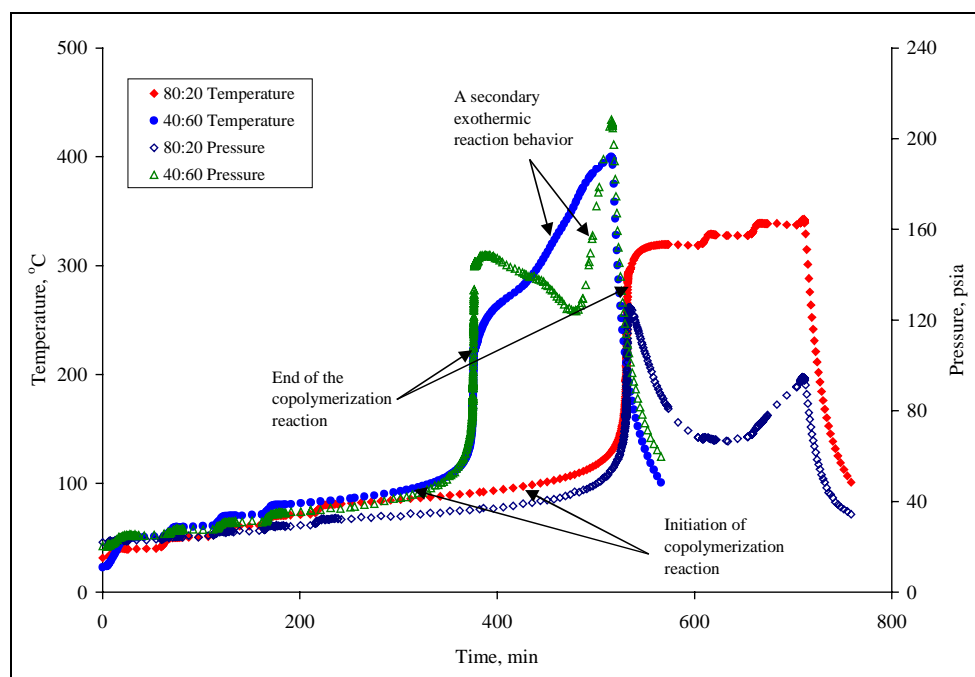


Figure 6.12. Maximum temperature and pressure for SAN reactions

The overall heat of reaction for copolymerization step of SAN was calculated using Equation 4.7 while time to maximum rate was calculated using Equation 4.13. A first-order kinetic model was assumed to fit the copolymerization reaction time-temperature profiles. Arrhenius parameters were obtained by plotting $(-\log k)$ vs. $(1/T)$ as presented in Figure 6.13 with an average linear fitting regression coefficient of 0.992. Table 6.9

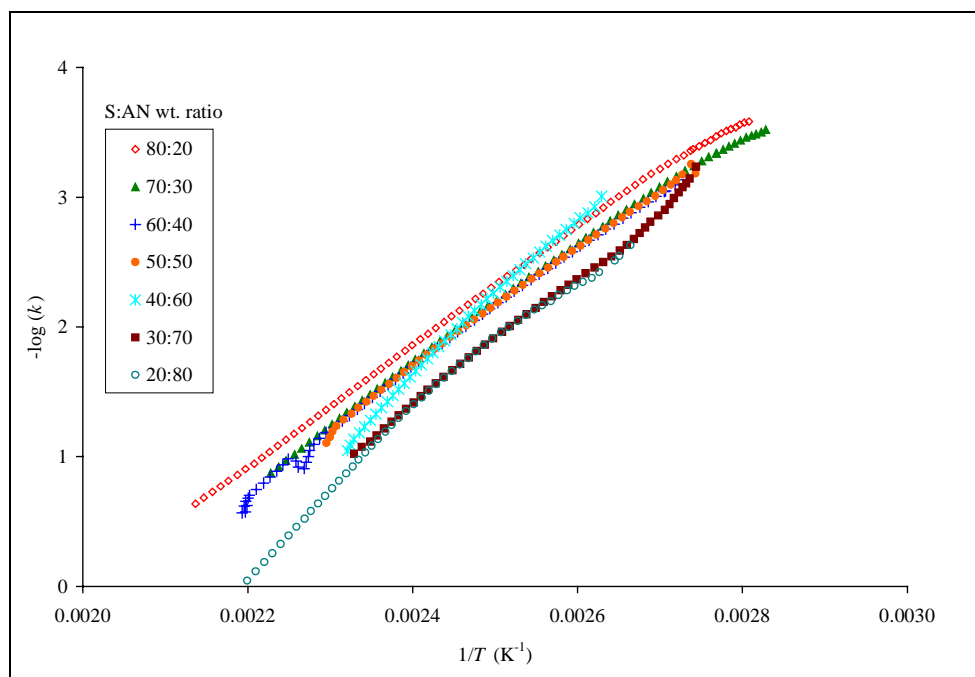


Figure 6.13. First-order kinetics of SAN copolymerization with the APTAC™

Table 6.9

Summary of the experimental thermodynamic and kinetic parameters of SAN copolymerization with the APTAC™

S:AN wt. ratio	T_o (°C)	ΔH_r (kcal/mol)	TMR_{ad} (min)	Reaction order, n	E_A (kcal/mol)	$\log(A)$ (s^{-1})
80:20	91 ± 3	-260 ± 2	128 ± 2	1	20.5 ± 0.5	8.9 ± 0.2
70:30	91 ± 3	-261 ± 2	124 ± 2	1	21.2 ± 0.6	9.6 ± 0.4
60:40	90 ± 0	-245 ± 10	119 ± 0	1	21.9 ± 0.2	9.9 ± 0.2
50:50	89 ± 2	-269 ± 5	122 ± 1	1	21.2 ± 0.3	9.5 ± 0.2
40:60	91 ± 6	-249 ± 10	92 ± 3	1	28.6 ± 0.3	13.6 ± 0.5
30:70	98 ± 6	-229 ± 5	107 ± 4	1	25.5 ± 3.9	12.0 ± 2.0
20:80	93 ± 4	-227 ± 5	111 ± 2	1	23.8 ± 0.9	9.32 ± 0.5

summarizes parameters obtained from the APTAC™ data. No significant variation in the reaction onset temperature is observed, however, as has the case with the RSST™, generally as the styrene concentration decreases the heat of reaction decreases. Below styrene ratio of 50 wt.%, changes in reaction mechanism are expected.

Self-heating rate and pressurization rate of reaction are also measured with the APTAC™ with the advantage of maintaining almost adiabatic conditions. Direct measurement of these two rates was applicable with no further mathematical treatment.

Figure 6.14 demonstrates measured self-heating rate of four styrene-acrylonitrile feeding ratios. These samples were tested with different ϕ factors as indicated. Clearly as the sample styrene content increases, the maximum self-heating rate increases. Also, an increase in the self-heating rate is measured with decreasing ϕ factor. Comparing these self-heating rate curves with those measured with the RSST™ (Figure 6.8), we notice the similarity in the general behavior; however, the maximum self-heating rates are quite different due to the heat and material losses associated with RSST™. In fact the APTAC™ results justify the explanation provided earlier. The APTAC™ closed cell experiment will minimize the effects of heat and material losses on the self-heating rate.

Pressurization rates are also measured with the APTAC™ and presented in Figure 6.15. Measured pressurization rates show similar behavior at the different styrene-acrylonitrile feeding ratio. Initially pressurization rates increase with temperature at a slow rate, and suddenly a sharp increase is measured. This sudden pressure increase may be associated with the rapid temperature increase during the copolymerization reaction, which causes the un-reacted styrene and acrylonitrile monomers to vaporize.

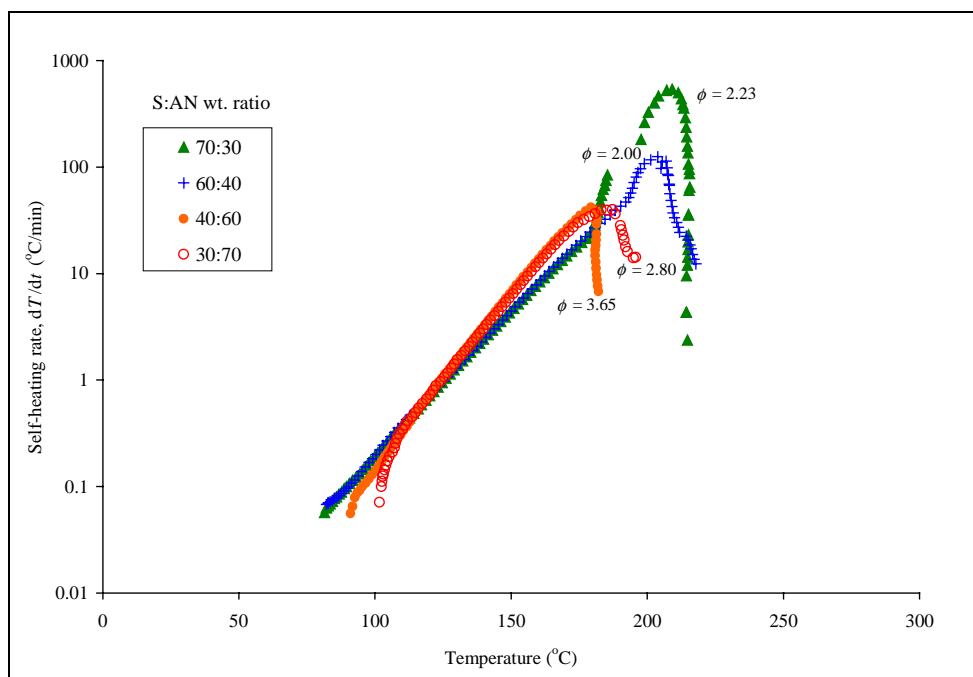


Figure 6.14. Self-heating rates of SAN copolymerization with the APTAC™

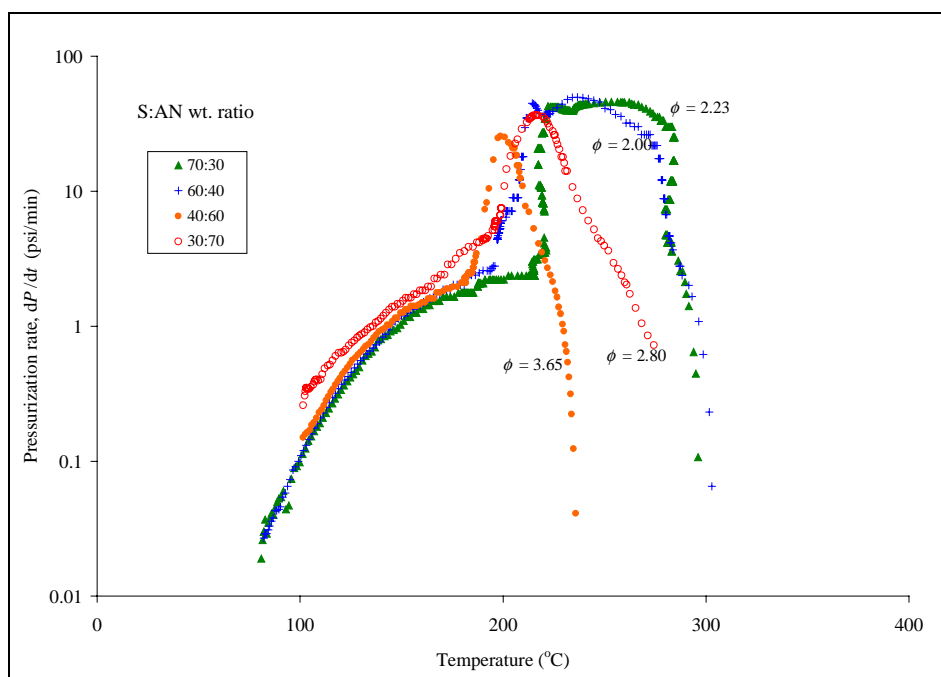


Figure 6.15. Pressurization rates of SAN copolymerization with the APTAC™

Once these monomers react, a drop in the pressurization rate is measured. It also can be noticed from Figure 6.15, that the effects of styrene-acrylonitrile feed ratio and the ϕ factor on the maximum pressurization rates are minimal when compared to their effects on the maximum self-heating rates. Values of maximum self-heating and pressurization rates are presented in Table 6.10. It is clear that these rates are strong functions of several parameters including thermal inertia factors, sample size, and sample concentrations.

Table 6.10

Maximum self-heating and pressurization rates of SAN copolymerization in the APTAC™

S:AN wt. ratio	ϕ -Factor	$(dT/dt)_{\max}$ (°C/min)	$(dP/dt)_{\max}$ (psi/min)
80:20	1.65	88 ± 16	61 ± 3
	2.29	127	31
	1.87	186	32
70:30	2.23	540	46
	1.94	282 ± 249	77 ± 24
60:40	1.96	258 ± 43	56 ± 15
50:50	1.85	50	49
	2.28	229	50
40:60	3.07	47	49
	3.65	42	26
30:70	2.80	72	37
	3.01	19	17
80:20	1.92	41	105
	3.57	22	13

4.6. Experimental Analysis Discussion

The RSST™ screening analysis results show that the onset temperature, T_o , for the copolymerization runaway reaction was about 106°C while from the APTAC™ analysis the onset temperature was about 91°C. From both RSST™ and APTAC™ results we can conclude that monomer feed ratio does not significantly affect the reaction T_o temperature. However the difference in T_o values for RSST™ and APTAC™ is due to heat losses from the open cell of the RSST™, which results in higher measured T_o values, compared to the closed cell and nearly adiabatic conditions of the APTAC™.

The effects of heat losses in the RSST™ are obvious also when comparing the measured overall heats of reaction as shown in Figure 6.16. An average difference of about 107 cal/g (43% of the APTAC™ measured ΔH_r) is observed between the APTAC™ and the RSST™ measured heat of reaction values. Generally, there is a reduction in the heat of reaction as the acrylonitrile concentration is increased. The slight reduction in heat of reaction at 60% styrene content, that looks inconsistent with the general trend, may require additional analysis that is beyond the scope of this research.

The RSST™ analysis temperature profiles show that the maximum temperature reached by the exothermic runaway reaction is decreased as the styrene concentration is reduced, and the same phenomena is noticed from the APTAC™ analysis temperature profiles. However in the APTAC™ profiles, another temperature activity is observed after reaching the maximum temperature. A temperature increase is observed even after

reaching the copolymerization runaway maximum temperature, and it is more noticeable as the acrylonitrile concentration increases. RSST™ did not measure these temperature changes because of the nature of the test. During the test, the RSST™ applies a constant temperature ramping, which obscures the secondary temperature activity, while for the APTAC™ the adiabatic operating mode continues to detect temperature changes even after the first maximum temperature is attained. A study of the APTAC™ pressure profile may enhance the understanding of this phenomenon.

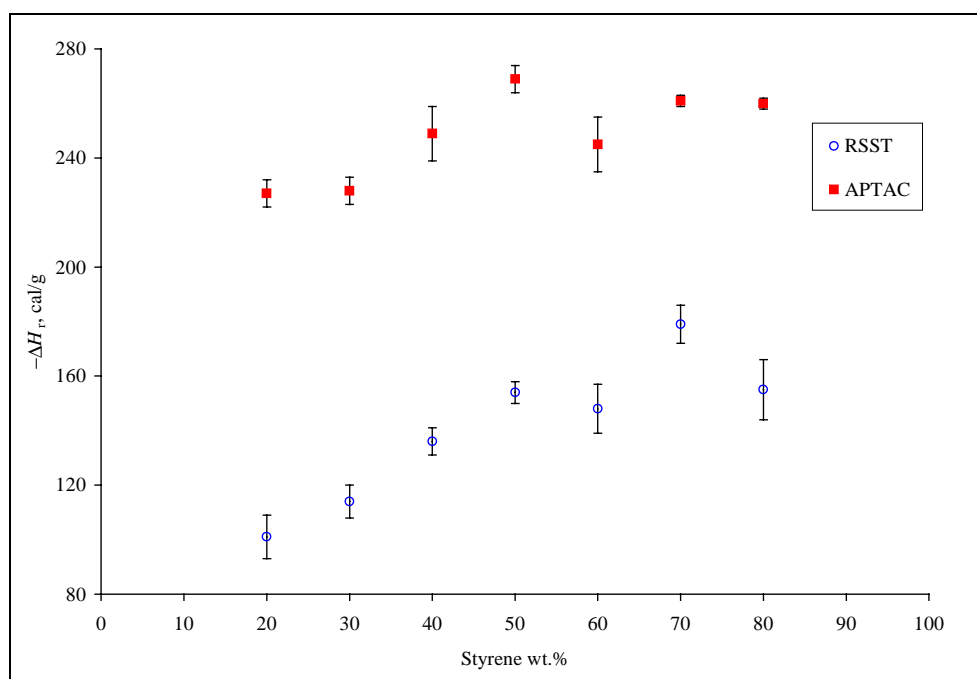


Figure 6.16. Comparison of measured heats of reaction of SAN copolymerization

For each copolymerization feed ratio, there were two maximum pressure peaks. A comparison of the temperature and pressure profiles indicates that the first pressure peak is for the copolymerization reaction. It was found that styrene-acrylonitrile in bulk copolymerizes in the vapor phase [120]. So initially the monomers evaporate causing a pressure increase and then copolymerize to the liquid phase causing the pressure to decrease, and this activity forms the first pressure peak. However, due to the high temperature increase caused by the thermal runaway, acrylonitrile monomers begin to decompose exothermally. The decomposition products cause the temperature and pressure to increase again forming the second maximum peak. As the acrylonitrile monomer increases in the feed, the second decomposition temperature and pressure peak reaches higher values. Also as the acrylonitrile concentrations increase, the main copolymerization reaction peaks and acrylonitrile decomposition peaks are grouped together more closely, until they form a single wide peak as in the styrene-acrylonitrile feed ratios of 30:70 and 20:80.

These significant differences between the RSST™ and APTAC™ results can reflect critically on the design of pressure relief systems. For example, using the RSST™ alone for designing pressure relief systems will not provide a sufficient understanding of the homopolymerization/copolymerization behavior of the SAN system, and it will underestimate the complex pressure behavior under reaction runaway scenarios. For the copolymerization part of the reaction, the Arrhenius parameters show less significant differences between the two calorimeters, which indicates that the overall reaction kinetics are about the same, but this overall reaction modeling was developed based on

the temperature-time data only. It is well known that for an open-cell testing such as with the RSST™, the measured pressure behavior is associated with material losses to the surrounding environment making the results of less value for relief system design when compared to closed-cell testing.

To enhance an understanding of the styrene-acrylonitrile reaction mechanism, a theoretical evaluation was conducted as discussed earlier. The APTAC™ results were used to compare the measured heats of reaction to the AM1 predictions of propagation reactions. In order to perform this comparison, the APTAC™ heats of reaction were corrected for the enthalpies of vaporization, ΔH_{vap} , of SAN mixtures as follows

$$\text{Corrected } \Delta H_r = \text{APTAC}^{\text{TM}} \text{ measured } \Delta H_r - \Delta H_{\text{vap}} \quad (6.2)$$

Values of enthalpies of vaporization were estimated at reaction onset temperature, T_o , considering the proportion of styrene to acrylonitrile in the mixture and based on the correlations available in the literature [105]. A pseudo molecular weight based on the mean molecular weight of the initial mixture styrene-acrylonitrile ratio was used for this comparison, and Table 6.11 presents the corrected heats of reaction. According to the results obtained from Table 6.1, the calculated heats of reaction for the most exothermic reactions among the cross-propagation reactions were about -57.8 kcal/mol. This value is much higher than the APTAC™ values measured and then corrected. As mentioned earlier, the AM1 level of theory was not used for absolute property estimation but as a relative prediction approach to determine the most critical or dominant reactions. According to these values, AM1 systematically overestimated the heats of reaction. In

addition, the density functional level of theory B3LYP/6-31G(d) was used to calculate the heats of Reactions 23, 24, 41, and 42 as presented in Table 6.2. This higher and more expensive level of theory provides more reliable values of heats of reaction on an absolute basis (-30.8 to -38.7 kcal/mol), and the calculated values are more consistent with the APTACTM measured values as shown in Table 6.11.

Table 6.11

Enthalpy of vaporization corrections for the APTACTM heats of reaction of styrene-acrylonitrile copolymerization

S:AN wt. ratio	Pseudo molecular weight (g/mol)	Enthalpy of vaporization (kcal/mol)	APTAC TM measured heat of reaction (cal/g)	APTAC TM measured heat of reaction (kcal/mol)	Corrected heat of reaction (kcal/mol)
80:20	87.1	9.00	-260	-22.7	-31.7
70:30	80.9	8.67	-261	-21.1	-29.8
60:40	75.8	8.40	-245	-18.6	-27.0
50:50	70.1	8.17	-269	-18.9	-27.0
40:60	64.9	7.92	-249	-16.2	-24.1
30:70	61.6	7.64	-228	-14.0	-21.7
20:80	57.7	7.53	-227	-13.1	-20.6

From a comparison of these calculations to the results of the experimental analysis, a conclusion is that as the concentration of acrylonitrile increases, the copolymerization rate must decrease since most of styrene monomers are consumed either by the cross-propagation copolymerization reaction or by the homopolymerization reaction. Since

the tendency of acrylonitrile for homopolymerization is low in the presence of styrene monomer, most of the un-copolymerized acrylonitrile monomers will start to decompose at the rapidly increased temperatures due to the copolymerization runaway, and this activity will cause another increase in temperature and pressure.

Also we can see from the results of Table 6.1 that heat of reaction is a function of the chain end active site regardless of what is attached to that site from the other side. For example, comparing Reactions 41 and 42 shows that heat of reaction will be the same (57-58 kcal/mol) as long as the reactive site on the copolymer chain and the monomer are the same with no effect from what is attached to the other end of the copolymer chain or in what order. This conclusion also is consistent with the random arrangement of monomers in the styrene-acrylonitrile copolymer chain.

Table 6.12

Summary of the APTACTM corrected parameters of SAN copolymerization at $\phi \approx 1$

S:AN wt. ratio	T_o (°C)	T_{max} (°C)	TMR_{ad} (min)	$(dT/dt)_{max}$ (°C/min)
80:20	83 ± 2	502 ± 14	71 ± 9	14,485
70:30	83 ± 3	471 ± 41	61 ± 4	21,743
60:40	82 ± 0	472 ± 8	61 ± 2	18,923
50:50	89 ± 4	493 ± 21	60 ± 9	24,680
40:60	80 ± 4	503 ± 5	27 ± 3	66,694
30:70	86 ± 6	458 ± 8	37 ± 3	174,023
20:80	82 ± 1	405 ± 10	44 ± 7	161,598

Experimental analysis parameters were corrected for near adiabatic conditions ($\phi \approx 1$) to simulate the real process conditions. Thermal inertia factor, ϕ , correction was presented in Chapter IV. In this analysis the adiabatic calorimeter (APTAC™) results were corrected for near adiabatic conditions ($\phi \approx 1$). Table 6.12 presents the onset temperatures, maximum temperature, time to maximum rate, and maximum self-heating rate at adiabatic conditions. Adjusting self-heating rates had significantly affected the maximum self-heating rate values. Corrected time to maximum rate was reduced to about half the experimental values, however, onset temperature were not affected significantly.

5. Conclusions

The effect of the monomer feed ratio of styrene-acrylonitrile copolymerization runaway scenario was evaluated using thermal (calorimetric) analysis. As the styrene monomer concentration increases, the copolymerization heat of reaction increases. A secondary exothermic reaction was detected as the acrylonitrile concentration increases. Screening thermal techniques are not able to predict the SAN copolymerization runaway behavior and the need for advanced thermal analysis is essential.

Theoretical analysis shows that a cross-propagation reaction is the main mechanism of styrene and acrylonitrile monomers. However, the very low tendency of homopolymerization by acrylonitrile causes the remaining acrylonitrile monomers to decompose at high temperatures due to the copolymerization runaway reaction.

The combination of the experimental analysis with screening theoretical calculations through the suggested systematic approach for chemical reactivity evaluation improved the understanding of the runaway reaction scenario of styrene-acrylonitrile copolymerization and yielded a good agreement with other research findings concerning this reaction mechanism.

The predicted heats of reaction are comparable to the measured heats of reaction especially at high styrene content. These finding supports the reaction mechanism conclusions achieved through this study.

CHAPTER VII

THERMAL POLYMERIZATION OF 1,3-BUTADIENE

1. Précis

1,3-Butadiene is produced in very large amounts every year from the petroleum industry and it is mainly used in the manufacturing of rubbers and plastics. Every day, large quantities of 1,3-butadiene are manufactured, transported, and handled in a safe manner. However, 1,3-butadiene's inherent tendency to react with large number of chemicals, to dimerize and polymerize, and its high toxicity requires that specific handling, storage, and shipping procedures be followed [121]. 1,3-butadiene has been involved in many incidents (8 incidents from 1994-1999) due to its reactivity [122]. Figure 7.1 presents some of the physical properties of the 1,3-butadiene.

The effective evaluation of reactivity hazards associated with 1,3-butadiene manufacturing, transporting, and handling stems from the ability to predict reaction stoichiometries under various scenarios and to quantify thermodynamic and kinetic parameters of these stoichiometries.

Experimental calorimetric analysis is a traditional technique for evaluating reactivity hazards. Various calorimeters are available for researchers; however, few of these calorimeters are suitable for testing gaseous and toxic substances such as 1,3-butadiene. The special considerations and testing procedures make the experimental analysis quite expensive.

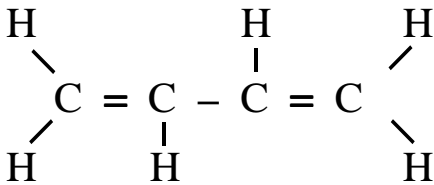
	
Molecular formula	C ₄ H ₆
CAS number	106-99-0
Molecular mass	54.1
Boiling point	-4.4 °C
Melting point	-108.9 °C
Density (liquid at 25°C)	0.619 g/mL
Solubility in water	735 ppm
Vapor pressure at 20°C	
Flash point	-85°C
Relative vapor density (air = 1)	1.9

Figure 7.1. 1,3-butadiene molecular structure and physical properties

In this research, polymerization of inhibited 1,3-butadiene in the presence and absence of oxygen was evaluated for its thermal reactivity and runaway behavior using theoretical computational models and thermal analysis techniques. The Automatic Pressure Tracking Adiabatic Calorimeter (APTAC™) was used for overall thermodynamic and kinetic parameter measurements. At the same time, theoretical evaluation was conducted to predict some possible hazardous reaction pathways.

Thermokinetic parameters of these predicted pathways are calculated to provide an explanation for the experimental results and to compare with literature values. A better understanding of butadiene reactivity hazards is achieved through the application of the proposed systematic approach for chemical reactivity evaluation.

2. Thermal Hazards Evaluation

Butadiene is known for its high tendency to react through numerous highly exothermic pathways of which the most significant pathways are dimerization, polymerization, and decomposition.

Several researchers studied the dimerization of butadiene under various conditions [123–126]. The general conclusion derived from a number of investigations is that dimerization is a homogeneous bimolecular reaction, not catalyzed by oxygen, unaffected by anti-oxidants, and with the same kinetics in the liquid and gaseous phases.

The thermally initiated dimerization reaction is very difficult to prevent except by lowering the butadiene storage temperature. Since the reaction rate increases about nine fold for every 20°C increase in temperature, care must be taken to maintain butadiene at a low temperature [91].

Also, 1,3-butadiene reacts readily with oxygen to form polymeric peroxides, which are not very soluble in liquid 1,3-butadiene and tend to settle at the bottom of the container because of their higher density. The peroxides are shock sensitive; therefore it is imperative to exclude any source of oxygen from butadiene. Oxygen or peroxides may initiate long-chain polymerization reactions to form rubbery polymers [127]. Some

of these polymers are known as popcorn polymers, which are hard, opaque, and porous and have been reported to ignite spontaneously on exposure to air. They grow faster in the presence of seeds, or oxygen, and rust. Because popcorn polymers can grow exponentially [128], they can generate tremendous pressure resulting in sudden rupture or plugging of containers, distillation towers, and pipes [16].

It is reported that rigorous exclusion of oxygen from the system, metal surface passivation, and removal of popcorn polymer seeds can mitigate most of this problem [128]. Addition of antioxidants such as *t*-butylcatechol (TBC) or butylated hydroxy toluene (BHT) removes free radicals that can cause rapid exothermic polymerizations. However, the high boiling points of many of these materials render them effective primarily in the liquid phase leaving the gaseous phase more vulnerable to reaction initiation. Because of these reasons, the various hazardous pathways butadiene may take cannot be prevented by low-temperature storage and antioxidants addition only. High temperature, oxidants, and free radicals may still initiate vigorous exothermic reactions.

As discussed in Chapter III, the evaluation of thermal hazards due to chemical reactivity should be based on a thorough understanding of reaction chemistry, which includes reaction thermodynamic, kinetic, and stoichiometric parameters. Calorimetric analysis is a very fundamental procedure for reactivity thermal hazards evaluation. However, the reactivity and toxicity hazards associated with butadiene thermal analysis make this procedure dangerous, expensive, and time consuming. Also, calorimetric analysis will provide an overall thermal hazard evaluation, with poor reaction stoichiometric information especially with this kind of reaction mechanisms.

Introducing theoretical analysis steps to the experimental evaluation process will help to reduce the cost of experimental analysis and it will help to improve the understanding of the reaction mechanisms and pathways.

Theoretical analysis may be based on thermodynamic and kinetic parameters available in the literature or they can be calculated using computational quantum chemistry methods and empirical thermodynamic-energy correlations. Literature information were utilized to provide possible reaction mechanisms.

3. Computational Models

Scientists observed nature's methods of joining elements into chains and duplicated that natural process to produce macromolecules or polymers. Polymerization is the linking together of smaller units (monomers) into long chains. The repeating units (mers) of some polymer chains are identical. Copolymers contain two or more different types of monomers. Isomers are variations in the molecular structure of the same composition. Most polymers are produced by unsaturated hydrocarbons, which means that they have one or more multiple covalent bonds, such as ethylene.

The main polymerization processes are addition (chain reaction) polymerization and condensation (step reaction) polymerization. The addition process is the simpler of the two. By use of heat and pressure in an autoclave or reactor, double bonds of unsaturated monomers break loose and then link up into a chain. These addition reactions (in addition polymerization for unsaturated hydrocarbons) are atoms or groups of atoms that attach themselves to the carbon atoms at the sites of multiple bonds. No products other

than the polymer are formed. Saturated hydrocarbons undergo substitution reactions in which hydrogen atoms are replaced by other atoms or groups of atoms.

A gradual accumulation of experimental data and data modeling on the kinetics of 1,3-butadiene has led to the realization that these processes are complex and follow various reaction pathways [123–126,129–139]. In this research the reactions of 1,3-butadiene in the presence and absence of oxygen were investigated through the application of theoretical computational models and experimental adiabatic thermal analysis. The focus of this study was on the dimerization and polymerization reaction pathways.

3.1. Dimerization of Butadiene

Butadiene dimerization was found to follow the Diels-Alder reaction. They are generally thermally reversible and can proceed in both the gas and liquid phases. The reactions are exothermic and follow second-order kinetics; first-order with respect to each reactant. Three possible mechanisms have been proposed for the Diels-Alder reactions: a concerted mechanism, a two-step mechanism, and an asynchronous two-stage mechanism [140]. The concerted mechanism suggests that the butadiene monomers will dimerize directly to the final product through an activated transition state barrier. However, the two-step mechanism suggests the formation of various diradicals as the first step is followed by the formation of the product as the final step. The asynchronous two-stage mechanism is a combination of the two earlier mechanisms. Years of controversy over which mechanism is most dominant has not been resolved, although it is likely to be an asynchronous two-stage mechanism [141].

Dimerization of butadiene through the Diels-Alder reaction is second order in the gas phase and in solution [125]. In general the gas phase reactions are fairly clean, but the second order rate constants do show marked drifts in later stages of a run [125]. In his study, Vaughan [123] demonstrated that only after some 50-percent butadiene conversion, the deviation from the second-order mechanism is appreciable. Vaughan interpreted the deviations as caused by a secondary reaction of the dimer with unreacted monomer. A different study [126] suggests that intermediate free radicals undergo an addition reaction with monomer molecules as an alternate to its isomerization into the stable cyclic dimer.

In this study a reaction mechanism (as in Figure 7.2) is suggested based on previous work to predict a reaction mechanism and calculate thermokinetic parameters [141–144].

In this mechanism, *trans*-butadiene (*t*-BD) and *cis*-butadiene (*c*-BD) will dimerize into 4-vinylcyclohexane (VCH), *cis*, *cis*-cycloocta-1,5-diene (COD), *trans*-1,2-divinylcyclobutane (*t*-DVCB), and *cis*-1,2-divinylcyclobutane (*c*-DVCB) dimers. These reactions will take place through the formation of the intermediate octa-1,7-diene-3,6-diyl diradicals (*trans, trans*), (*cis, trans*), and (*cis, cis*).

To investigate the dominant reaction pathway and its thermokinetic parameters, computational quantum chemistry (*ab initio* method) calculations were performed. Three levels of theory were applied; Hartree-Fock, HF, with 6-31G(d) basis set, density functional theory, B3LYP, with 6-31G(d) basis set, and the complete basis set, CBS-4M. All quantum chemistry calculations were performed using the Gaussian 98 program [84]. These levels of quantum calculations have been discussed briefly in Chapters IV

and V. The calculated Gibbs free energies and enthalpies of reactions components are presented in Table 7.1, while Table 7.2 presents the calculated Gibbs free energy and enthalpy of the various reactions.

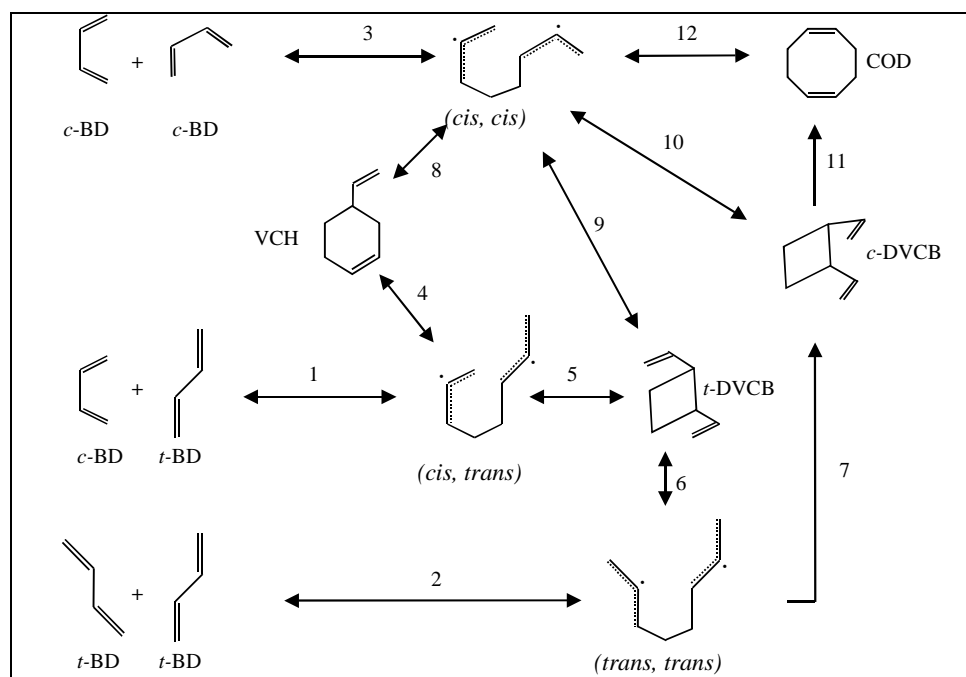


Figure 7.2. Proposed reaction pathways of 1,3-butadiene dimerization

As discussed earlier in Chapters IV, V, and VI, the findings of Evans and Polanyi can be used to predict reaction activation barriers. In this work, Polanyi equation was applied to determine dominant pathway for this set of reactions (Figure 7.2) based on activation energy predictions. Since Reactions 1, 2, and 3 share the same mechanism, E_A^o and γ_p values are expected to be the same for these reactions [72]. In this case, the

predicted values of heat of reaction were sufficient to show that Reaction 1 is dominant over 2 and 3 since it has the lowest heat of reaction. Therefore, diradical (*cis, trans*) will be the main intermediate. Similarly, Reaction 4 to form VCH and Reaction 5 to form *t*-DVCB compete with each other, however Reaction 4 has a much lower heat of reaction, which suggests that it will have a lower activation barrier and that is more dominant. For the (*cis, cis*) intermediate, Reactions 8, 9, 10, and 12 compete and Reaction 8 to form VCH is expected to have the lowest activation energy barrier. According to this analysis, the butadiene dimerization main pathway could be the formation of VCH through the (*cis, trans*) intermediate and to lesser extent through the (*cis, cis*) intermediate. In fact, this conclusion is in agreement with other researchers findings that

Table 7.1

Gibbs free energies and enthalpies (in Hartree/particle^{*}) of 1,3-butadiene dimerization components calculated using three levels of theory

Component	HF/6-31G(d)		B3LYP/6-31G(d)		CBS-4M	
	<i>G</i>	<i>H</i>	<i>G</i>	<i>H</i>	<i>G</i>	<i>H</i>
<i>c</i> -BD	-154.848178	-154.817430	-155.926885	-155.895831	-155.727865	-155.696927
<i>t</i> -BD	-154.853845	-154.822705	-155.932450	-155.901062	-155.733539	-155.702119
<i>cis, cis</i>	-309.595496	-309.549280	-311.743480	-311.696953	-311.349480	-311.302165
<i>cis, trans</i>	-309.695311	-309.650347	-311.857991	-311.811852	-311.464917	-311.418828
<i>trans, trans</i>	-309.641840	-309.599610	-311.783646	-311.740986	-311.398686	-311.354857
<i>c</i> -DVCB	-306.693903	-309.652355	-311.852068	-311.809652	-311.468381	-311.425913
<i>t</i> -DVCB	-309.696651	-309.654885	-311.854675	-311.811907	-311.470766	-311.428006
VCH	-309.734778	-309.694992	-311.890919	-311.850338	-311.508433	-311.467690
COD	-309.717747	-309.678112	-311.877639	-311.837109	-311.492173	-311.452242

* Hartree/particle = 627.51 kcal/mol

Table 7.2

Gibbs free energies and heats of reactions (in kcal/gmol) of 1,3-butadiene dimerization calculated using three levels of theory

Reaction	HF/6-31G(d)		B3LYP/6-31G(d)		CBS-4M	
	ΔG_r	ΔH_r	ΔG_r	ΔH_r	ΔG_r	ΔH_r
1	4.2	-6.4	0.8	-9.4	-2.2	-12.4
2	41.3	28.7	51.0	38.4	42.9	31.0
3	63.3	53.7	69.2	59.4	66.7	57.5
4	-24.8	-28.0	-20.7	-24.2	-27.3	-30.7
5	-0.8	-2.9	2.1	-0.0	-3.7	-5.8
6	-34.4	-34.7	-44.6	-44.5	-45.2	-45.9
7	-32.7	-33.1	-42.9	-43.1	-43.7	-44.6
8	-87.4	-91.4	-92.5	-96.3	-99.7	-103.9
9	-63.5	-66.3	-69.8	-72.1	-76.1	-79.0
10	-61.8	-64.7	-68.1	-70.7	-74.6	-77.7
11	-15.0	-16.2	-16.1	-17.2	-14.9	-16.5
12	-76.7	-80.8	-84.2	-88.0	-89.5	-94.2

VCH is the main product of the butadiene dimerization reaction [123–126,129,130].

The heats of reaction to form the four major products are presented in Table 7.3 although the formation of VCH is dominant. Group contribution method (using CHETAH™) was also used to calculate heat of reactions for comparison. Since group contribution methods cannot differentiate between isomers, *c*-DVCB and *t*-DVCB are having the same heat of reaction values. Generally, CHETAH™ is predicting heat of reactions that are comparable to CBS-4M predictions except for the VCH formation reaction.

Table 7.3

Heats of reactions (in kcal/gmol) of 1,3-butadiene dimerization to form the four major products calculated using four levels of theory

Product	HF/6-31G(d)	B3LYP/6-31G(d)	CBS-4M	CHETAH™
VCH	-34.4	-33.5	-43.1	-36.6
COD	-23.8	-25.2	-33.4	-34.7
<i>c</i> -DVCB	-7.7	-8.0	-16.9	-13.2
<i>t</i> -DVCB	-9.3	-9.4	-18.2	-13.2

3.2. Polymerization of Butadiene

In the presence of air, peroxide, or any free radical initiator, butadiene will start to polymerize with itself. In this article the reaction of butadiene with singlet oxygen, SO, is discussed. This reaction will lead to the formation of 3,6-dihydro-1,2-dioxin (DHD), which is a highly reactive peroxide that may initiate the polymerization of the butadiene. Possible reaction pathways leading to the formation of DHD are suggested based on previous research and are illustrated in Figure 7.3 [91,145]. HF/6-31g(d), B3LYP/6-31G(d), and CBS-4M quantum computational levels of theory were used to predict reaction thermodynamic parameters of components and reactions as presented in Tables 7.4 and 7.5, respectively.

Applying the same concepts of reaction pathway predictions suggests that DHD will be formed through Reactions 1 and 2 dominantly. Since Reaction 3 has a lower enthalpy of reaction than Reaction 2, then it is expected to have a higher activation barrier.

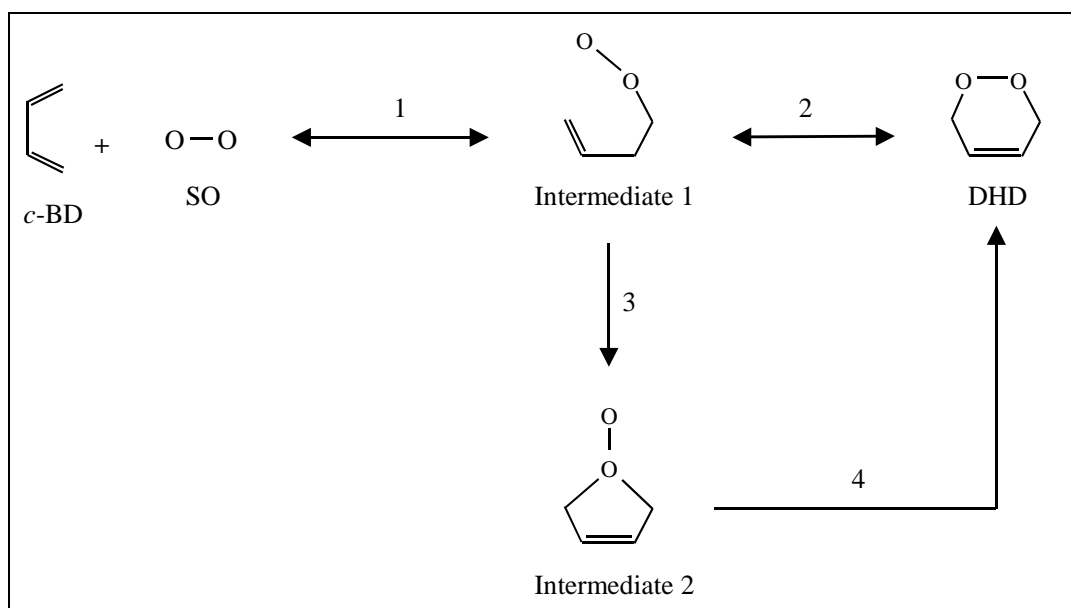


Figure 7.3. 1,3-butadiene reaction with singlet oxygen to form 3,6-dihydro-1,2-dioxin

Table 7.4

Gibbs free energies and enthalpies (in Hartree/particle^{*}) of 1,3-butadiene reaction with singlet oxygen components calculated using three levels of theory

Component	HF/6-31G(d)		B3LYP/6-31G(d)		CBS-4M	
	<i>G</i>	<i>H</i>	<i>G</i>	<i>H</i>	<i>G</i>	<i>H</i>
<i>c</i> -BD	-154.848178	-154.817430	-155.926885	-155.895831	-155.727865	-155.696927
SO	-149.547309	-149.525140	-150.272628	-150.250376	-150.141174	-150.118880
Intermediate 1	-304.410938	-304.375758	-306.209414	-306.173668	-305.871834	-305.835756
Intermediate 2	-304.442570	-304.406103	-306.180911	-306.141895	-305.918616	-305.881656
DHD	-304.475354	-304.441785	-306.287056	-306.252872	-305.951491	-305.917174

* Hartree/particle = 627.51 kcal/mol

Table 7.5

Gibbs free energies and heats of reactions (in kcal/gmol) of 1,3-butadiene with singlet oxygen reactions calculated using three levels of theory

Reaction	HF/6-31G(d)		B3LYP/6-31G(d)		CBS-4M	
	ΔG_r	ΔH_r	ΔG_r	ΔH_r	ΔG_r	ΔH_r
1	-9.7	-20.8	-6.2	-17.2	-1.8	-12.5
2	-40.4	-41.4	-48.7	-49.7	-50.0	-51.1
3	-19.9	-19.0	17.9	19.9	-29.4	-28.8
4	-20.6	-22.4	-66.6	-69.6	-20.6	-22.3

When comparing the dimerization Reaction 1 and the peroxide formation Reaction 1, it is noticed that they have almost the same heat of reaction (-12.41 and -12.52, respectively, based on CBS-4M level of theory), which may indicate that they have very similar activation barriers. However, when the following reactions in every pathway are compared, it was found that the peroxide formation reactions generally have lower activation barriers and hence may have dominance over the dimerization reactions. This peroxide reaction dominance will increase the chances of polymerization reaction initiation and therefore increase the reactivity hazard potential.

Polymerization of butadiene can proceed via Isotactic 1,2-, Syndiotactic 1,2-, Cis-1,4-, and Trans-1,4-additions as presented in Figure 7.4. More information about these polymer geometries is available in the literature [91]. Heats of reaction for the polymerization propagation step were calculated using the Hartree-Fock, HF/6-31g(d), level of theory [63] and are presented in Table 7.6. It is obvious that the energy release associated with the polymerization reactions exceeds those of the dimerization reaction

and more favorable. The reactivity hazards of butadiene can therefore be predicted to be more significant in the presence of air or any other free radical initiator than the dimerization pathway.

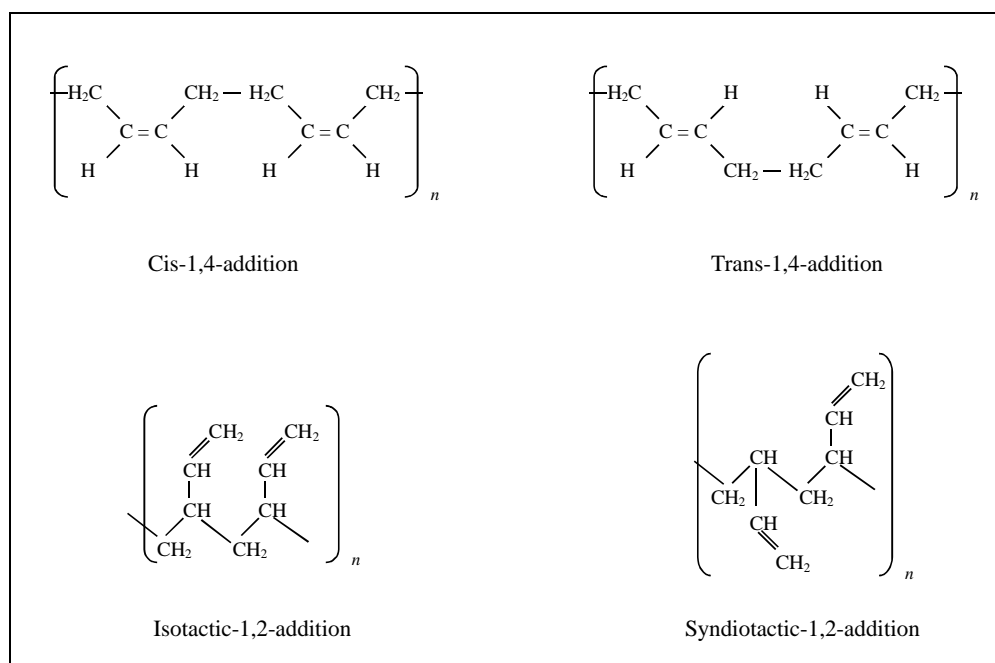


Figure 7.4. Modes of addition reactions of 1,3-butadiene

Table 7.6

Heats of reaction for butadiene polymerization propagation steps calculated using HF/6-31G(d) level of theory

Reaction	Heat of reaction (kcal/gmol)
Isotactic 1,2-addition	-97.6
Syndiotactic 1,2-addition	-88.1
Cis-1,4-addition	-79.3
Trans-1,4-addition	-84.7

4. Experimental Analysis

The theoretical evaluation of 1,3-butadiene reactions had indicated the high potential of exothermic pathways. It also provided an idea about a possible dominance of certain reaction pathways over others. Although theoretical evaluation was useful in providing this preliminary information, but still experimental adiabatic thermal analysis is expected to deliver an exact characterization of the reactive system under the various scenarios. Generally, experimental analysis is performed when the theoretical approach indicates a potential for exothermal activity or high-pressure generation and for more exact parameter determinations.

A detailed thermal analysis using the APTAC™ calorimeter was conducted. Because of the butadiene's high reactivity, gaseous nature, and toxicity, the RSST™ (open-cell) calorimeter was not capable of performing this analysis. High caution was taken during the experimental thermal analysis of the butadiene including testing relatively small quantities. In this section the results of inhibited 1,3-butadiene adiabatic thermal analysis in the presence and absence of oxygen are presented and discussed.

4.1. Materials

Aldrich 99+% 1,3-butadiene monomer that was inhibited with about 100 ppm of TBC was employed in this thermal analysis. A single pressurized cylinder supplied the butadiene for all experiments. The butadiene was used with no additional purification or treatment processes. Some of the experiments were conducted under nitrogen environment following evacuation of air from the test cells. High purity compressed

nitrogen was used in the APTAC™ experiments to provide the no-air environment, reduce liquid boil-off, and backup the cell.

4.2. Apparatus

Thermal analysis of these samples was performed using the APTAC™. A detailed description of this calorimeter, operating procedure, and data quality was discussed in detail in Chapter IV. However, because of the gaseous nature of the 1,3-butadiene, special arrangements for sample loading to the test cell were developed.

The butadiene monomer was transferred to the APTAC™ from a 500-ml compressed cylinder. Special apparatus setup was developed to transfer and measure the weight of the butadiene sample. Figure 7.5 illustrates the special setup that was performed. Initially the APTAC™ test cell and transferring line were evacuated of air to 2 psia. Then a series of test cell and transferring line purging with nitrogen and then vacuuming to 2 psia were performed to ensure the absence of oxygen from the test cell and transferring line. Then valve 1 (as illustrated in Figure 7.5) was closed and valve 2 was opened to fill the line with butadiene. A period of time was allowed to ensure thermal stabilization in the transferring line. Then valve 1 was reopened and the butadiene started to flow into the test cell. The weighing scale measured the transferred butadiene sample size with accuracy of ± 0.01 g. To enhance the butadiene transfer process a bath of liquid nitrogen (-102°C) surrounding the test cell was used to cool down the collected liquid butadiene in the test cell and enhance the thermal driving forces between the pressurized cylinder and the collecting test cell. In the case of

butadiene thermal analysis in the presence of oxygen, the test cell was pressurized with 5 psia of atmospheric air prior to the butadiene transfer process. Both titanium and stainless steel APTAC™ test cells were used in this analysis to allow various ϕ factors.

Similar to the operating procedures described in Chapter IV, initially 1,3-butadiene samples were heated to either 50 or 80 °C, then the heat-wait-search mode of operation with 2°C/min heating rate, 10°C heating increments, and 0.1°C/min threshold was applied. This APTAC™ mode of operation, as discussed earlier, is useful to measure and calculate various reactivity parameters such as, onset temperature, T_o , adiabatic time to maximum rate, TMR_{ad} , maximum self heating rate $(dT/dt)_{max}$, and maximum pressurizing rate $(dP/dt)_{max}$.

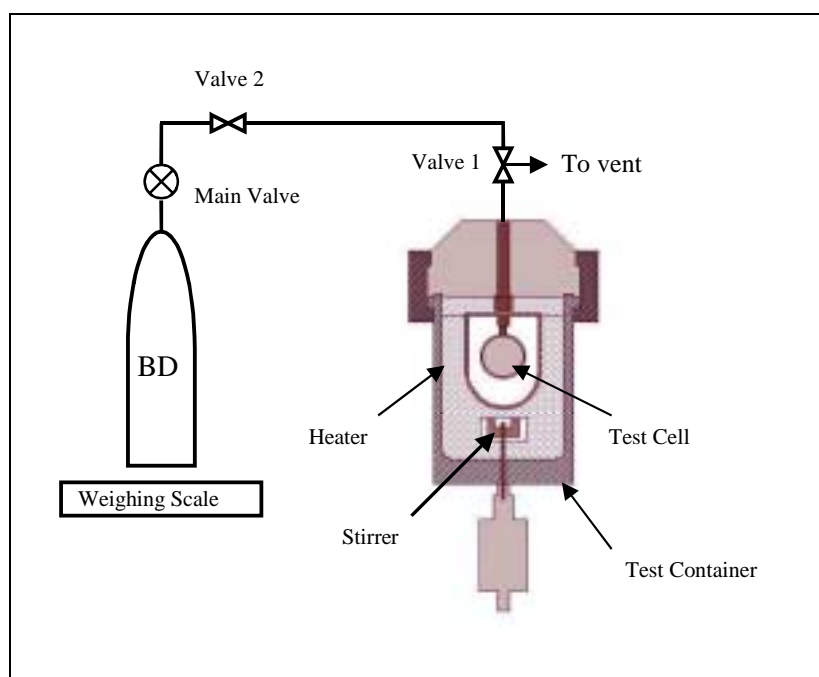


Figure 7.5. Schematic of special APTAC™ setup to transfer butadiene to the test cell

4.3. Data Analysis

Experimental data analysis was performed on the time-temperature-pressure data that was collected. Thermodynamic and kinetic parameters of the suggested reaction pathways were calculated according to the methods and procedures described in Chapter IV and later in this chapter.

4.4. 1,3-Butadiene in the Absence of Oxygen

A total of five samples were tested with sample weights ranged from 8.5 to 12.1 g. 130-ml APTAC™ test cells of titanium and stainless steel were used in these tests. The combinations of test cell and sample resulted in thermal inertia factors, ϕ , ranging from 1.20 – 1.34. The correction for the ϕ effects on measured parameters for scale-up procedures will be presented later in this chapter.

Temperature and pressure profiles for the butadiene tests in the APTAC™ are shown in Figures 7.6 and 7.7, respectively. Table 7.7 summarizes the experimental measured temperatures for the tested samples. The reported onset temperature for each APTAC™ test was determined at a self-heating rate of 0.1°C/min.

Figure 7.6 indicates a gradual increase in temperature to reach substantial levels. The APTAC™ did not continue to further heating steps after the reached maximum temperature because the sample self-heating rate had exceeded the maximum APTAC™ heating rate capability (400°C/min) that resulted in heater shutdown. This is expected to affect the measured maximum temperature. The reproducibility of the tested samples

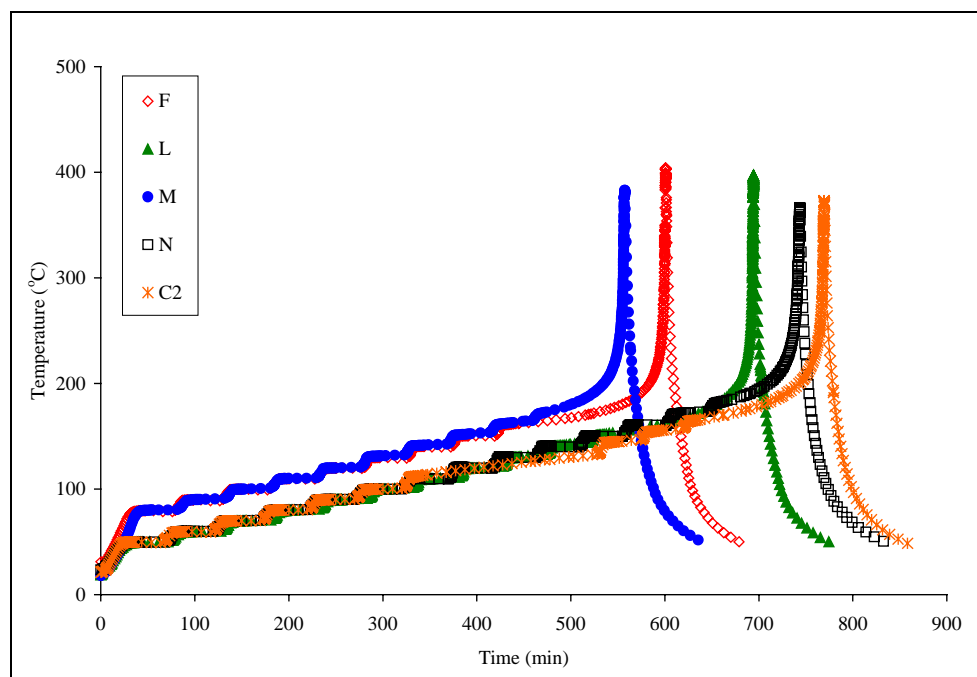


Figure 7.6. Butadiene temperature profiles in the absence of oxygen

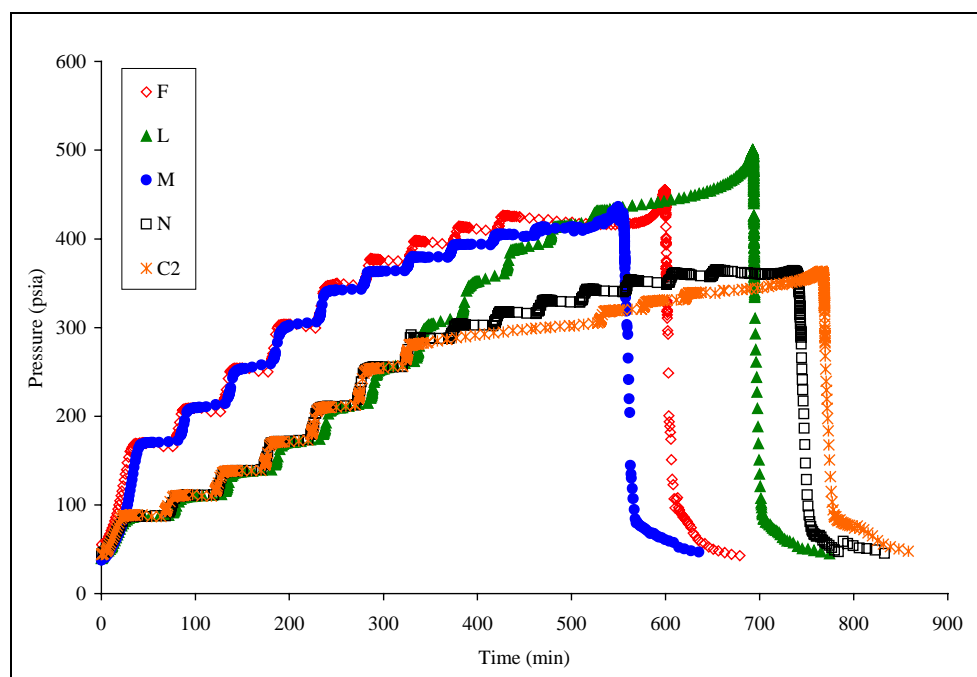


Figure 7.7. Butadiene pressure profiles in the absence of oxygen

Table 7.7

Summary of the experimental results of butadiene tests in the absence of oxygen with the APTAC™

Test No.	Sample wt. (g)	Cell material	ϕ -Factor	T_o (°C)	T_{max} (°C)	ΔT_{ad} (°C)	C_s (cal/(g · K))
F	11.2	Titanium	1.20	166	404	238	0.685
L	12.1	Stainless Steel	1.30	148	397	249	0.646
M	10.9	Stainless Steel	1.34	160	383	223	0.670
N	8.5	Titanium	1.31	175	366	190	0.691
C2	8.8	Titanium	1.29	160	373	213	0.667

was acceptable and expected to reduce the effect of the APTAC™ heaters shutdown. Studying the pressure profiles of the same samples does not reveal similar rapid increase in the pressure. The pressure increase was gradual and consistent with the heating steps that had been applied. This indicates that the reaction that took place was almost pure dimerization that did not lead to any rapid pressure increase. Also, this behavior supports the opinion that dimerization of 1,3-butadiene can take place in the liquid and vapor phases without resulting in higher pressure increase. In fact, the maximum temperatures reached by the samples were below the level (around 475°C) where polybutadienes have been observed to thermally decompose [146]. In this analysis the final sample was clear yellowish liquid. Therefore, these temperature and pressure profiles primarily exhibit dimerization reaction pathways. Different pressure profiles were observed for larger amount of butadiene samples [130]. For those larger samples

higher temperatures were reached that initiated a thermal decomposition reaction that led to rapid pressure increase.

No significant variation in the reaction onset temperature was observed, except for Sample L, which measured a 148°C while the average onset temperature was 162 ± 10 °C. Also the maximum temperatures are comparable, and the slight variations are due to the butadiene sample size. Based on these temperatures, the overall heat of the butadiene reaction in the absence of oxygen is calculated using Equation 4.7.

A pseudo zero-order rate constant, k , at temperature, T , was assumed as discusses in Chapter IV to be

$$k = \frac{(dT/dt)}{\left(\frac{T_{\max} - T}{\Delta T_{\text{ad}}}\right)^n \Delta T_{\text{ad}} C_o^{n-1}} \quad (7.1)$$

A second-order kinetic model was assumed to fit the dimerization reaction of the measured time-temperature profiles. Arrhenius parameters (activation energy and frequency factor) were obtained by plotting $(-\log k)$ vs. $(1/T)$ for Equation 7.2

$$\log k = \log(C_o A) - \frac{E}{2.303 R} \left(\frac{1}{T}\right) \quad (7.2)$$

This plot is presented in Figure 7.8. This plot validates a second-order reaction kinetic assumption with an average linear fitting regression coefficient of 0.998. An overall first-order kinetic model was also assumed for comparison to fit the same dimerization data using Equation 7.3

$$\log k = \log(A) - \frac{E}{2.303 R} \left(\frac{1}{T} \right) \quad (7.3)$$

The derivation of these equations was discussed in Chapter IV. Table 7.8 summarizes onset temperature, heat of reaction, time to maximum rate, and Arrhenius parameters obtained from the APTAC™ data.

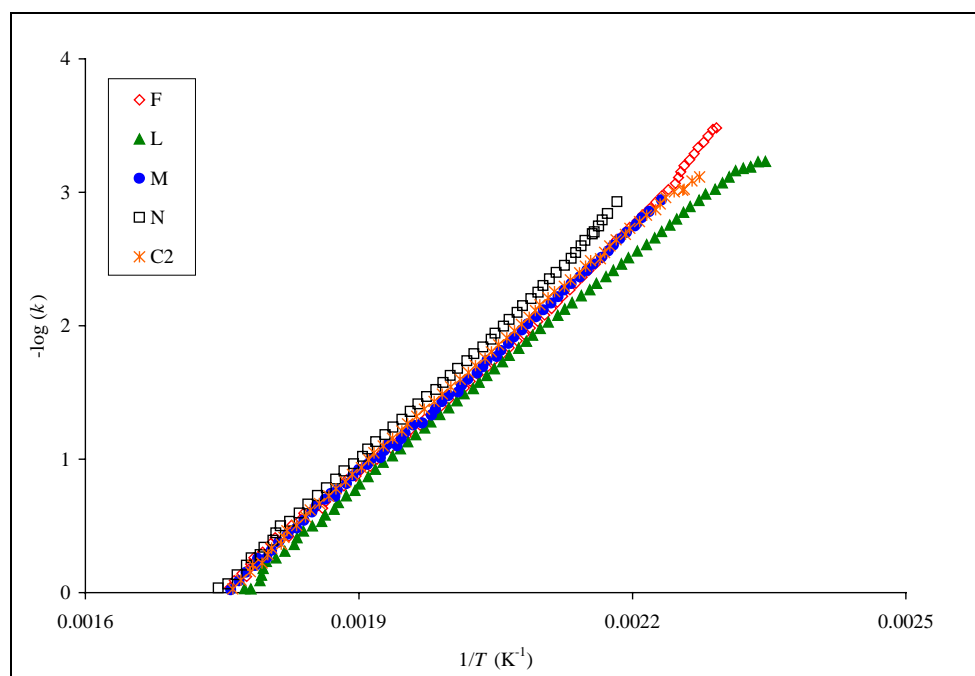


Figure 7.8. Second-order kinetics of 1,3-butadiene dimerization

Table 7.8

Summary of the experimental thermodynamic and kinetic parameters of butadiene reaction in the absence of oxygen with the APTAC™

T_o (°C)	162 ± 10
ΔH_r (kcal/mol)	-14.1 ± 1.5
TMR_{ad} (min)	133 ± 6
Reaction order, n	2
E_A , (kcal/mol)	28.3 ± 1.3
$\log(A C_o)$	10.9 ± 0.5
Reaction order, n	1
E_A , (kcal/mol)	24.3 ± 0.7
$\log(A)$	8.9 ± 0.2

Self-heating and pressurization rates are presented in Figures 7.9 and 7.10, respectively. It is evident that complete exotherms are reached in these plots since the observed self-heating rate reduces to negligible values indicating reaction completion. The self-heating rate plot is typical of second-order kinetics [130]. The measured self-heating rates are, generally, comparable since the differences in the thermal inertia factors are insignificant except for Sample F, which has the lowest thermal inertia factor that resulted in significant increase in the measured maximum self-heating rate (2 – 3 times the maximum self-heating rate of other samples). However, more significant variations in the pressurization rates are observed for the same samples and this could be related to the small variations in the thermal inertia factors. Moreover, since the measured maximum pressurization rates were relatively small, this made the error associated with the pressure measurement more considerable. Generally, these small

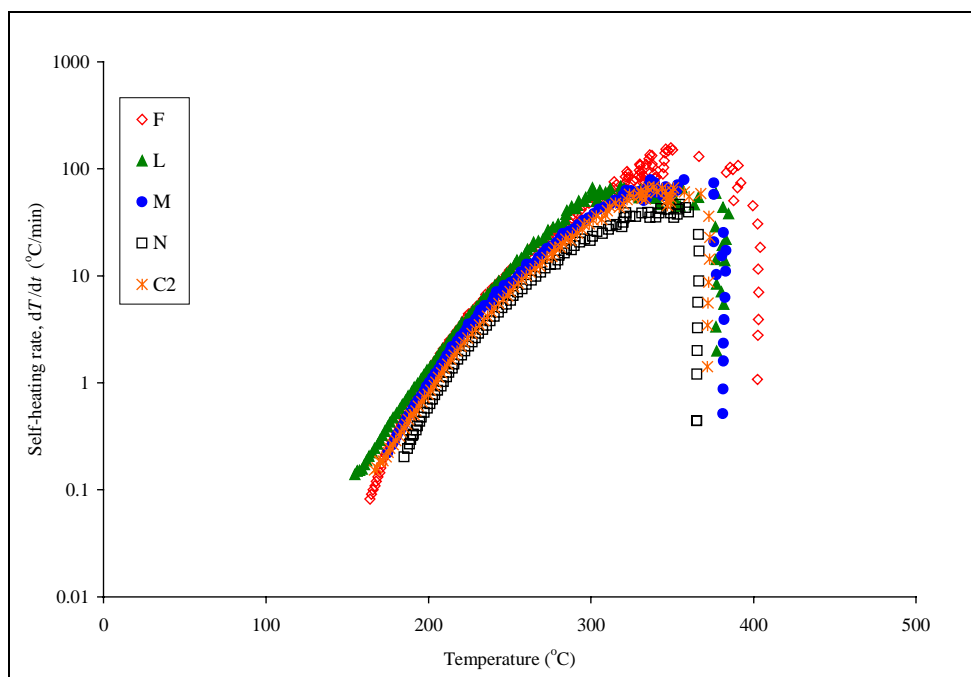


Figure 7.9. Self-heating rate of 1,3-butadiene dimerization

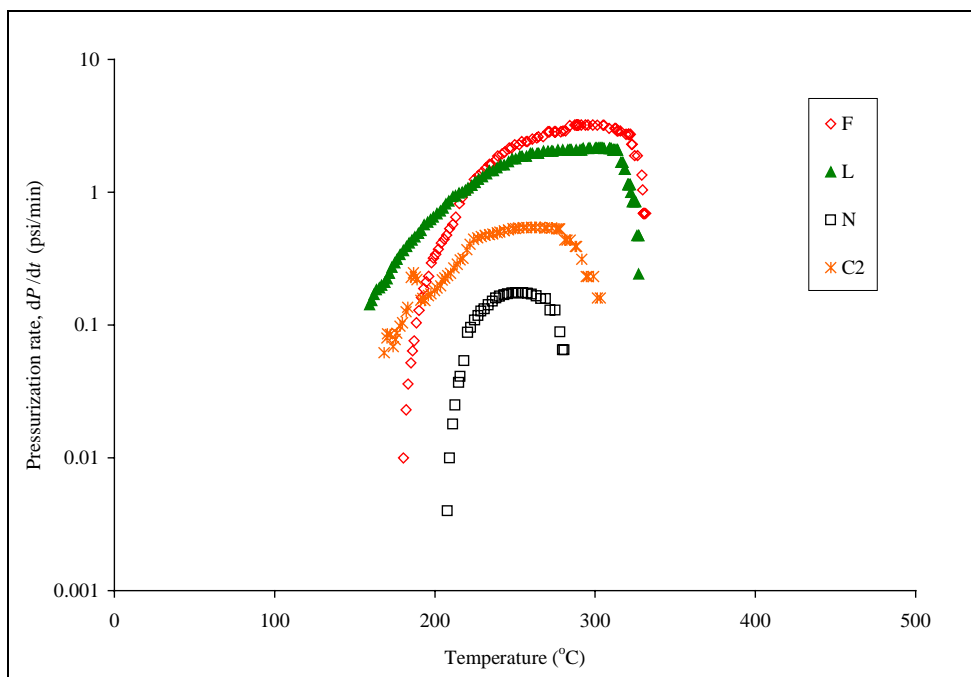


Figure 7.10. Pressurization rate of 1,3-butadiene dimerization

values of maximum pressurization rates are consistent with the observed pressure profiles in Figure 7.7 that indicates the dominance of the butadiene dimerization reaction. Table 7.9 presents the maximum self-heating and pressurization rates. Sample M maximum pressurization rate was not reported due to a measurement error.

Table 7.9

Maximum self-heating and pressurization rates of butadiene reaction in the absence of oxygen with the APTAC™

Test No.	ϕ -Factor	$(dT/dt)_{\max}$ (°C/min)	$(dP/dt)_{\max}$ (psi/min)
F	1.20	157	3.2
L	1.30	66	2.2
M	1.34	79	---
N	1.31	46	0.18
C2	1.29	68	0.54

4.5. 1,3-Butadiene in the Presence of Oxygen

A total of six samples were tested with sample weights ranging from 10.5 to 13.2 g. 130-ml APTAC™ test cell of titanium was used for these tests. The combinations of test cell and sample resulted in thermal inertia factors, ϕ , ranging from 1.09 – 1.19. Air at 5 psia was added to the test cell prior to the butadiene loading.

Temperature and pressure profiles for the butadiene tests in the APTAC™ are shown in Figures 7.11 and 7.12, respectively. Table 7.10 summarizes the experimental temperatures for the tested samples. The reported onset temperature for each APTAC™ test was determined at a self-heating rate of 0.1°C/min.

Similar to the butadiene experiments in the absence of oxygen, Figure 7.11 indicates a gradual increase in temperature; however, the maximum temperature in the presence of oxygen is substantially higher than those in the absence of oxygen. Again, the APTAC™ did not continue to further heating steps after the maximum temperature because the sample's self-heating rate had exceeded the maximum APTAC™ heating rate capability (400°C/min) that resulted in heater shutdown. The reproducibility of the tested samples was acceptable keeping in mind the effect of the APTAC™ heater shutdown on the measured maximum temperature. The average detected onset temperature (123 ± 8 °C) of butadiene in the presence of oxygen reveals a significantly lower value than that in the absence of oxygen. This makes the system reaction more sensitive to for thermal initiation.

The pressure profiles (Figure 7.12) show a rapid increase in pressure to substantial levels. The sample size has a noteworthy effect on the maximum pressure reached due to the runaway reaction. This pressure behavior is incomparable to that with absence of oxygen. The presence of oxygen and thermal initiation starts the butadiene polymerization reaction. Although the butadiene was inhibited with the TBC antioxidant, this antioxidant was found to be ineffective in the presence of high oxygen

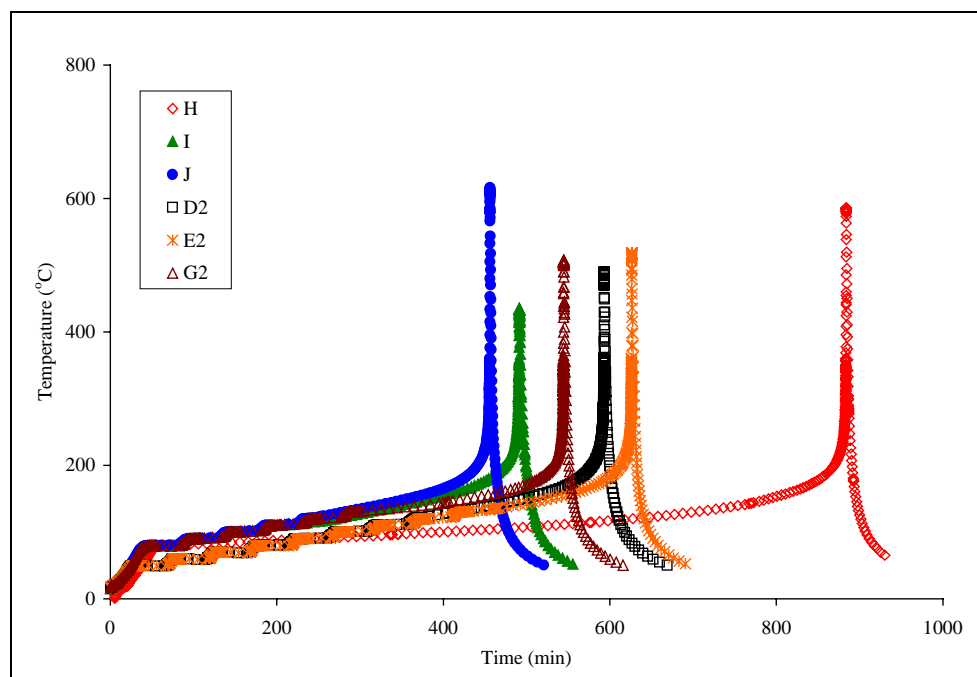


Figure 7.11. Butadiene temperature profiles in the presence of oxygen

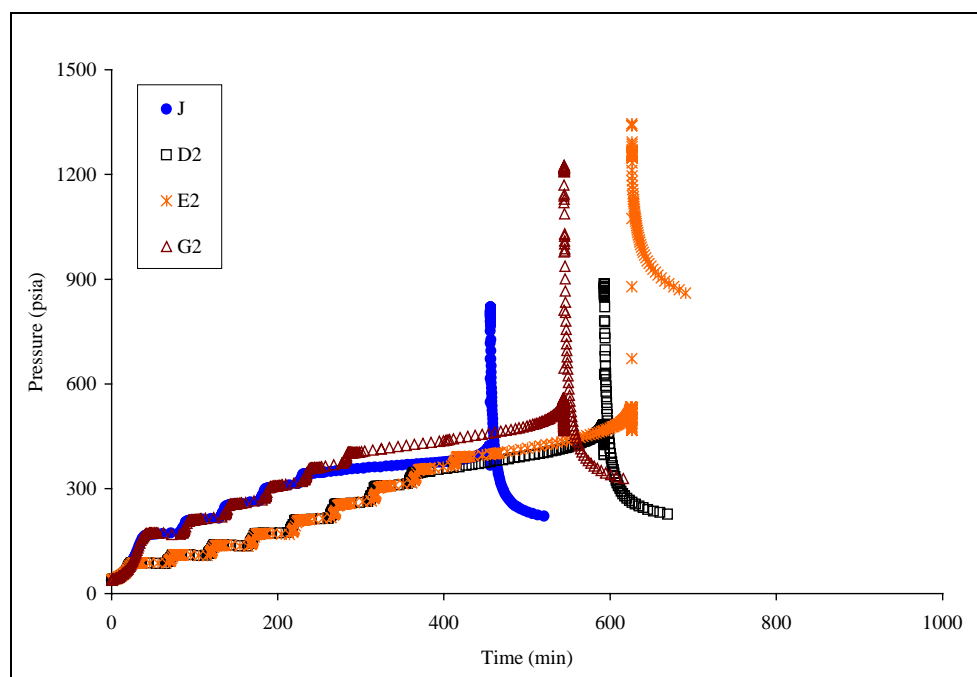


Figure 7.12. Butadiene pressure profiles in the presence of oxygen

Table 7.10

Summary of the experimental results of butadiene tests in the presence of oxygen with the APTAC™

Test No.	Sample wt. (g)	Cell material	ϕ -Factor	T_o (°C)	T_{max} (°C)	ΔT_{ad} (°C)	C_s (cal/(g · K))
H	13.2	Titanium	1.09	115	586	471	0.615
I	10.5	Titanium	1.19	113	435	322	0.590
J	11.0	Titanium	1.10	123	616	493	0.605
D2	10.7	Titanium	1.16	122	490	368	0.598
E2	12.0	Titanium	1.13	133	519	386	0.620
G2	12.9	Titanium	1.12	132	508	376	0.624

concentrations and high temperature levels. The high temperature associated with these exothermic polymerization reactions had reached the level (475°C) where polybutadiene thermal decomposition reactions may be initiated. The gaseous and volatile products of these decomposition reactions and the energy released will cause a significant pressure increase. The residue of these tests was black with a consistency resembling chalk with strong organic odor, indicating decomposition products.

The overall heat of 1,3-butadiene reaction in the absence of oxygen was calculated using Equation 4.7. Second-order and first-order kinetic models were assumed to fit the polymerization reaction of the measured time-temperature profiles using Equations 7.2 and 7.3, respectively. Arrhenius parameters (activation energy and frequency factor) were obtained by plotting $(-\log k)$ vs. $(1/T)$.

First-order kinetics is presented in Figure 7.13 with an average linear fitting regression coefficient of 0.995. Table 7.11 summarizes onset temperature, heat of reaction, time to maximum rate, and the Arrhenius parameters obtained using the APTAC™.

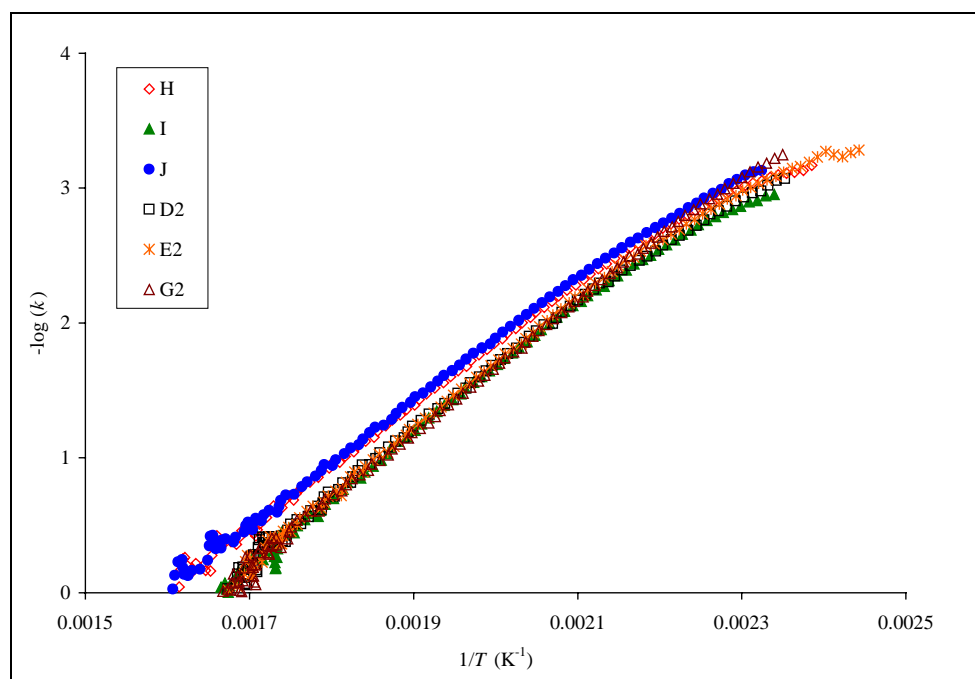


Figure 7.13. First-order kinetics of 1,3-butadiene polymerization

Table 7.11

Summary of the experimental thermodynamic and kinetic parameters of butadiene reaction in the presence of oxygen with the APTAC™

T_o (°C)	123 ± 8
ΔH_r (kcal/mol)	-24.4 ± 4.2
TMR_{ad} (min)	138 ± 6
Reaction order, n	2
E_A , (kcal/mol)	22.6 ± 1.3
$\log(A C_o)$	8.3 ± 0.7
Reaction order, n	1
E_A , (kcal/mol)	20.7 ± 1.0
$\log(A)$	7.4 ± 0.5

Self-heating and pressurization rates are presented in Figures 7.14 and 7.15, respectively. Complete exotherms are reached in these plots since the observed reduction in the self-heating rate to negligible rates indicate reaction completion. The effect of thermal inertia is inevitable, low thermal inertia exhibit higher maximum self-heating rate, although the variations in the thermal inertia factors are not that significant. Multiple self-heating rate curves exist as it appears clearly in Samples H and J (Figure 7.16). This is an indication of a two-stage exothermic activity. The first stage is the polymerization reaction initiated thermally in presence of oxygen, while the second stage is the decomposition of the polymer due to high temperatures reached by polymerization.

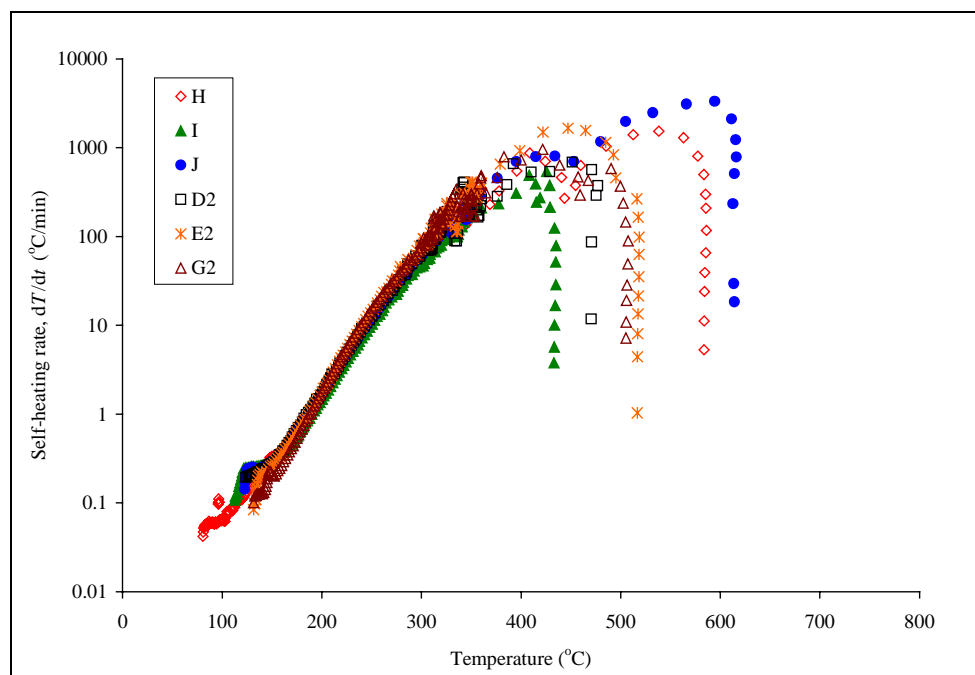


Figure 7.14. Self-heating rate of 1,3-butadiene polymerization

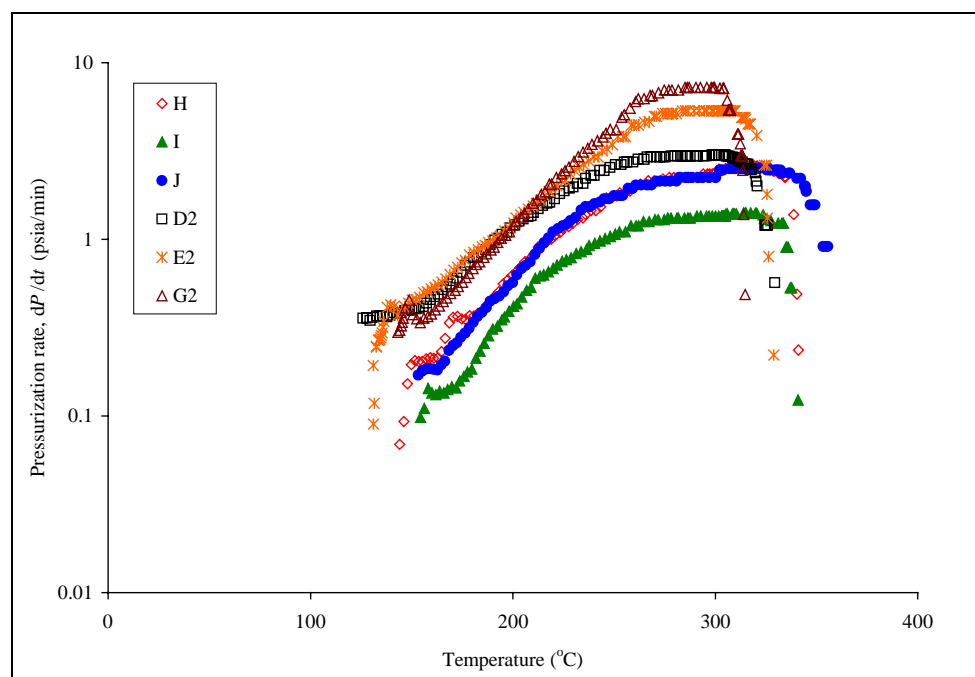


Figure 7.15. Pressurization rate of 1,3-butadiene polymerization

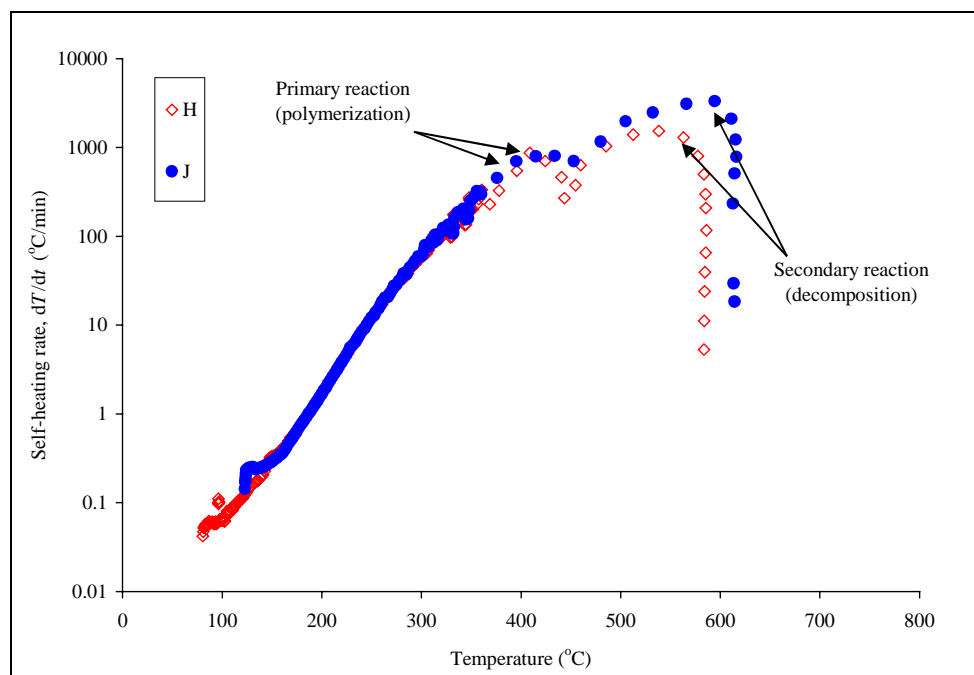


Figure 7.16. Two-stage reaction of 1,3-butadiene in the presence of oxygen

Pressurization rate curves did not reveal the same phenomenon; instead they showed a single-peak curve with significant effect of thermal inertia factors. Generally, the values of the maximum pressurization rates are not that hazardous and more significant values may be reached with larger sample sizes [130].

Table 7.12 presents the maximum self-heating and pressurization rates of butadiene reaction in presence of oxygen. Two maximum self-heating rates were reported for the primary and secondary reactions.

Table 7.12

Maximum self-heating and pressurization rates of butadiene reaction in the presence of oxygen with the APTAC™

Test No.	ϕ -Factor	Primary $(dT/dt)_{\max}$ (°C/min)	Secondary $(dT/dt)_{\max}$ (°C/min)	$(dP/dt)_{\max}$ (psi/min)
H	1.09	873	1533	2.6
I	1.19	258	541	1.4
J	1.10	804	3316	2.5
D2	1.16	409	688	3.0
E2	1.13	409	1654	5.3
G2	1.12	955	579	7.2

5. Results Discussion

The various computational levels of theory performed in this evaluation demonstrated the same relative trends among the proposed reaction pathways. This outcome predicts, qualitatively, the dominant reaction pathways irrespective of the level of theory used. However, when the enthalpy of VCH, COD, *c*-DVCB, and *t*-DVCB formation were quantitatively compared as in Table 7.3, some variations were found especially for the CBS-4M level of theory. Experimental enthalpy of reaction to form VCH was found to be -36.7 ± 0.5 kcal/mol at 25°C [129], and that to form COD was found to be -29.0 ± 0.20 kcal/mol at 252°C and 1 atm standard state [130].

According to that, CBS-4M level of theory was found to overestimate the enthalpy of reaction by about 4 – 6 kcal/mol, however HF/6-31G(d) and B3LYP/6-31G(d) levels underestimated the enthalpies by about 2 – 5 kcal/mol. Benson group contribution

method predicted VCH formation heat of reaction to about 0.1 kcal/mol difference from experimental value, and within 5.7 kcal/mol for COD formation reaction. Generally, these calculated values are in good agreement with the experimental ones.

The theoretical predictions indicated that the thermal hazards associated with the 1,3-butadiene reactions in the presence of oxygen are more significant. Comparing the activation energy barriers, based on Polanyi Equation, of the proposed elementary reactions in Figures 7.2 and 7.3 pointed up that reactions leading to the formation of 3,6-dihydro-1,2-dioxin (DHD) are relatively dominant. For instance, Reaction 4, Figure 7.2, which is a ring closing of the biradical (*cis, trans*) to VCH with a small strain energy of 1.4 kcal/mol [147] is expected to have no intrinsic activation energy [28,148]. Similarly, Reaction 3, Figure 7.3, which is another ring closing of the Intermediate 1 to DHD is expected to have the same reaction mechanism. In this case, the application of Polanyi Equation was possible using the calculated heats of reaction, which clearly revealed that the more exothermic reaction (formation of DHD) is more dominant over the less exothermic reaction (formation of VCH). The formation and accumulation of DHD peroxide will initiate polymerization reactions. Relatively, the calculated enthalpies of reaction of possible polymerization pathways are about 3 times the enthalpy of butadiene dimerization to VCH using HF/6-31g(d) level of theory.

These theoretical conclusions were confirmed with the outcome of the adiabatic thermal analysis. The measured thermodynamic and kinetic parameters indicated that butadiene polymerization (in presence of oxygen) is more thermally hazardous than butadiene polymerization (in absence of oxygen). The measured onset temperatures, at

self-heating rate of 0.1°C/min, of butadiene polymerization (in presence of oxygen) were found to be lower by about 39°C. The first- and second-order activation energies of the polymerization reaction were found to be lower by about 3.6 and 3.9 kcal/mol, respectively. Since it is expected that the polymerization reaction will follow free radical polymerization mechanism, a first-order reaction parameter is more appropriate to represent this reaction. Therefore, the difference in activation energy between the dimerization and polymerization is more significant (about 7.6 kcal/mol). The overall heat of reaction for the polymerization reaction is -24.4 ± 4.2 kcal/mol while that of butadiene dimerization is -14.1 ± 1.5 kcal/mol. These are clear indications of less thermally stable butadiene in presence of oxygen.

When comparing the theoretically calculated butadiene to VCH reaction enthalpy as the primary dimerization pathway with the overall measured heat of reaction of butadiene in absence of oxygen, significant differences were noticed. The differences between the predicted and measured values of heats of reaction are due, in part, to the thermal effects of butadiene vaporization. Also, the heat capacity of the butadiene sample was estimated at the onset temperature of the reaction for both liquid and vapor phases assuming ideal gas conditions and using correlations available in the literature. The uncertainty in this heat capacity estimation and the continuous changes in temperature and composition during the experiment will be reflected negatively on the measured overall heat of reaction. Therefore, the heat capacity estimation is a main source of error in the measured overall heat of reaction.

The overall measured dimerization second-order Arrhenius parameters ($E_A = 28.3 \pm 1.3$ kcal/mol and $\log (A C_o) = 10.9 \pm 0.5$) are comparable with those found in the literature. Table 7.13 summarizes some of others researchers values of these parameters. The reported values assume that 1,3-butadiene dimerization to VCH is the primary reaction pathway. These literature results were obtained by testing uninhibited 1,3-butadiene monomer.

Table 7.13
Literature values of 1,3-butadiene dimerization

Activation energy, E_a (kcal/mol)	Frequency factor, $\log (A C_o)$	Pressure (psia)	Temperature (°C)	Reference
25.30	10.67	0.03 – 14	326 – 436	[123]
26.80	11.14	2 – 15	418 – 650	[124]
23.69	9.97	10 – 96	173 – 387	[125]
24.53	6.95	0.9 – 8.7	191 – 284	[130]

The effect of the thermal losses associated with test cell (thermal inertia) was found to affect the measured parameters. When the experimental results were corrected for almost adiabatic conditions ($\phi \approx 1$) to simulate the real process conditions, a modified set of parameters were achieved and presented in Table 7.14. Thermal inertia factor correction methods and relations were presented in Chapter III. Significant effects of thermal inertia on maximum self-heating and pressurization rates were found, however,

they were limited on the reaction onset temperatures and time to maximum rate. The exponential nature of the self-heating and pressurization rates relationships with ϕ factor is responsible for these behaviors.

Table 7.14

Summary of the corrected experimental parameters of butadiene reactions with the APTAC™ at $\phi \approx 1$

Reaction	T_o (°C)	T_{max} (°C)	TMR_{ad} (min)	$(dT/dt)_{max}$ (°C/min)
Butadiene in absence of oxygen	158 ± 10	445 ± 19	103 ± 7	543
Butadiene in presence of oxygen	119 ± 8	580 ± 61	122 ± 7	1,473 (primary) 3,608 (secondary)

6. Conclusions

Successful qualitative theoretical predictions of 1,3-butadiene dimerization and polymerization reaction pathways were possible through the application of quantum chemistry calculations and thermodynamic-energy correlations. Theoretical evaluation was able to predict relative reaction tendencies of butadiene in presence and absence of oxygen even with low cost quantum computational levels of theory. Higher levels of theory may predict good thermodynamic estimates for dimerization reactions.

The combination of experimental thermal analysis and the theoretical calculations improved the understanding of the inhibited 1,3-butadiene reactions in presence and

absence of oxygen. Under thermal initiation conditions of the reaction, the inhibitors did not prevent polymerization reactions from proceeding although they may cause some delay to the reaction that was reflected on reaction onset temperature and activation energy when compared to literature values; however, they are not expected to prevent dimerization reactions.

This approach of evaluation provides the most required stoichiometric, thermodynamic, and kinetic parameters for chemical reactivity evaluation of 1,3-butadiene reactions including the corrected parameters due to thermal inertia effects. The measured and calculated parameters were found to be in a good agreement with literature information.

CHAPTER VIII

CONCLUSIONS AND RECOMMENDATIONS

1. Conclusions

Reactive chemical incidents are a significant safety problem for the chemical process industry. The current and traditional approaches for chemical reactivity evaluation were found to be inadequate either to provide the required understanding of reactive system chemistry or to quantify thermodynamic and kinetic parameters. Advanced methods of evaluation are primarily thermal analysis techniques and are capable of providing overall thermodynamic and kinetic description, however, these techniques are expensive and unable to provide detailed stoichiometric understanding of the system.

Since reactive chemical incidents are not limited to certain chemical groups or process conditions, the evaluation methodology should depend on a multi-level approach that addresses all chemicals as reactive chemicals under likely conditions. Various techniques of evaluation should be applied in a systematic methodology to screen reactive systems and reduce the number of chemicals to be investigated in detail. This approach should be practical, effective, and inexpensive.

A systematic approach for evaluating reactive chemical hazards was presented. In this approach a combination of computational quantum chemistry methods, thermodynamic-energy correlations, and experimental analysis results in a better understanding of reaction stoichiometry and better estimations of the thermodynamics and kinetics of reactive systems.

Computation quantum chemistry calculations together with screening experimental analysis at the early stages of system evaluation will focus research on the most possible and most hazardous reaction stoichiometries and hence reduce the need for detailed experimental analysis. More detailed and advanced experimental analyses may be still required for more complex systems.

Computational quantum chemistry calculations were applied at various levels of theory to predict the thermodynamic parameters of proposed reaction pathways. The most probable reaction stoichiometries were investigated through the application of thermodynamic-energy correlations such as Polanyi and Marcus equations. Based on that, heats of reaction of the most possible pathways were calculated.

The application of various levels of theory indicated the importance of appropriate selection of the method. In case where relative reaction behaviors are needed as the case with predicting dominant pathways, low-cost levels of theory, such as the AM1 and HF methods, can be applied with acceptable results. However, when accurate thermodynamic predictions are required, higher levels of theory such as B3LYP, CBS, and G2 should be used. Group contribution methods are valuable as a computational screening tool, however they still have some limitations.

Thermal analysis is considered a primary level of evaluation and it was conducted in two levels: screening thermal analysis using the RSST™ and C80D calorimeters, and adiabatic thermal analysis using the APTAC™ calorimeter. The adiabatic thermal analysis is the most acceptable technique for reactivity hazards evaluation since it is expected to simulate, successfully, the real process runaway scenarios.

Applying this reactivity evaluation approach for *di-tert*-butyl peroxide, styrene-acrylonitrile, and 1,3-butadiene systems led to successful predictions of primary reaction pathways and their thermodynamic parameters. A set of reactivity hazardous evaluation parameters was calculated using the experimental thermal analysis data and corrected to perfect adiabatic conditions. When these findings were compared to the literature information, a great level of agreement and consistency existed.

In general, this approach for evaluating chemical reactivity can be applied to a variety of systems. The degree of success in applying this approach will depend on the system complexity and on the appropriate levels of experimental analysis and theory to measure and predict the thermochemical data. The application of theoretical and experimental levels of evaluation should be conducted in parallel to enhance the understanding of reaction chemistry.

2. Recommendations

This approach may be applied to investigate real incident scenarios (case studies) for further evaluation of its validity. Real incidents evaluation may dramatically show the degree of success that can be achieved in predicting reactivity hazards scenarios.

This approach can also be expanded to investigate some other reactive systems of additional chemical groups. Investigating various reactive chemical groups will also expand the knowledge of this approach's capabilities and limitations.

In this research, the focus was on evaluating a single reactive system. The validity of this approach may be extended to include mixtures of reactive systems. Although this may appear as a significantly difficult task, however, the same principles of theoretical computational chemistry and experimental analysis are applied. To simplify dealing with mixtures of systems, one may start with combinations of two reactive compounds at a time to investigate their compatibility. This will lead to the formation of a chemical matrix that will identify the reactive chemical combinations for advanced studies.

For more complex reactive systems, other experimental techniques may be applied. Although, in this research, the focus was on thermal analysis techniques, however, the intermediates and products in these experiments can be analyzed for their composition. The knowledge of chemical composition will significantly improve the reactive system chemistry understanding.

REFERENCES

- [1] U.S. Chemical Safety and Hazard Investigation Board (CSB), Hazard Investigation: Improving Reactive Hazard Management, Report No. 2001-01-H, Washington, D.C., 2002.
- [2] Center for Chemical Process Safety (CCPS), Guidelines for Chemical Reactivity Evaluation and Application to Process Design, American Institute of Chemical Engineers, New York, 1995.
- [3] T. Yoshida, Y. Wada, Natalie Foster, Safety of Reactive Chemicals and Pyrotechnics, Industrial Safety Series, vol. 5, Elsevier, Amsterdam, 1995.
- [4] J. Steinbach, Safety Assessment for Chemical Processes, Wiley-VCH, Weinheim, Germany, 1999.
- [5] Health and Safety Executive (HSE), Designing and Operating Safe Chemical Reaction Processes, HSE Books, Rugby, UK, 2000.
- [6] Expert Commission for Safety in the Swiss Chemical Industry (ESCIS), Thermal Process Safety: Data Assessment Criteria Measures, Booklet 8, ESCIS, Basel, 1993.
- [7] J. Barton, R. Rogers (Eds.), Chemical Reaction Hazards: A Guide to Safety, second ed., The Institution of Chemical Engineers, Rugby, UK, 1997.
- [8] T. Grewer, Thermal Hazards of Chemical Reactions, Industrial Safety Series, vol. 4, Elsevier, Amsterdam, 1994.
- [9] R. Seyler, *Thermochim. Acta* 41 (1980) 55.
- [10] E. Donoghue, *J. Therm. Anal.* 49 (1997) 1609.
- [11] D. Laggett, *Thermochim. Acta* 367-368 (2001) 351.
- [12] H. Kohlbrand, *Chem. Eng. Prog.* 4 (1985) 52.
- [13] HarsBook: A Technical Guide for the Assessment of Thermal Hazards in Highly Reactive Chemical Systems, Industrial and Materials Technologies Programme of European Commission, Project: BET2-0572, Brussels, 2001.
- [14] L. Bretherick, Reactive chemical hazards: an overview, in: J. Woodward (Ed.), Proceedings of the International Symposium on Preventing Major Chemical Accidents, American Institute of Chemical Engineers/Center for Chemical Process Safety, New York, 1987, pp. 4.1-4.15.
- [15] T. Grewer, *Thermochim. Acta* 187 (1991) 133.
- [16] L. Bretherick, Handbook of Reactive Chemical Hazards: An Indexed Guide to Published Data, sixth ed., Butterworth-Heinemann, Oxford, 1999.

- [17] U. S. National Oceanic and Atmospheric Administration (NOAA), The Chemical Reactivity Worksheet, version 1.5, U. S. National Oceanic and Atmospheric Administration, Washington D.C., 2002.
- [18] National Fire Protection Association (NFPA), Manual of Hazardous Chemical Reactions, 4th edition, 491M, National Fire Protection Association, Boston, 1971.
- [19] C. Winder, A. Zarie, *J. Hazardous Materials* A79 (2000) 19.
- [20] D. Mosley, A. Ness, D. Hendershot, *Chem. Eng. Prog.* 11 (2000) 51.
- [21] T. Hofelich, D. Frurip, J. Powers, *Process Safety Progress* 13 (1994) 227.
- [22] C. Dahn, *J. Hazardous Materials* 4 (1980) 121.
- [23] A. Tompa, W. Bryant, Jr., *Thermochim. Acta*, 367-368 (2001) 433.
- [24] R. Gygax, *Chem. Eng. Prog.* 2 (1990) 53.
- [25] A. Keller, D. Stark, H. Fierz, E. Heinzle, K. Hungerbühler, *J. Loss Prev. Process Ind.* 10 (1997) 31.
- [26] T. Grewer, R. Rogers, *Thermochim. Acta* 225 (1993) 289.
- [27] T. Hofelich, R. Thomas, The use/misuse of the 100 degree rule in the interpretation of thermal hazard tests, in: *Proceedings of the International Symposium on Runaway Reactions*, The American Institute of Chemical Engineers, New York, 1989, pp. 74-85.
- [28] S. Benson, *Thermochemical Kinetics*, second ed., John Wiley, New York, 1976.
- [29] S. Benson, J. Buss, *Journal of Chem. Phys.* 29 (1958) 546.
- [30] N. Cohen, S. Benson, *Chem. Rev.* 93 (1993) 2419.
- [31] S. Verevkin, *Thermochim. Acta* 307 (1997) 17.
- [32] ASTM, CHETAH: the ASTM computer program for chemical thermodynamic and energy release evaluation, version 7.2, American Society for Testing and Materials, West Conshohocken, 1998.
- [33] D. Frurip, *Plant/Operation Progress* 11 (1992) 224.
- [34] E. Shanley, G. Melhem, *J. Loss Prev. Process Ind.* 13 (2000) 67.
- [35] T. Grewer, D. Frurip, B. Harrison, *J. Loss Prev. Process Ind.* 12 (1999) 391.
- [36] A. Carven, A simple method of estimating exothermicity by average bond energy summation, in: *Hazardous from Pressure: Exothermic Reactions, Unstable Substances, Pressure Relief, and Accidental Discharge*, Symposium Series 102, The Institution of Chemical Engineers, Rugby, UK, 1987, pp. 97-111.
- [37] E. Shanley, G. Melhem, *Process Safety Progress* 14 (1995) 29.

- [38] C. Bruneton, C. Hoff, P. Barton, *Computers Chem. Engng.* 21 (1997) Suppl. S311.
- [39] C. Bruneton, C. Hoff, P. Barton, *Computers Chem. Engng.* 22 (1998) 735.
- [40] K. Irikura, D. Frurip (Eds.), *Computational Thermochemistry*, American Chemical Society, Washington, D.C., 1996.
- [41] R. Landau, *Thermochim. Acta* 289 (1996) 101.
- [42] S. Rowe, *Thermochim. Acta* 289 (1996) 167.
- [43] Y. Duh, C. Hsu, C. Kao, S. Yu, *Thermochim. Acta* 285 (1996) 67.
- [44] F. Stoessel, *J. Therm. Anal.* 49 (1997) 1677.
- [45] H. Fauske, *Chem. Eng. Prog.* 2 (2000) 17.
- [46] R. Rota, G. Ruggeri, M. Morbidelli, S. Ditali, *J. Loss Prev. Process Ind.* 15 (2002) 49.
- [47] J. Singh, *Process Safety Progress* 16 (1997) 43.
- [48] J. Leonhardt, P. Hugo, *J. Therm. Anal.* 49 (1997) 1535.
- [49] J. Sempere, R. Nomen, R. Serra, P. Cardillo, *J. Loss Prev. Process Ind.* 10 (1997) 55.
- [50] K. Heldt, H. Anderson, *Thermochim. Acta* 271 (1996) 189.
- [51] J. Sun, Y. Li, K. Hasegawa, *J. Loss Prev. Process Ind.* 14 (2001) 331.
- [52] D. Jones, R. Augsten, *Thermochim. Acta* 286 (1996) 355.
- [53] A. West, *Process Safety Progress*, 12 (1993) 55.
- [54] W. Fenlon, *Plant/Operation Progress* 3 (1984) 197.
- [55] J. Pastré, U. Wörsdörfer, A. Keller, K. Hungerbühler, *J. Loss Prev. Process Ind.* 13 (2000) 7.
- [56] E. Wilcock, R. Rogers, *J. Loss Prev. Process Ind.* 10 (1997) 289.
- [57] L. Tuma, *Thermochim. Acta* 392-393 (2002) 41.
- [58] G. Melhem, H. Fisher, D. Shaw, *Process Safety Progress* 14 (1995) 1.
- [59] T. Hofelich, M. LaBarge, *J. Loss Prev. Process Ind.* 15 (2002) 163.
- [60] D. Townsend, J. Tou, *Thermochim. Acta* 37 (1980) 1.
- [61] M. Gordon, G. O'Brien, C. Hensler, K. Marcali, *Plant/Operation Progress* 1 (1982) 27.
- [62] H. Liaw, C. Yur, Y. Lin, *J. Loss Prev. Process Ind.* 13 (2000) 499.
- [63] C. Roothan, *Rev. Mod. Phys.* 23 (1951) 69.
- [64] J. Ochterski, G. Petersson, J. Montgomery, Jr., *J. Chem. Phys.* 104 (1996) 2598.

- [65] L. Curtiss, K. Raghavachari, G. Trucks, J. Pople, *J. Chem. Phys.* 94 (1991) 7221.
- [66] C. Lee, W. Yang, R. Parr, *Phys. Rev.* B37 (1989) 785.
- [67] A. Becke, *J. Chem. Phys.* 98 (1993) 5648.
- [68] M. Dewar, E. Szoebisch, E. Healy, *J. Am. Chem. Soc.* 107 (1985) 3902.
- [69] D. Young, *Computational Chemistry*, Wiley, New York, 2001.
- [70] M. Evans, M. Polanyi, *Trans. Faraday Soc.* 32 (1936) 1333.
- [71] M. Evans, M. Polanyi, *Trans. Faraday Soc.* 34 (1938) 11.
- [72] R. Masel, *Chemical Kinetics and Catalysis*, Wiley, New York, 2001.
- [73] R. Masel, *Principles of Adsorption and Reaction on Solid Surfaces*, Wiley, New York, 1996.
- [74] J. Bockris, A. Reddy, M. Gamboa-Aldeco, *Modern Electrochemistry: Fundamentals of Electrode Processes*, vol. 2A, second ed., Kluwer Academic/Plenum Publishers, New York, 2000.
- [75] R. Masel, W. Lee, *J. Catal.* 165 (1997) 80.
- [76] M. Mannan, A. Aldeeb, S. Saraf, W. Rogers, unpublished work.
- [77] W. Kohn, L. Sham, *Phys. Rev.* 140 (1965) A1133.
- [78] R. Marcus, *J. Chem. Phys.* 24 (1956) 966.
- [79] R. Marcus, *J. Phys. Chem.* 72 (1968) 891.
- [80] G. Maria, E. Heinzle, *J. Loss Prev. Process Ind.* 11 (1998) 187.
- [81] J. Foresman, Æ. Frisch, *Exploring Chemistry with Electronic Structure Methods*, second ed., Gaussian Inc., Pittsburgh, 1996.
- [82] R. Krishnan, J. Binkley, R. Seeger, J. Pople, *J. Chem. Phys.* 72 (1980) 650.
- [83] J. Montgomery, Jr., M. Frisch, J. Ochterski, G. Petersson, *J. Chem. Phys.* 112 (2000) 6532.
- [84] M. Frisch, G. Trucks, H. Schlegel, G. Scuseria, M. Robb, J. Cheeseman, V. Zakrzewski, J. Montgomery, Jr., R. Stratmann, J. Burant, S. Dapprich, J. Millam, A. Daniels, K. Kudin, M. Strain, O. Farkas, J. Tomasi, V. Barone, M. Cossi, R. Cammi, B. Mennucci, C. Pomelli, C. Adamo, S. Clifford, J. Ochterski, G. Petersson, P. Ayala, Q. Cui, K. Morokuma, D. Malick, A. Rabuck, K. Raghavachari, J. Foresman, J. Cioslowski, J. Ortiz, A. Baboul, B. Stefanov, G. Liu, A. Liashenko, P. Piskorz, I. Komaromi, R. Gomperts, R. Martin, D. Fox, T. Keith, M. Al-Laham, C. Peng, A. Nanayakkara, M. Challacombe, P. Gill, B. Johnson, W. Chen, M. Wong, J. Andres, C. Gonzalez, M. Head-Gordon, E. Replogle, J. Pople, *Gaussian 98*, revision A.9, Gaussian, Inc., Pittsburgh, 1998.

- [85] H. Fauske, Reactive System Screening Tool, United States Patent Number 5,229,074, 1993.
- [86] H. Fauske, Process Safety Progress 17 (1998) 190.
- [87] S. Chippett, P. Ralbovsky, R. Granville, The APTAC: a high pressure, low thermal inertia, adiabatic calorimeter, in: G. Melhem, H. Fisher (Eds.), International Symposium on Runaway Reactions, Pressure Relief Design, and Effluent Handling, American Institute of Chemical Engineers, New York, 1998, pp. 81–108.
- [88] F. Incropera, D. DeWitt, Fundamentals of Heat and Mass Transfer, fifth ed., Wiley, New York, 2002.
- [89] H. Fisher, H. Forrest, S. Grossel, J. Huff, A. Muller, J. Noronha, D. Shaw, B. Tilley, Emergency Relief System Design Using DIERS Technology, The American Institute of Chemical Engineers, New York, 1992.
- [90] A. Kossoy, E. Koludarova, J. Loss Prev. Process Ind. 8 (1995) 229.
- [91] R. Kirk, D. Othmer, Encyclopedia of Chemical Technology, fourth ed., Wiley, New York, 1991.
- [92] A. Hordijk, J. De Groot, Thermochem. Acta 101 (1986) 45.
- [93] R. Antrim, M. Bender, M. Clark, Jr., L. Evers, D. Hendershot, J. Magee, J. McGregor, P. Morton, J. Nelson, C. Zeszotarski, Process Safety Progress 17 (1998) 225.
- [94] T. Ho, Y. Duh, J. Chen, Process Safety Progress 17 (1998) 259.
- [95] N. Milas, D. Surgenor, J. Am. Chem. Soc. 68 (1946) 205.
- [96] J. Raley, F. Rust, W. Vaughan, J. Am. Chem. Soc. 70 (1948) 88.
- [97] J. Raley, F. Rust, W. Vaughan, J. Am. Chem. Soc. 70 (1948) 1336.
- [98] F. Rust, F. Seubold, W. Vaughan, J. Am. Chem. Soc. 70 (1948) 95.
- [99] J. Murawski, J. Roberts, M. Szwarc, J. Chem. Phys. 19 (1951) 698.
- [100] A. Williams, E. Oberright, J. Brooks, J. Am. Chem. Soc. 78 (1956) 1190.
- [101] E. Huyser, C. Bredeweg, J. Am. Chem. Soc. 86 (1964) 2401.
- [102] J. Baker, J. Littlefair, R. Shaw, J. Thynne, J. Am. Chem. Soc., 1286 (1965) 6970.

- [103] P. Molyneux, *Tetrahedron* 22 (1966) 2929.
- [104] D. Shaw, H. Pritchard, *Can. J. Chem.* 46 (1968) 2721.
- [105] C. Yaws, *Chemical Properties Handbook: Physical, Thermodynamic, Environmental, Transport, Safety, and Health Related Properties for Organic and Inorganic Chemicals*, McGraw-Hill, New York, 1999.
- [106] M. Chase, Jr., *NIST-JANAF Thermochemical Tables*, fourth ed., *J. Phys. Chem. Ref. Data*, Monograph 9, 1998, pp. 1-1951.
- [107] Y. Iizuka, M. Surianarayanan, *Ind. Eng. Chem. Res.* 42 (2003) 2987.
- [108] J. Tou, L. Whiting, *Thermochim. Acta* 48 (1981) 21.
- [109] J. Leung, H. Fauske, H. Fisher, *Thermochim. Acta* 104 (1986) 13.
- [110] M. Chanda, *Advanced Polymer Chemistry*, Marcel Dekker, New York, 2000.
- [111] R. Boundy, R. Boyer, S. Stoesser, *Styrene: Its Polymers, Copolymers, and Derivatives*, Reinhold Publishing, New York, 1952.
- [112] D. Sebastian, J. Biesenberger, Nonisothermal behavior and thermal runaway phenomena in chain addition copolymerization, in: V. Weekman, Jr., D. Luss (Eds.), *The Fifth International Symposium on Chemical Reaction Engineering*, American Chemical Society, Washington, D.C., 1978, pp. 173-186.
- [113] D. Sebastian, J. Biesenberger, *Polym. Eng. Sci.* 19 (1979) 190.
- [114] D. Sebastian, J. Biesenberger, *J. Appl. Polym. Sci.* 23 (1979) 661.
- [115] D. Sebastian, J. Biesenberger, *J. Macromol. Sci., Chem.* A15 (1981) 553.
- [116] F. Billmeyer, Jr., *Textbook of Polymer Science*, third ed., Wiley, New York, 1984.
- [117] D. Hill, J. O'Donnell, P. O'Sullivan, *Macromolecules* 15 (1982) 960.
- [118] D. Hill, A. Lang, P. Munro, J. O'Donnell, *Eur. Polym. J.* 28 (1992) 391.
- [119] F. Lewis, F. Mayo, W. Hulse, *J. Am. Chem. Soc.* 67 (1945) 1701.
- [120] American Cyanamid Company, *The Chemistry of Acrylonitrile*, American Cyanamid Company, New York, 1959.

- [121] M. Sittig, Handbook of Toxic and Hazardous Chemicals and Carcinogens, third ed., Noyes Publications, Park Ridge, New Jersey, 1991.
- [122] U.S. Environmental Protection Agency, RMP*Info Database, USEPA, Washington, D.C., 2000.
- [123] W. Vaughan, *J. Am. Chem. Soc.* 54 (1932) 3863.
- [124] D. Rowley, H. Steiner, *Discuss. Faraday Soc.* 10 (1951) 198.
- [125] G. Kistiakowsky, W. Ransom, *J. Chem. Phys.* 7 (1939) 725.
- [126] J. Harkness, G. Kistiakowsky, W. Mears, *J. Chem. Phys.* 5 (1937) 682.
- [127] R. Robey, H. Wiese, C. Morrell, *Ind. Eng. Chem.* 36 (1944) 3.
- [128] G. Miller, R. Eliason, G. Pritchard, *J. Polym. Sci., Pt. C* 5 (1964) 1109.
- [129] N. Duncan, G. Janz, *J. Chem. Phys.* 20 (1952) 1644.
- [130] G. Huybrechts, L. Luyckx, TH. Vandenboom, V. Mele, *Int. J. Chem. Kinet.* 9 (1977) 283.
- [131] H. Fried, D. Schisla, J. Zoeller, M. Levin, A study of free-radical and thermally-initiated butadiene polymerization, in: *Proceeding of the Process Plant Safety Symposium*, vol. 1, The American Institute of Chemical Engineers, New York, 1996, pp. 363–390.
- [132] R. Fourent, J. Bauge, F. Battin-Leclerc, *Int. J. Chem. Kinet.* 31 (1999) 361.
- [133] A. Laskin, H. Wang, C. Law, *Int. J. Chem. Kinet.* 32 (2000) 589.
- [134] M. Bartke, A. Wartmann, K. Reichert, *Chem. Ing. Tech.* 73 (2001) 660.
- [135] P. Philips, C. Giavarini, R. Silla, *Chem. Ing. Tech.* 73 (2001) 681.
- [136] W. Tsang, V. Mokrushin, Mechanism and rate constants for 1,3-butadiene decomposition, in: *Proceeding of the Combustion Institute*, vol. 28, Pittsburgh, 2000, pp. 1717–1723.
- [137] J. Ling, X. Ni, Y. Zhang, Z. Shen, *Polymer* 41 (2000) 8703.
- [138] H. Fisher, G. Melhem, M. Levin, J. Leung, 1,3-Butadiene; thermal dimerization/trimerization, free-radical polymerization, and polymer

decomposition reactions, in: G. Melhem, H. Fisher (Eds.), *International Symposium on Runaway Reactions, Pressure Relief Design, and Effluent Handling*, American Institute of Chemical Engineers, New York, 1998, pp. 445–460.

- [139] W. Tsang, *J. Chem. Phys.* 42 (1965) 1805.
- [140] R. Woodward, R. Katz, *Tetrahedron* 5 (1959) 70.
- [141] W. Doering, M. Neumann, D. Hasselmann, R. Kaye, *J. Am. Chem. Soc.* 94 (1972) 3833.
- [142] Y. Li, K. Houk, *J. Am. Chem. Soc.* 115 (1993) 7478.
- [143] J. Berson, P. Dervan, *J. Am. Chem. Soc.* 95 (1973) 267.
- [144] J. Gajewski, *Hydrocarbon Thermal Isomerization*, Academic Press, New York, 1981.
- [145] M. Bobrowski, A. Liwo, S. Oldziej, D. Jeziorek, T. Ossowski, *J. Am. Chem. Soc.* 122 (2000) 8112.
- [146] S. Madorsky, *Thermal Degradation of Organic Polymers*, Interscience Publishers, New York, 1964.
- [147] S. Benson, F. Cruickshank, D. Golden, G. Haugen, H. O'Neal, A. Rodgers, R. Shaw, R. Walsh, *Chem. Rev.* 69 (1969) 279.
- [148] S. Benson, *J. Chem. Phys.* 46 (1967) 4920.

VITA

Abdulrehman Ahmed Aldeeb was born in Kuwait in 1973. He holds a Ph.D. in chemical engineering from Texas A&M University (2003), M.S. degree in environmental engineering from the University of Texas at Arlington (1999), and B.S. degree in chemical engineering from Jordan University of Science and Technology (1995). During his Ph.D. studies, he joined the Mary Kay O'Connor Process Safety Center for four years as a graduate researcher with focus on chemical reactivity hazards evaluation using thermal analysis and computational techniques. Previously, he worked for the pharmaceutical industry and was a research and development chemical engineer. Aldeeb is a member of the American Institute of Chemical Engineers, an associate member of the Institution of Chemical Engineers, UK, and a member of the North American Thermal Analysis Society. He received the Texas Chemical Council Sponsorship (2003), Brunner Barnes Graduate Fellowship, Texas A&M University (2003), International Study Grant, Texas A&M University (2003), Civil and Environmental Engineering Department Scholarship, University of Texas at Arlington (1999), and the Honor Student award, Jordan University of Science & Technology (1994 and 1995). Aldeeb's permanent address is Suweileh, P.O. Box 938, Amman 11910, Jordan.